Development of a Novel Protein Sensor For The Intracellular Imaging of

Zinc

by

Tamiika Kache Hurst

A dissertation submitted in partial fulfillment
of the requirements for the degree of
Doctor of Philosophy
(Chemistry)
in The University of Michigan
2010

Doctoral Committee:

    Professor Carol A. Fierke, Chair
    Professor Raoul Kopelman
    Professor Adam J. Matzger
    Professor Mark E. Meyerhoff
    Professor Martin A. Philbert

ACKNOWLEDGEMENTS

TABLE OF CONTENTS

LIST OF FIGURES

LIST OF SCHEMES

LIST OF TABLES

LIST OF ABBREVIATIONS

AF594	AlexaFluor 594
BFP	Blue Fluorescent Protein
BME	β-mercaptoethanol
CA(II)	Carbonic Anhydrase Isozyme II
CFP	Cyan Fluorescent Protein
CIP	Calf Intestinal Alkaline Phosphatase
DNSA	Dansylamide
DPA	Dipicolinic acid
Dps	Dapoxyl Sulfonamide
DTT	Dithiothreitol
E117A	Glutamate to alanine mutation at position 117
EDTA	(Ethylenedinitrilo) etraacetic acid
FRET	Förster resonance energy transfer
Glu-117	Glutamate at position 117
GFP	Green Fluorescent Protein
HEPES	4-(2-hydroxyethyl)-1-piperazineethanesulfonic acid
H94	Histine at position 94, Zinc Ligand
H96	Histine at position 96, Zinc Ligand
H119	Histine at position 119, Zinc Ligand
ICP-MS	Inductively Coupled Plasma Emission Mass Spectrometry

IPTG	Isopropyl-β-D-thiogalactopyranoside
LPS	Lipopolysaccharide
MOPS	3-(N-morpholino)ethanesulphonic acid
N67C	Aspargine to cysteine mutation at position 67
NEB	New England Biolabs
NTA	Nitrilo-triacetic acid
PMSF	Phenylmethanesulfonyl fluoride
PTD	Protein Transduction Domain
Q92A	Glutamine to alanine mutation at position 92
Q92L	Glutamine to leucine mutation at position 92
SDS Page	Sodium dodecyl sulfate polyacrylamide gel electrophoresis
T199A	Threonine to alanine mutation at position 199
T199G	Threonine to glycine mutation at position 199
T199I	Threonine to isoleucine mutation at position 199
T199N	Threonine to asparagine mutation at position 199
T199S	Threonine to serine mutation at position 199
T199V	Threonine to valine mutation at position 199
TAME	Tosyl-L-Argininyl-methyl ester
TAT	Transactivator of transcription
TCEP	Tris(2-carboxyethyl)phosphine hydrochloride
TFA	Trifluoroacetic acid
TSQ	N-6-methoxy-8-quinolyl)-p-toluenesulfonamide
XRF	X-ray Fluorescence Spectrometry

ABSTRACT

Development Of A Novel Protein Sensor For The Intracellular imaging Of Zinc

by

Tamiika Kache Hurst

Chair: Carol A. Fierke

Zinc is the second most abundant transition metal in the human body. In recent years, research on zinc homeostasis in mammalian cells has revealed distinct pools of zinc. Zinc is tightly bound to metalloproteins as a cofactor or structural component including metallothioneins that may provide a specific labile pool of zinc. The zinc-binding protein, Carbonic Anhydrase II (CA(II)) can be compartmentalized in intracellular organelles such as lysosomes, endosomes, endoplasmatic reticulum, mitochondria and the Golgi apparatus or in specialized organelles like synaptic vesicles and secretory granules. However, the concentration of "free" zinc inside cells is estimated to be at or below the

picomolar level. Disruption of cellular Zn^{2+} homeostasis is implicated in several major disorders including Alzheimer's disease, diabetes, and cancer.

The molecular mechanisms of Zn^{2+} physiology and pathology are insufficiently understood, owing in part to the lack of tools for measuring changes in intracellular Zn^{2+} concentrations with high spatial and temporal fidelity. To address this critical need, we have designed, characterized, and applied an intracellular protein-based sensor expressed in BL21(DE3) cells for the ratiometric imaging of Zn^{2+} based on the carbonic anhydrase (CA(II)) platform. FRET excitation ratiometric detection of intracellular Zn^{2+} occurs through Zn^{2+}-mediated energy transfer between dapoxylsulfonamide (Dps) bound to carbonic anhydrase and the fluorescent protein, mCherry fused to the C-termini of (CA(II)).

The series of probes developed are expressible in various cell types, feature visible excitation and emission profiles, and show excellent selectivity responses for Zn^{2+} at intracellular concentrations. Furthermore, the ratio of the binding affinity for Zn^{2+}/Cu^{2+} can be varied by mutations at Q92 and T199. We demonstrate the value of the (CA(II))_mCherry sensor for biological applications by imaging induced changes in intracellular $[Zn^{2+}]$ in *E. coli.*. We anticipate that (CA(II))_mCherry and related probes will prove useful for elucidating the biology of Zn^{2+} in a number of *in vivo* processes.

CHAPTER 1: Carbonic Anhydrase II-Based Metal Ion Sensing

Role of zinc in biology:

Transition metals, including zinc, copper, iron and nickel, are essential minerals for living organisms. Zinc, the second most abundant trace element after iron, plays important catalytic, structural, and regulatory roles in cells. Bioinformatic analysis indicates that 3%-10% of the human genome encodes potential zinc binding proteins [1]. More than 300 zinc enzymes covering all six classes of enzymes have been discovered (reviewed in [2], [3], [4]); in many cases, the zinc ion is an essential cofactor for the observed biological function of these metalloenzymes. Carbonic anhydrase was the first zinc-dependent enzyme discovered [5]. Additionally, various zinc-binding motifs that are important for stabilizing protein structure mediate diverse biological processes [6].

Disturbance of zinc homeostasis can cause multiple disorders in human health. Humans require a daily intake of several mg of zinc to maintain normal zinc levels [7]. Zinc deficiency, resulting from either genetic defect or dietary limitation, causes growth retardation, lethargy, gastrointestinal disorders, dermatological lesions, defects in reproductive organs, and dysfunction of the immune system [8]. Loss of function in zinc absorption transporters in the small intestine causes severe zinc deficiency and death in utero [9]. Furthermore,

increased vulnerability to infections is the leading cause of death among zinc-deficient populations in developing countries [10]. Zinc supplementation has successfully been used as a treatment of many disorders, including acrodermatitis enteropathica (inflammation of the skin and the small intestine), age-related macular degradation and pediatric diarrhea [11]. Accumulating evidence also supports a role for zinc in the development of chronic diseases such as Alzheimer's disease, diabetes, and asthma [12]. Excess zinc can induce aggregation of amyloid-β and formation of plaque [13], the hallmark of Alzheimer's disease, and oral administration of zinc chelators substantially reduces the plaque formation in mouse models [14]. Decreased serum zinc levels are seen in Type I diabetes patients, and dietary supplementation with zinc reduces the incidence of chemically-induced diabetes in mice [15]. Furthermore, a missense mutant of the zinc transporter (ZnT8), believed responsible for inserting zinc into pancreatic beta cell insulin-containing vesicles, was identified as a risk factor for Type 2 diabetes [16]. Therefore, development of methods to better understand zinc homeostasis in cells and organs should have implications for the treatment of a number of diseases.

Methods to measure total metal concentrations:

      A wide variety of analytical techniques are available for the determination and quantitation of metal ions in solutions. Measurement of low concentrations of analytes in complex media, like seawater and blood, is increasingly important

for both biomedical and environmental applications. In particular, determination of the concentrations of transition metals, including copper and zinc, is of great interest as these metal ions are essential for human health and can be toxic at elevated levels.

Unlike iron or copper, zinc contains a filled d orbital ($3d^{10}4s^0$) and therefore is not amenable to direct determination by optical absorption, emission, electron paramagnetic resonance, or related techniques. Therefore, techniques such as atomic absorption spectroscopy, mass spectrometry and X-ray absorption spectroscopy have been employed to measure zinc. Hybrid techniques (i.e. HPLC-atomic absorption spectroscopy, ICP-MS), in which separation of the species of interest is coupled with a metal specific detector, have been established as reliable and robust analytical tools for analysis of multiple metal ions in biological and environmental applications [17, 18]. The separation component of the coupled system is important when the target analytes have related chemical properties. The choice of the detector depends on both the analyte concentration, and the required limit of detection. Because of its multi-element capability and low detection limits, inductively coupled plasma mass spectrometry (ICP-MS) is the most widely used method to measure the concentration of a given metal in complex mixtures [18]. Like all analytical techniques, ICP-MS has inherent limitations. First, the sample is destroyed during metal analysis. Second, ICP-MS measures the total metal concentration in a sample irrespective of the speciation of that metal, whereas in biological or environmental matrices it is often the concentration of the readily exchangeable

3

or bio-available metal ion that is of interest. Finally, ICP-MS cannot be used for real-time intracellular monitoring of metals. Therefore, additional methods to quantify zinc concentrations are needed.

New methods to measure and image metals in biological samples are under development. Recently X-ray fluorescence spectrometry (XRF) has been employed to measure and image metal ions in cells and tissues [19]. XRF is a nondestructive method for the elemental analysis of solids and liquids, but is destructive to cells and typically requires dehydration of the sample prior to imaging. In this method, the sample is irradiated by an intense x-ray beam that causes the emission of fluorescent x-rays from inner shell electrons of metal ions. The spectrum of emitted x-rays is detected using either an energy dispersive or wavelength dispersive detector. The elements in the sample are identified by the wavelengths of the emitted x-rays, while the concentrations of the elements are determined by the intensity of those x-rays in comparison to standards [20]. This technique allows for simultaneous detection of >10 elements with detection limits typically varying between 10 and 100 ppm dry weight, depending on the elements to be analyzed and the sample matrix [21]. X-ray fluorescence has been useful for imaging metal ions within cells [22]; coupling XRF with traditional light microscopy allows the coupling of cell morphology with *in vivo* metal ion distribution. Like ICP-MS, an issue with XRF imaging is that quantitation is based on the total metal content and not the free metal ion concentration.

Methods to measure "free" metal concentrations:

The methods above allow for the measurement of the total metal concentration in a sample. However, zinc in biological systems is bound to myriad proteins and small molecules, thereby decreasing the "free" or readily exchangeable metal concentration by orders of magnitude and complicating analyses. Consequently, fluorescence methods based on indicators whose emissions respond to bound metal have become the most prevalent approach for quantifying many divalent metals in both aqueous and biological samples. Fluorescent sensors are classified according to the receptor molecule and the fluorescent signal. If the transducer is a molecule that is biological in origin, the sensor is called a biosensor (Figure 1.1).

Figure 1:1: Biosensor Paradigm:

A sensor is termed a "biosensor" if the analyte is recognized by a molecule that is biological in origin
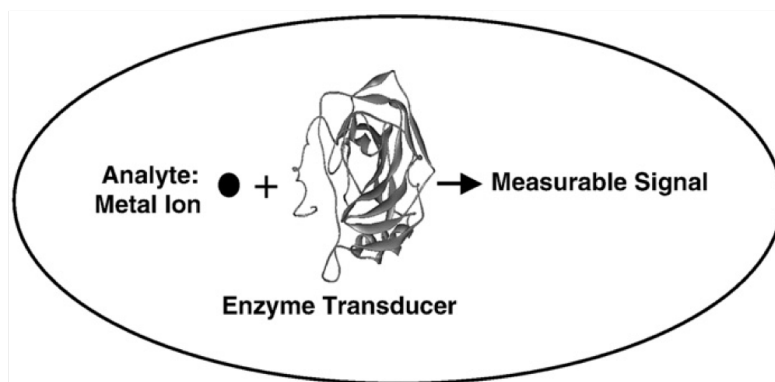
The success of fluorescent sensors in biology has been due in part to their ability to correlate analyte concentration distributions with the physical structures of cells and tissues. An array of fluorescent, zinc-selective chelators have been

developed and applied to zinc measurements (recently reviewed in [23], [24], [25], [26]). Many desirable traits of fluorescent metal ion indicator systems are now apparent. Perhaps the most important consideration is high affinity and selectivity for zinc or other target metal ions; the probe must not only respond to free zinc but reject potentially interfering metal ions present at up to billion-fold higher concentrations. Metal selectivity has been a limitation of many fluorescent sensors; these chelators often retain affinity for ions such as Ca^{2+} and Mg^{2+}. While calcium or magnesium do not produce interference when present at equal concentrations with zinc, intracellular concentrations of these metals are significantly higher than that of free zinc [27], [28], [29], and therefore can interfere by saturating all of the metal binding sites of the fluorophore. To quantify zinc concentrations in real-time, zinc should equilibrate with the sensor; therefore metal binding should be fast, reversible, and ideally of 1:1 stoichiometry. Furthermore, the sensor should have a metal affinity comparable to the free metal concentration. Reliable quantitation is essential for many studies, so a wavelength ratiometric, polarization, or lifetime response is necessary. A sensor where the analyte binding only induces a change in fluorescence intensity is of modest use for quantitation because so many other factors can also cause apparent intensity changes, including: changes in the probe concentration due to photobleaching or washout, variations in the excitation intensity or sample thickness, the presence of adventitious quenchers, and so on. The potential for these artifacts led to the introduction of wavelength ratiometric indicators for pH and calcium [30], and later lifetime- [31], [32] and

6

polarization-based chemical analyses [33], all of which are largely free of these artifacts.   An excitation wavelength in the visible range or near IR is preferred so as to reduce damage to the cell and confounding autofluorescence. For both *in vitro* and *in vivo* intracellular applications, solubility and membrane permeability are vital; furthermore, washout and nonspecific binding (e.g., to proteins) must be minimal. The optimal properties of fluorescent sensors can depend on the proposed use for the sensor.

Specific tools for monitoring Zn^{2+}:

Among the most important tools for studying the roles of metal ions such as Zn^{2+} in biology have been metallofluorescent indicators (sometimes called sensors). These indicators recognize the presence of free metal ions and indicate a change in fluorescence signal, which can be measured or photographed. The change may be in the intensity (either enhancement or quenching), the excitation or emission wavelength, or in a few cases, the polarization or lifetime of the fluorescence [34], [35], [36]. There are several advantages to the fluorescence approach for studying metals in biology. First, fluorescence can be imaged in cells, tissues, or living organisms, which enables analyte distribution to be related to the structure of the living cells or organisms. Most imaging is done on a microscope, which permits the use of small samples. Second, in good examples indicators are quite sensitive and specific for analyte, and respond rapidly enough to follow physiologically important processes. Third, in some cases the indicators permit quantitative determination of analytes *in situ*, without sample

7

collection or processing, which may be infeasible on a subcellular level. Fourth, by using protein or organelle-specific fluorescent stains and other indicators emitting at different wavelengths, the analyte level may be spatially related to a specific structure or organelle, or the distribution of another analyte in the cell. Finally, imaging or scanning can be used to screen a large number of specimens at high rates for fluorescence changes, which is routinely used to test candidate drugs for efficacy in treating disease. For all these reasons, hundreds of fluorescent indicators and stains have been developed for different purposes.

Various fluorescent indicators have been described for measuring zinc ion in solution and excellent reviews article have appeared recently [25], [24], [25], [26]; unfortunately, the scope of this necessitates the omission of much important work. Most of these indicators are small organic fluorophores that also have multiple chelating moieties, such as amines or carboxylates, capable of binding the metal ion. Early indicators (such as 8-hydroxyquinoline) were mostly ill-suited for studying biological systems mainly due to a lack of specificity for zinc and toxicity compared to other metal ions more prevalent in biological matrices, such as calcium and magnesium [34], [35]. Frederickson developed the first zinc indicator widely used for biological specimens (TSQ: N-6-methoxy-8-quinolyl)-p-toluenesulfonamide), which served as an histological stain for granular zinc in brain, pancreas, and other tissues [37]. However, the pH-dependence and insolubility of the 2:1 complex made TSQ poorly suited for soluble zinc and quantitation problematic. Several important advances appeared with the introduction of the more soluble Zinquin [38], including exploitation of

dequenching by binding amine moieties [39], higher selectivity zinc binding

moieties [40]; ratiometric response [41]; targeting to mitochondria [42] and high

affinity [43], [44]. A significant proportion of these indicators are available

commercially and, where appropriate, widely used. While the development of

these indicators has come a long way, no indicator or family of indicators offers

high (or tunable) affinity, ratiometric or other accurate quantitation, rapid

response, and targeting to desired cell types and/or organelles.

Knowing the high selectivity with which biomolecules, such as proteins,

bind metal ions, several workers constructed peptides or proteins with biomimetic

metal ion binding sites and transduced the binding as changes in fluorescence

using attached labels [45], [46], [47]. These indicators may be termed

"biosensors" because of their use of biologically-derived molecules for

recognition of the analyte.   Other investigators drew on the pioneering work of

Miyawaki in developing FRET-based sensors [48], where the binding of zinc ion

to a protein induces a conformational change, bringing two tethered fluorescent

protein moieties closer together, thereby improving their energy transfer

efficiency [49], [50], [51]. While these approaches have been promising

(particularly the prospect of an expressible indicator), until recently [52] they had

not demonstrated the high affinity and selectivity observed for natural metal ion

binding sites.   As will be seen, the CA(II)-based biosensors offer all these

desirable traits, and more.

Carbonic Anhydrase:

Meldrum and Roughton discovered a new enzyme present in red blood cells that catalyzed the reverse hydration of CO_2 to HCO_3^- [53], [54]. This enzyme, named carbonic anhydrase, was identified as the first zinc metalloenzyme. For both the *in vivo* function and the use of CA in sensors, the affinity and selectivity of metal ion binding to the active site is key. The crystal structure of human CA(II) demonstrates that the active site, located in the central region of a ten stranded, twisted β-sheet, is comprised of a cone shaped cleft, 15 Å deep, with a tetrahedral Zn^{2+} ion at the bottom of the cleft [55], [56]. The imidazole side chains of three histidine ligands, at positions 94, 96 and 119, are directly coordinated to the metal center. These direct ligands form hydrogen bonds to the indirect ligands Gln-92, Asn-244 and Glu-117, respectively. Filling out the coordination sphere of zinc is a hydroxide ion that forms a hydrogen bond to Thr-199 at neutral pH. With the exception of Asn-244, which is hydrogen bonded to His-96 through the main chain carbonyl oxygen, the direct and indirect metal ligands are invariant in all sequenced catalytically active α-carbonic anhydrases [57], [58]. This prototypical metal site is completed by hydrophobic residues that surround the zinc site. By comparison, the beta class of carbonic anhydrases contains a $HisCys_2H_2O$ zinc polyhedron [59].

Determinants of metal affinity of CA(II):

Metal affinity is determined by optimal interactions between the CA(II) metal ligands and the bound metal ion. The nature of the metal ligands, the

hydrogen bond network and the hydrophobic shell all contribute to the picomolar

metal affinity of CA(II) [55], [56]. Large changes in metal affinity occur by altering

the number of metal ligands. Substitution of one of the histidine side chains with

alanine decreases the metal affinity by at least 10^5-fold (Figure 1.2), while

introduction of a fourth ligand into the metal coordination sphere of CA(II) by

replacing T199 with Glu, Asp or Cys increases the affinity up to 100-fold [60],

[61]. Spectroscopy and crystallography demonstrate that the new thiolate side

chain coordinates to the metal ion, displacing the metal-bound solvent molecule.

Furthermore, substitution of any of the His ligands with another side chain

capable of coordinating the zinc ion, such as Asp, Glu, Gln, Asn or Cys,

substantially decreases zinc affinity [62], [63], [64], [65], [66]. Crystal structures

of these variants demonstrate that none of these side chains position the

coordinating atom at the same place as the imidazole nitrogen, leading to

movements in the location of the bound zinc ion.

K_{Zn} pM $t_{1/2}$ k_{off}

	K_{Zn} pM	$t_{1/2}$ k_{off}
Thr199	1	95 days
Ala199	60	15 days

Thr199

Glu106

	K_{Zn} pM	$t_{1/2}$ k_{off}
Gln92	1	95 days
Asn92	5	1 day
Ala92	18	3 days

Zn^{2+}

Gln92

His119

Glu117

His94

	K_{Zn} pM	$t_{1/2}$ k_{off}
His94	1	95 days
Ala94	270,000	0.3 min

His96

HN Asn244

C_a

	K_{Zn} pM	$t_{1/2}$ k_{off}
Glu117	1	95 days
Asp117	12	37 min
Ala117	40	27 min
Gln117	4400	0.5 s
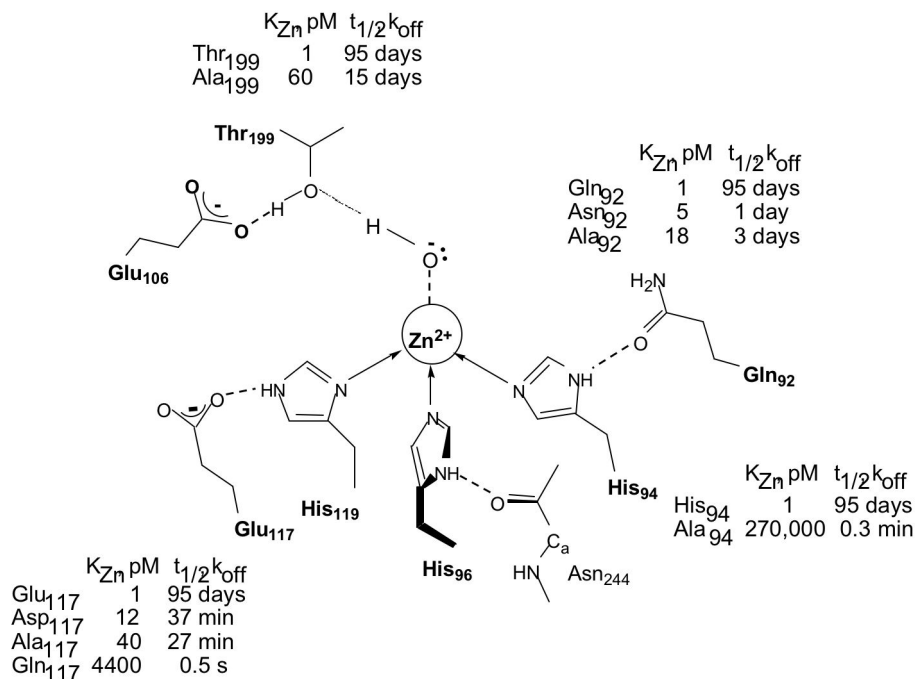
Figure 1:2: Schematic diagram of the active site of WT CA(II):

Substitutions in both direct (H94) and indirect (E117, T199, Q92) ligands decrease the zinc affinity of CA(II) by 5- to 10^5 –fold, and dramatically reduce equilibration time

Deletion of any one of the hydrogen bonds with the second shell ligands also reduces zinc affinity although this effect is more modest, decreasing zinc affinity 10 – 40-fold [67], [68]. Thermodynamic measurements of metal binding demonstrate that modifications in the metal polyhedron of CA(II) lead to a complex series of changes in both the enthalpy and entropy of ligand binding that is most readily rationalized in terms of metal and protein desolvation, rather than

in terms of changes in the direct interactions of ligand and protein [69]. Although the second shell ligands were proposed to function primarily by orienting the direct ligands, mutations in these residues produce profoundly different effects on the enthalpy of binding, depending on the nature of the residue. These results indicate that the second shell ligands make both enthalpic and entropic contributions to metal binding.

Finally, alterations in the hydrophobic residues (Phe-93, Phe-95 and Trp-97) underneath the zinc binding site decrease the metal affinity of CA(II) by as much as 100-fold [70], [71]. Crystal structures of these mutant proteins demonstrate alterations in the structure of the apo-enzyme such that the histidine side chains are no longer correctly oriented to bind zinc [72]. In addition to providing fundamental insight into the determinants of metal affinity, the metal affinity of these CA(II) variants span the range from subpicomolar to micromolar thereby providing an array of CA(II) proteins that could be used to measure a wide range of zinc concentrations.

Kinetics of zinc ion binding to CA(II):

In CA(II), zinc equilibration is limited by both the high zinc affinity (pM) and the slow dissociation rates. The measured association rate constant at $\sim 10^5 \ M^{-1} s^{-1}$ is much slower than a diffusion-controlled limit of $10^7\text{-}10^8 \ M^{-1} s^{-1}$ leading to a half-time for dissociation estimated at several months [67], [73]. The slow association rate constant suggests that metal binding occurs in a two-step mechanism: formation of an initial complex followed by a conformational change

(Scheme 1.1). The apparent association rate constant increases significantly for mutants with one of the histidine ligands replaced with alanine (His_2 zinc site) or the second shell hydrogen bond between His119 and E117 removed (E117A mutant) [64], [67]. These mutations suggest that the kinetic mechanism for zinc binding occurs via an intermediate where the zinc ion is bound to the two ligands nearest the active site surface, His94 and His96, followed by slow addition of the third His ligand (H119) and dissociation of water ligands to form the tetrahedral metal site (Scheme 1.1; [67]). The E117A mutation has proven particularly useful for zinc sensing since this mutation decreases the half-time for zinc dissociation by 5000-fold while only decreasing the zinc affinity by 40-fold [67].

$$E\begin{matrix} His_{94} \\ His_{96} \\ His_{119} \end{matrix} + Zn(H_2O)_6 \rightleftharpoons E\begin{matrix} His_{94} \\ His_{96} \\ His_{119} \end{matrix} Zn(H_2O)_4 \rightleftharpoons E\begin{matrix} His_{94} \\ His_{96} \\ His_{119} \end{matrix} Zn\text{-}OH^- \\ + 2\,H_2O \qquad\qquad + 3\,H_2O + H^+$$
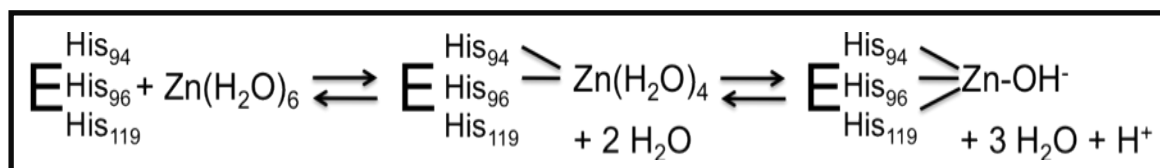
Scheme 1.1: Proposed Mechanism of Zinc Binding to CA(II)

Equilibration of CA(II) with zinc can be facilitated by the addition of certain chelators, including dipicolinic acid (DPA) [74], [75], but not others, including EDTA. Catalysis of metal exchange by DPA is proposed to occur by the formation of a CA(II)-DPA-Zn^{2+} ternary complex (Scheme 1.2); the apparent association rate is increased because CA(II) binds DPA-bound Zn^{2+} which is in higher concentration than the "free" zinc and the dissociation rate constant is enhanced by the bound DPA [75]. This type of chelator-catalyzed zinc exchange

could mimic intracellular mechanisms that are proposed to enhance zinc

equilibration [29], [76].

$$E + Zn \cdot DPA \rightleftharpoons E \cdot Zn \cdot DPA$$
$$\updownarrow \qquad\qquad \updownarrow$$
$$E + Zn + DPA \rightleftharpoons E \cdot Zn + DPA$$
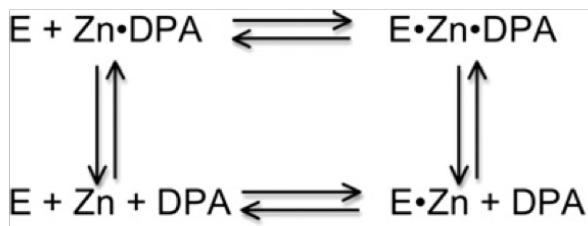
Scheme 1.2: Proposed mechanism for catalysis of zinc exchange by DPA

Metal specificity of CA(II):

Through evolution, the structure of CA(II) has been selected to bind Zn^{2+}

in the presence of a variety of potential cellular interferents, including: Mg^{2+}

(estimated free concentration of 0.5-1 mM) [27], Ca^{2+} (est. free concentration of

0.05-1 µM) [28], [77], [78] Fe^{2+} (est. free concentration of 0.1-10 µM) [79], [80],

[81], [82], and Cu^{2+} (est. free concentration of ~ 10^{-18} M [83].) Like small

molecule ligands, the metal affinity of wild type CA(II) follows the Irving-Williams

series ($Mn^{2+} < Co^{2+} < Ni^{2+} < Cu^{2+} > Zn^{2+}$) although the zinc affinity is increased

significantly compared to the rest of the transition metals (Figure 1.3) [66], [84],

[85]. Copper could potentially compete with zinc for binding to CA(II) in a cell

since the affinity is 10-fold higher than zinc; however, the readily exchangeable

copper concentration is estimated at >>1000-fold lower than that of zinc [86].

CA(II) has little affinity for other possible competitors; the dissociation constant of CA(II) for Ca^{2+} and Mg^{2+} is larger than 10 mM and the affinity of Fe^{2+} is estimated to be significantly higher than 100 µM [85]. Therefore, CA(II) has significantly higher metal selectivity compared to small molecule chelators such as EDTA, NTA, DPA and TPEN that have little discrimination in binding affinity between Co, Ni, Zn and Cd (Table 1.1).
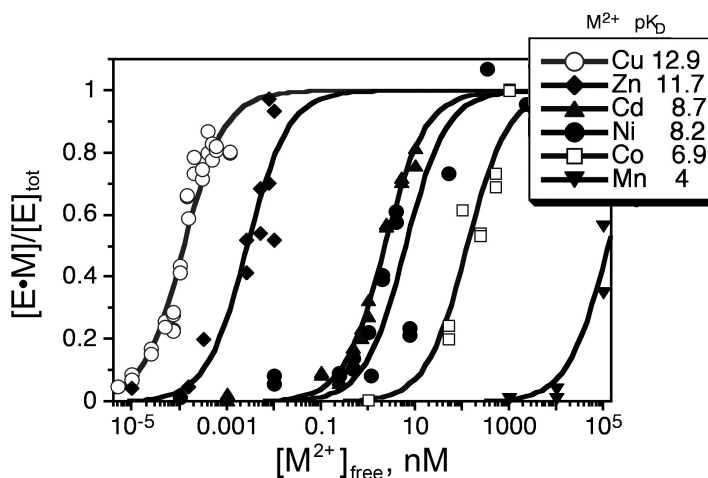
Figure 1:3: Divalent metal ion affinities of WT CA(II):

The metal ion affinity of CAII follows the inherent metal ion-ligand affinity trend termed the Irving-William series ($Mn^{2+}<Co^{2+}<Ni^{2+}<Cu^{2+}>Zn^{2+}$)

Table 1.1: Selectivity of CA(II):

	Mn	Co	Ni	Cu	Zn	Cd	Fe	Ca	Mg
wt CAII	<3.4	6.8	7.8	13	12	8.6	*	<2	<1.3
EDTA	14.0	16.0	18.6	18.8	16.5	16.5	14.2	10.6	8.7
EGTA	12.1	12.3	11.8	17.7	12.9	16.5	11.8	11.0	5.2
NTA	7.4	10.8	11.5	13.1	10.4	9.78	15.9	6.5	5.5
DPA	5.01	6.65	6.91	9.1	6.32	6.45	5.71	4.2	2.7
TPEN	10.3				15.6		14.6	4.4	1.7

pK_d of M^{2+} of several small molecules chelators of CA(II). Asterisk indicates that no affinity measurements are published to date

Structures of metal-substituted CA(II) enzymes reveal that the geometry of the metal site often varies with the identity of the metal. For example, copper binds to wild-type CA(II) in a trigonal bipyramidal geometry, accepting an additional water as a ligand while both bound manganese and nickel are octahedral with three water molecules [56], [87]. The enthalpy of metal binding to CA(II) decreases through the series $Co^{2+} \rightarrow Zn^{2+} \rightarrow Cu^{2+}$, mirroring the enthalpy of hydration, suggesting that desolvation of the metal ion plays an important role in metal affinity and selectivity [88].

The metal selectivity of CA(II) is also determined by the structure of the active site. Mutagenesis of the His ligands to another side chain capable of coordinating Zn^{2+}, including Asp, Glu, Gln, Asn, and Cys, leads to CA(II) variants with altered metal selectivity [66]. For example, the selectivity for zinc compared to copper (K_{Zn}/K_{Cu}) varies from 0.1 to 2 x 10^{-4} to 15 for wild-type, H119N, and H119Q CA(II), respectively Similarly, the selectivity for zinc compared to nickel (K_{Zn}/K_{Ni}) varies from a value of 2 x 10^4 for wild-type CA(II) to 1 for the H94D mutant. Nonetheless, except for H119Q CA(II), the metal selectivity of all of these mutants follows the inherent metal ion affinity trend suggested by the Irving-Williams series, demonstrating the importance of this trend for metal ion selectivity in biology. Furthermore, neither the polarizability of the liganding side chains nor the size of the metal ion binding site correlate strongly with metal ion specificity; instead, changes in metal ion specificity in the variants correlate with the preferred coordination number and geometry of the metal ion [58]. This

correlation suggests that a primary feature driving deviations from the inherent ligand affinity trend is the positioning of active site groups such that a given metal ion can adopt a preferred coordination number/geometry.

The hydrophobic residues underneath the zinc binding site in CA(II) also contribute to metal selectivity. As the hydrophobicity and size of the amino acids at positions 93, 95 and 97 decrease, the affinity of CA(II) for metal ions that bind with a tetrahedral geometry, zinc^{2+} and cobalt^{2+}, decreases [71, 89]. In contrast, the affinity of CA(II) for the trigonal bipyramidal Cu^{2+} increases significantly. These two trends contribute to the enhanced copper selectivity for these mutants with values of K_{Cu}/K_{Zn} as high as 10^6. A comparison of the crystal structures of the apo forms of wild-type and F93I/F95M/W97V CA(II) demonstrates that mutations in the hydrophobic residues disrupt the positioning of the His ligands in a tetrahedral geometry in the absence of bound metal [72]. Therefore, this hydrophobic shell is important for stabilizing the tetrahedral metal ion geometry for zinc and destabilizing alternative geometries, such as the trigonal bipyramidal geometry of copper.

CA-based zinc sensing: ratiometric fluorescent sensors:

Most of the CA-based zinc sensors rely on the zinc-dependent binding of a ligand to the protein. Aryl sulfonamides have long been known to inhibit holo-carbonic anhydrase [90]. Hundreds of these compounds with various structural properties and activity have been identified, some of which are being used to

treat glaucoma. The mechanism for inhibition is well-understood; aryl sulfonamides contain the weakly acidic SO_2NH_2 moiety that directly coordinates the zinc ion through the ionized NH^- group, displacing the zinc bound water [91]. The first approach to fluorometrically determine zinc using carbonic anhydrase as a recognition element evolved from the work of Chen and Kernohan [92]. They discovered that the fluorescence emission of the aryl sulfonamide, dansylamide (DNSA), upon binding to holo-carbonic anhydrase is both enhanced significantly and blue-shifted. Thompson and Jones [93] determined that DNSA has very weak affinity for apo-CA and thus the fraction of CA with bound DNSA reflects the fraction of zinc-bound CA, which is determined by the free zinc concentration. Therefore the ratio of emissions from free and bound dansylamide could be used to determine the free zinc concentration. To optimize CA-based fluorescence sensors for accurate quantitation, the metal ion binding has been transduced using wavelength ratiometric indicators as well as lifetime- and polarization-based methods [94], [95], [96], [97]. Wavelength ratiometric measurements have been applied to quantification of free zinc in biological samples. Zinc release from brain cells in a rabbit ischemia model was measured by adding apo–CA to the dialysate in the brain of a living rabbit and then quantifying zinc concentrations from the fluorescence emission ratio after addition of DNSA [98]. Similarly, neuronal zinc release from organotypic cultures of mammalian hippocampus following electrical stimulation was measured using apo-CA(II) and a water-soluble aryl sulfonamide, ABD-N, with an improved extinction coefficient and a longer excitation wavelength [94]. In both of these cases the exchangeable

zinc concentrations (1-100 nM) are much higher than the K_{Zn} for CA(II) (1 pM), therefore the measurements were carried out using high concentrations of apo-CA(II) and sulfonamide (1-20 µM) such that zinc binds to CA(II) stoichiometrically. In this linear relationship, the detection limit is established by the lowest fractional occupancy that can be reliably measured, which is usually considered as 0.1%; therefore, the dynamic range is thus largely determined by the concentration of apo-CA(II). Stoichiometric methods depend on accurate knowledge of the concentration of CA(II) and maintaining an excess concentration of both CA(II) and sulfonamide. Therefore, stoichiometric methods do not work for *in vivo* measurements where the total zinc concentration is high (~0.2 mM) and well buffered by numerous ligands and consequently difficult to deplete.

To address these issues, an excitation ratiometric method was developed based on Förster resonance energy transfer (FRET) [99] between a cell-permeable sulfonamide, Dapoxyl sulfonamide, and a second fluorophore attached to CA(II) (Figure. 1.4) [100]. The fluorophore that is covalently attached to CA(II) serves as a FRET acceptor for the bound sulfonamide, such that emission from the bound sulfonamide is efficiently transferred to the label on the protein, which emits at much longer wavelengths. In this case, the label is AlexaFluor594 maleimide (AF594, Ex 594/Em 617) that is attached to the thiol group of a unique cysteine (H36C/C206S) engineered on the surface of CA(II); the position of the label on CA and the overlap of its absorbance with the emission of Dapoxyl sulfonamide are chosen so that energy transfer from the

sulfonamide to the AF594 is nearly quantitative.   For this sensor, when Dapoxyl

sulfonamide bound to AF594-CA(II) is excited at 365 nm, fluorescence emission

is observed at 617 nm from the AF594 because of FRET. Thus the UV-excited

red emission (Ex 365 nm/Em 617 nm) represents the fraction of AF594-CA(II)

with sulfonamide (and therefore zinc) bound, whereas the signal of the directly

excited AF594 (Ex 548 nm/Em 617 nm) represents the total amount of the

AF594-CA(II). The fluorescent ratio of UV excited (365 nm) to directly excited

(548 nm) emissions correlates with the zinc-bound fraction of the sensor and

thus free zinc. *In vivo* calibrations are carried out using a series of nitrilotriacetic

acid (NTA)-chelated zinc buffers in which the free zinc concentration is

maintained at a fixed level, indicating that the apparent zinc affinity of this sensor

is ~140 pM. An important advantage of this approach is the relative insensitivity

to the sulfonamide level, sulfonamide bound to membranes and proteins, and

adventitious holo-CA(II) present in the specimen, since only the fraction of the

sulfonamide in close proximity (effectively, bound) to the labeled CA(II) is

observed. Also, even though UV excitation is used, the large difference between

the excitation and emission wavelengths leads to a very low autofluorescence

background.

This sensor was applied to measure the intracellular free zinc

concentration in the mammalian cell line PC-12 under resting conditions [29].

Because AF594-CA(II) is ordinarily cell-impermeant, an 11 amino acid cell-

permeating peptide (TAT-tag derived from HIV-1 protease) was fused to the N-

terminus to facilitate uptake [101]. Using this method, the concentration of free

zinc is measured at 5-10 pM compared to a standard curve and assuming
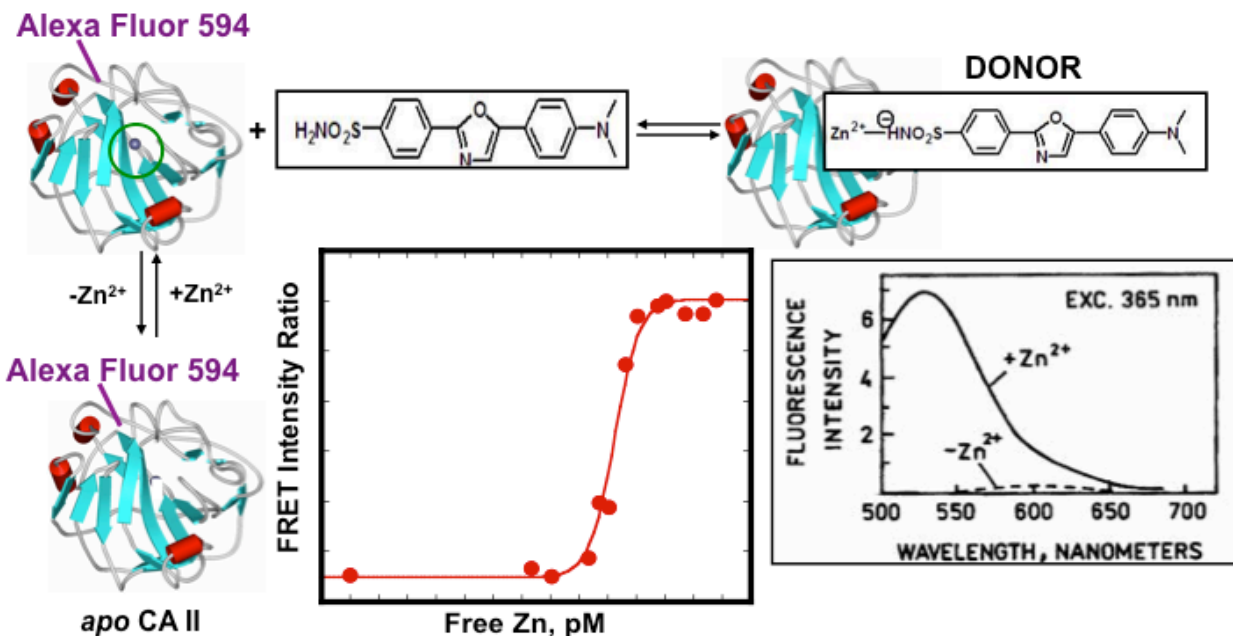
Figure 1:4: FRET excitation ratiometric Zn^{2+} sensing scheme:

In the presence of zinc, dapoxyl sulfonamide binds to holo-CA(II) and transfers energy to the acceptor, AlexaFluor 594. The ratio of the acceptor fluorescence emission with excitation of the donor to that with excitation of the acceptor is measured. The FRET intensity ratio increases with zinc concentration as the fraction of zinc-bound CA(II) increases, producing a binding curve with picomolar affinity (inset)

equilibration between CA(II) and the readily exchangeable zinc concentration.

To examine whether zinc equilibration *in vivo* occurs readily despite the slow zinc

association rate constant *in vitro*, we demonstrated that the measured zinc

concentration is not dependent on the concentration of sensor or on the equilibration time (20 min to 24 h). Furthermore, the same "free" zinc concentration in PC12 cells is observed using the AF594-labeled E117A CA(II) mutant as the receptor molecule where the zinc equilibration rate is increased by 800-fold [102]. The picomolar affinity of this CA(II) sensor is the most sensitive sensor used to measure cellular zinc to date.

In addition to measuring the readily exchangeable zinc concentration, these data have further implications for the mechanism of cellular zinc homeostasis. First, these data indicate that there is a substantial exchangeable zinc pool in the cell; the concentration of the CA(II) sensor is in the nanomolar regime providing a lower limit for the exchangeable zinc pool. Since the total zinc concentration in cells is ~0.2 mM, an exchangeable zinc pool in the nanomolar to micromolar range is still a small percentage of the total cellular zinc. Second, the rapid equilibration of the sensor with the readily exchangeable zinc concentration is inconsistent with the CA(II) sensor binding the picomolar "free" zinc with the 10^5 $M^{-1}s^{-1}$ association rate constant measured *in vitro* since the estimated equilibration half-time for this reaction is on the order of several hours. These data suggest that zinc may bind to CA(II) via a zinc-chelator complex *in vivo*, where the chelator is either a small molecule or protein chaperone, perhaps similar to the mechanism of DPA-catalyzed zinc binding to CA(II) (Scheme 1.2). In summary, these data indicate that there is a readily exchangeable pool of cellular zinc that equilibrates rapidly with zinc-binding proteins such as carbonic anhydrase.

Carbonic anhydrase with wild-type zinc affinity is ideal for measuring the cellular zinc concentration under equilibrium conditions for most cells. However, free zinc concentrations in neuronal models vary over 7 orders of magnitude from 10 pM in normal resting cells to more than 10 μM outside the neurons after stimulation of synaptic zinc release [29], [103], [104]. To measure zinc concentrations over this wide dynamic range, CA(II) receptors with altered zinc affinities, such as CA(II) mutants described previously will be of great utility [105].

Other zinc sensing methods using CA(II):

Fluorescence anisotropy is another ratiometric approach that provides an accurate alternative for quantification, especially for fluorophores with smaller changes in lifetime and quantum yield. In some cases fluorescence anisotropy offers a particular advantage of an expanded dynamic range, as observed for the carbonic anhydrase-based sensor [106], [107], [108]. Fluorescence anisotropy-based sensing has not been widely used for cellular studies, perhaps because fluorescence polarization microscopes are less common than those permitting wavelength ratiometric determinations of analytes.

CA-based sensors can also be used to measure zinc concentrations based on changes in fluorescence lifetime. Fluorescent aryl sulfonamides, including dansylamide and Dapoxyl sulfonamide, exhibit substantial changes in their average fluorescence lifetimes upon binding to holo-CA, consistent with the increases in the apparent quantum yield [92], [97]. Using standard time- or

frequency-domain methods, the proportions of the lifetimes corresponding to the free and bound forms of the sulfonamide can be determined, and therefore, the free zinc concentration can be calculated in the same manner as for the wavelength ratiometric approaches. Lifetime-based methods have advantages similar to those of ratiometric determinations; however, microscopes capable of imaging fluorescence lifetimes are still uncommon [109].

Environmental applications using CA(II)-based sensors:

CA(II)-based sensing has also been applied to the determination of metal ions, such as Cu^{2+} and Zn^{2+}, in natural waters. Cu^{2+}, Zn^{2+}, and to a lesser extent Cd^{2+}, Co^{2+}, and Ni^{2+} are of interest environmentally for two main reasons. First, Cu and Zn are nutrients required by essentially all organisms, and their availability (together with Fe) in natural waters effectively controls the growth of phytoplankton and thus all other organisms in the food chain as well. As a consequence, Cu and Zn typically exhibit a "nutrient distribution" in the ocean, with low levels in the sunlight-exposed photic zone near the surface, and elevated concentrations at greater depth [110]. Second, Cu and Zn at elevated levels are toxic to many life forms, and are thus important pollutants in many harbors and estuaries [111]. For instance, the blue mussel, a commercially important shellfish, is killed by Cu^{2+} at sub-ppb levels [112]. Speciation of metal ions in natural waters (e.g., the proportion of total metal bound to different ligands, particles and colloids in a sample) is important, because it determines the availability of the metal ions to various organisms; conversely, the marine

biota have a dramatic influence on the speciation and distribution of biologically important metals [110], [113]. The importance of these questions has led to substantial study of the marine geochemistry of these metal ions.

Copper sensing using CA(II) is based on copper binding to the His_3 metal site and quenching the fluorescence of a fluorophore, such as Oregon Green, that is covalently attached to a unique Cys residue near the metal site, such as L198C [114]. Copper binding to fluorophore-labeled CA(II) results in a concomitant decrease in fluorescence intensity and lifetime, the latter of which results in increased modulation and decreased phase angle [115], [116]. The free Cu^{2+} concentration can be determined under equilibrium conditions from the observed lifetime or phase angle in comparison to a standard curve. The CA(II) variants with altered copper affinity and enhanced copper selectivity will be useful for limiting interference from Zn and for measuring a variety of copper concentrations. Other metal ions such as Co^{2+}, Cd^{2+}, and Ni^{2+} also exhibit quenching of suitably positioned fluorophores upon binding to the active site of CA and can be quantified by changes in fluorescence intensity, lifetime, or fluorescence polarization [95].

The high sensitivity and selectivity of CA-based fluorescence sensors for zinc and copper are well suited to determining free metal ions in the complex matrix of sea water. CA-based sensors offer some unique advantages in comparison to other methods of determining free metal ion concentration (and thus speciation). First, compared to CA-based sensing, existing (mainly voltammetric) methods of determining free Cu^{2+} and Zn^{2+} in sea water are

relatively slow and labor intensive, such that only a few samples a day can be analyzed by a skilled practitioner [117], [118], [119]; by comparison, CA-based sensors can determine these metals in sea water without any processing or separation steps, and can also act as a true sensor, providing a continuous readout of metal ion concentration *in situ*, in real time [120]. Also, the fluorescent-labeled CA(II) can be immobilized at the end of an optical fiber, which can be immersed and the metal ion concentration determined remotely *in situ* at some depth in the water column [109]. This is of importance since collecting water samples is slow and expensive, and risks contamination of the samples compared with determination *in situ* with a fiber optic sensor. In view of the power and flexibility of the CA-based fluorescence sensors, we anticipate they will find many uses in environmental monitoring of metal ions.

CONCLUSIONS AND FUTURE WORK

CA(II)-based sensors have been demonstrated to quantify readily exchangeable zinc concentrations in mammalian cells and "free" Cu^{2+} concentration in seawater. These sensors have a bright future for examining zinc concentrations and changes in zinc concentrations in a wide variety of cells and subcellular organelles as well as in tissues. The ability to measure readily exchangeable zinc concentrations using CA(II)-based sensors is an important new tool for answering biological questions concerning intracellular zinc storage

and distribution, the role of zinc in signaling pathways as well as the pathological roles of zinc in human disease. In the future, this sensor may also find important applications in measuring the readily exchangeable concentration of other metal ions, including copper, in cells and in seawater.

Expressible ratiometric CA(II)-based sensors:

Although TAT-tag mediated delivery of ratiometric CA sensors has been successfully applied to mammalian cell lines, it cannot penetrate some other organisms without detrimental effects [121]. Also, the chemical labeling of the isolated protein with the AlexaFluor fluorophore is tedious, labor intensive, and does not always proceed in high yield. A further improvement in zinc sensors would be to further develop and optimize a protein-based sensor that can be readily expressed in cells [122], [123]. The expressible sensor can be constructed by fusing a fluorescent protein to CA(II) as a fluorescence acceptor and using a zinc-dependent FRET donor, like the Dapoxyl sulfonamide used in the previous sensor. The relatively small size of the fluorescent protein variants and CA(II) generally means that efficient energy transfer between the Dapoxyl sulfonamide and the fluoresecent protein acceptor is feasible. An ideal candidate fluorescent protein for an expressible CA sensor should meet the following criteria: excitation spectrum overlap with the emission of Dapoxyl sulfonamide to ensure good FRET efficiency, high extinction coefficient and quantum yield, fast maturation, and monomeric state. Directed evolution studies have generated a large pool of fluorescent proteins that can be used for this purpose [124], such as

28

variants of RFPs from *Discosoma sp.* and *Entacmaea quadricolor* [125], [126], [127]. Furthermore, fluorescent proteins with different spectra can be coupled to CA variants with different zinc affinities, thus creating a multicolor measurement covering a wide dynamic range in a single experiment.   Our initial experiments have used mOrange and mCherry [127] in fusion proteins; this work is ongoing, including the use of sequences to target the expression to particular organelles within the cell.

REFERENCES

[1]   C. Andreini, L. Banci, I. Bertini, A. Rosato, Counting the zinc-proteins encoded in the human genome, J Proteome Res 5 (2006) 196-201.

[2]   J.E. Coleman, Zinc proteins: Enzymes, storage proteins, transcription factors, and replication proteins, Annual Review of Biochemistry 61 (1992) 897-946.

[3]   D.W. Christianson, Structural biology of zinc, Advances in Protein Chemistry 42 (1991) 281-355.

[4]   B.L. Vallee, D.S. Auld, Zinc coordination, function, and structure of zinc enzymes and other proteins, Biochemistry 29 (1990) 5647-5659.

[5]   D. Keilin, T. Mann, Carbonic anhydrase. Purification and nature of the enzyme, Biochem J 34 (1940) 1163-1176.

[6]   J.M. Matthews, M. Sunde, Zinc fingers--folds for many occasions, IUBMB Life 54 (2002) 351-355.

[7]   W. Maret, H.H. Sandstead, Zinc requirements and the risks and benefits of zinc supplementation, J Trace Elem Med Biol 20 (2006) 3-18.

[8]   B.L. Vallee, K.H. Falchuk, The biochemical basis of zinc physiology, Physiological Reviews 73 (1993) 79-118.

[9]   J.P. Liuzzi, R.J. Cousins, Mammalian zinc transporters, Annu Rev Nutr 24 (2004) 151-172.

[10]   M.J. Tuerk, N. Fazel, Zinc deficiency, Curr Opin Gastroenterol 25 (2009) 136-143.

[11]   N. Bhandari, R. Bahl, S. Taneja, T. Strand, K. Molbak, R.J. Ulvik, H. Sommerfelt, M.K. Bhan, Substantial reduction in severe diarrheal morbidity by daily zinc supplementation in young north Indian children, Pediatrics 109 (2002) e86.

[12]   C. Devirgiliis, P.D. Zalewski, G. Perozzi, C. Murgia, Zinc fluxes and zinc transporter genes in chronic diseases, Mutat Res 622 (2007) 84-93.

[13]   A.I. Bush, W.H. Pettingell, G. Multhaup, M.d. Paradis, J.-P. Vonsattel, J.F. Gusella, K. Beyreuther, C.L. Masters, R.E. Tanzi, Rapid induction of Alzheimer AB amyloid formation by zinc, Science 265 (1994) 1464-1467.

[14]   R.A. Cherny, C.S. Atwood, M.E. Xilinas, D.N. Gray, W.D. Jones, C.A. McLean, K.J. Barnham, I. Volitakis, F.W. Fraser, Y.S. Kim, X. Huang, L.E. Goldstein, R.D. Moir, J.T. Lim, K. Beyreuther, H. Zheng, R.E. Tanzi, C. Masters, A.I. Bush, Treatment with a copper-zinc chelator markedly and rapidly inhibits beta-amyloid accumulation in Alzheimer's disease transgenic mice, Neuron 30 (2001) 665 - 676.

[15]   C.G. Taylor, Zinc, the pancreas, and diabetes: insights from rodent studies and future directions, Biometals 18 (2005) 305-312.

[16]   R. Sladek, G. Rocheleau, J. Rung, C. Dina, L. Shen, D. Serre, P. Boutin, D. Vincent, A. Belisle, S. Hadjadj, B. Balkau, B. Heude, G. Charpentier, T.J. Hudson, A. Monpetit, A.V. Psheszhetsky, M. Prentki, B.I. Posner, D.J. Balding, D. Meyre, C. Polychronakos, P. Froguel, A genome-wide

association study identifies novel risk loci for type 2 diabetes, Nature 445 (2007) 881 - 885.

[17]   J. Szpunar, Bio-inorganic speciation analysis by hyphenated techniques, Analyst 125 (2000) 963-988.

[18]   A. Sanz-Medel, M. Montes-Bayon, M. Luisa Fernandez Sanchez, Trace element speciation by ICP-MS in large biomolecules and its potential for proteomics, Anal Bioanal Chem 377 (2003) 236-247.

[19]   T. Paunesku, S. Vogt, J. Maser, B. Lai, G. Woloschak, X-ray fluorescence microprobe imaging in biology and medicine, J Cell Biochem 99 (2006) 1489-1502.

[20]   M. Ralle, S. Lutsenko, Quantitative imaging of metals in tissues, Biometals 22 (2009) 197-205.

[21]   R.M. Rousseau, Detection limit and estimate of uncertainty of analytical XRF results, Rigaku 18 (2001) 33-47.

[22]   C.J. Fahrni, Biological applications of X-ray fluorescence microscopy: exploring the subcellular topography and speciation of transition metals, Curr Opin Chem Biol 11 (2007) 121-127.

[23]   P. Jiang, Z. Guo, Fluorescent detection of zinc in biological systems: recent development on the design of chemosensors and biosensors, Coordination Chemistry Reviews 248 (2004) 205 - 229.

[24]   D.W. Domaille, E.L. Que, C.J. Chang, Synthetic fluorescent sensors for studying the cell biology of metals, Nat Chem Biol 4 (2008) 168-175.

[25]   T. Hirano, K. Kikuchi, T. Nagano, zinc fluorescent probes for biological applications, in: C.D. Geddes, J.R. Lakowicz (Eds.), Reviews in Fluorescence 2004, Kluwer Academic / Plenum Publishers, New York, 2004, pp. 55 - 73.

[26]   R.B. Thompson, Studying zinc biology with fluorescence: Ain't we got fun?, Current Opinion in Chemical Biology 9 (2005) 526 - 532.

[27]   B. Morelle, J.M. Salmon, J. Vigo, P. Viallet, Measurement of intracellular magnesium concentration in 3T3 fibroblasts with the fluorescent indicator Mag-indo-1, Analytical Biochemistry 218 (1994) 170-176.

[28]   L. Missiaen, W. Robberecht, L. Van Den Bosch, G. Callewaert, J.B. Parys, F. Wuytack, L. Raeymaekers, B. Nilius, J. Eggermont, H. De Smedt, Abnormal intracellular Ca^{2+} homeostasis and disease, Cell Calcium 28 (2000) 1-21.

[29]   R.A. Bozym, R.B. Thompson, A.K. Stoddard, C.A. Fierke, Measuring picomolar intracellular exchangeable zinc in PC-12 cells using a ratiometric fluorescence biosensor, ACS Chemical Biology 1 (2006) 103 - 111.

[30]   G. Grynkiewicz, M. Poenie, R.Y. Tsien, A new generation of calcium indicators with greatly improved fluorescence properties, Journal of Biological Chemistry 260 (1985) 3440-3450.

[31]   M.E. Lippitsch, J. Pusterhofer, M.J.P. Leiner, O.S. Wolfbeis, Fibre-optic oxygen sensor with the fluorescence decay time as the information carrier, Analytica Chimica Acta 205 (1988) 1.

[32]   J.R. Lakowicz, Principles of Fluorescence Spectroscopy, Second ed., Kluwer Academic / Plenum Publishers, New York, 1999.

[33]   W.B. Dandliker, R.J. Kelly, J. Dandliker, J. Farquhar, J. Levin, Fluorescence polarization immunoassay. Theory and experimental method, Immunochemistry 10 (1973) 219-227.

[34]   C.E. White, R.J. Argauer, Fluorescence Analysis: A Practical Approach, Marcel Dekker, Inc., New York, 1970.

[35]   A. Fernandez-Gutierrez, A. Munoz de la Pena, Determinations of inorganic substances by luminescence methods, in: S.G. Schulman (Ed.), Molecular Luminescence Spectroscopy, Part I: Methods and Applications, vol. 77, Wiley-Interscience, New York, 1985, pp. 371-546.

[36]   J.R. Lakowicz, I. Gryczynski, Z. Gryczynski, J.D. Dattelbaum, Anisotropy-based sensing with reference fluorophores, Analytical Biochemistry 267 (1999) 397 - 405.

[37]   C.J. Frederickson, E.J. Kasarskis, D. Ringo, R.E. Frederickson, A quinoline fluorescence method for visualizing and assaying histochemically reactive zinc (bouton zinc) in the brain, Journal of Neuroscience Methods 20 (1987) 91-103.

[38]   P.D. Zalewski, I.J. Forbes, W.H. Betts, Correlation of apoptosis with change in intracellular labile Zn(II) using Zinquin [(2-methyl-8-p-toluenesulphonamido-6-quinolyloxy)acetic acid], a new specific fluorescent probe for Zn(II), Biochemical Journal 296 (1993) 403-408.

[39]   M.E. Huston, K.W. Haider, A.W. Czarnik, Chelation-enhanced fluorescence in 9, 10-bis(TMEDA) anthracene, Journal of the American Chemical Society 110 (1988) 4460 - 4462.

[40]   S.C. Burdette, G.K. Walkup, B. Spingler, R.Y. Tsien, S.J. Lippard, Fluorescent sensors for Zn2+ based on a fluorescein platform: Synthesis, properties and intracellular distribution, Journal of the American Chemical Society 123 (2001) 7831-7841.

[41]   K.R. Gee, Z.L. Zhou, D. Ton-That, S.L. Sensi, J.H. Weiss, Measuring zinc in living cells. A new generation of sensitive and selective fluorescent probes, Cell Calcium 31 (2002) 245 - 251.

[42]   S.L. Sensi, D. Ton-That, P.G. Sullivan, E.A. Jonas, K.R. Gee, L.K. Kaczmarek, J.H. Weiss, Modulation of mitochondrial function by endogenous Zn2+ pools, Proceedings of the National Academy of Sciences 100 (2003) 6157 - 6162.

[43]   M.M. Henary, Y. Wu, C.J. Fahrni, Zinc(II)-selective ratiometric fluorescent sensors based on inhibition of excited state intramolecular proton transfer, Chemistry in Europe Journal 10 (2004) 3015 - 3025.

[44]   S. Aoki, D. Kagata, M. Shiro, K. Takeda, E. Kimura, Metal chelation-controlled twisted intramolecular charge transfer and its application to fluorescent sensing of metal ions and anions, Journal of the American Chemical Society 126 (2004) 13377 - 13390.

[45]   H.A. Godwin, J.M. Berg, A fluorescent zinc probe based on metal induced peptide folding, Journal of the American Chemical Society 118 (1996) 6514-6515.

[46] G.K. Walkup, B. Imperiali, Fluorescent chemosensors for divalent zinc based on zinc finger domains. Enhanced oxidative stability, metal binding affinity, and structural and functional characterization, Journal of the American Chemical Society 119 (1997) 3443-3450.

[47] J.S. Marvin, H.W. Hellinga, Conversion of a maltose receptor into a zinc biosensor by computational design, Proceedings of the National Academy of Sciences 98 (2001) 4955 - 4960.

[48] A. Miyawaki, J. Llopis, R. Heim, J.M. McCaffery, J.A. Adams, M. Ikura, R.Y. Tsien, Fluorescent indicators for Ca2+ based on green fluorescent proteins and calmodulin, Nature 388 (1997) 882-887.

[49] L.L. Pearce, R.E. Gandley, W. Han, K. Wasserloos, M. Stitt, A.J. Kanai, M.K. McLaughlin, B.R. Pitt, E.S. Levitan, Role of metallothionein in nitric oxide signaling as revealed by a green fluorescent fusion protein, Proceedings of the National Academy of Sciences 97 (2000) 477 - 482.

[50] K.K. Jensen, L. Martini, T.W. Schwartz, Enhanced fluorescence resonance energy transfer between spectral variants of green fluorescent protein through zinc-site engineering, Biochemistry 40 (2001) 938-945.

[51] W. Qiao, M. Mooney, A.J. Bird, D.R. Winge, D.J. Eide, Zinc binding to a regulatory zinc-sensing domain monitored *in vivo* by using FRET, Proc Natl Acad Sci U S A 103 (2006) 8674-8679.

[52] E.M.W.M.v. Dongen, T.H. Evers, L.M. Dekkers, E.W. Meijer, L.W.J. Klomp, M. Merkx, Variation of linker length in ratiometric fluorescent sensor proteins allows rational tuning of Zn(II) affinity in the picomolar to femtomolar range, Journal of the American Chemical Society 129 (2007) 3494 - 3495.

[53] N.U. Meldrum, F.J. Roughton, Carbonic anhydrase. Its preparation and properties, J Physiol 80 (1933) 113-142.

[54] H. Stadie W.C. and O'Brien, The catalysis of the hydration of carbon dioxide and the dehydration of carbonic acid by an enzyme isolated from red blood cells. , The Journal of Biological Chemistry
103 (1933) 521-529.

[55] A. Liljas, K.K. Kannan, P.C. Bergsten, I. Waara, K. Fridborg, B. Strandberg, U. Carlbom, L. Jarup, S. Lovgren, M. Petef, Crystal structure of human carbonic anhydrase C, Nat New Biol 235 (1972) 131-137.

[56] K. Hakansson, M. Carlsson, L.A. Svensson, A. Liljas, Structure of native and apo carbonic anhydrase II and structure of some of its anion-ligand complexes, Journal of Molecular Biology 227 (1992) 1192-1204.

[57] D.W. Christianson, C.A. Fierke, Carbonic anhydrase - Evolution of the zinc binding site by nature and by design, Accounts of Chemical Research 29 (1996) 331 - 339.

[58] K.A. McCall, C. Huang, C.A. Fierke, Function and mechanism of zinc metalloenzymes, J Nutr 130 (2000) 1437S-1446S.

[59] M.S. Kimber, E.F. Pai, The active site architecture of Pisum sativum beta-carbonic anhydrase is a mirror image of that of alpha-carbonic anhydrases, EMBO Journal 19 (2000) 1407 - 1418.

[60]   L.L. Kiefer, J.F. Krebs, S.A. Paterno, C.A. Fierke, Engineering a cysteine ligand into the zinc binding site of human carbonic anhydrase II, Biochemistry 32 (1993) 9896-9900.

[61]   J.A. Ippolito, T.T. Baird, Jr., S.A. McGee, D.W. Christianson, C.A. Fierke, Structure-assisted redesign of a protein-zinc-binding site with femtomolar affinity, Proc Natl Acad Sci U S A 92 (1995) 5017-5021.

[62]   L.L. Kiefer, J.A. Ippolito, C.A. Fierke, D.W. Christianson, Redesigning the zinc binding siteof human carbonic anhydrase II: Structure of a His2Asp-Zn2+ metal coordination polyhedron, Journal of the American Chemical Society 115 (1993) 12581 - 12582.

[63]   R.S. Alexander, L.L. Kiefer, C.A. Fierke, D.W. Christianson, Engineering the zinc binding site of human carbonic anhydrase II: structure of the His-94-->Cys apoenzyme in a new crystalline form, Biochemistry 32 (1993) 1510-1518.

[64]   L.L. Kiefer, C.A. Fierke, Functional characterization of human carbonic anhydrase II variants with altered zinc binding sites, Biochemistry 33 (1994) 15233-15240.

[65]   C.A. Lesburg, C. Huang, D.W. Christianson, C.A. Fierke, Histidine --> carboxamide ligand substitutions in the zinc binding site of carbonic anhydrase II alter metal coordination geometry but retain catalytic activity, Biochemistry 36 (1997) 15780-15791.

[66]   K.A. McCall, C.A. Fierke, Probing determinants of the metal ion selectivity in carbonic anhydrase using mutagenesis, Biochemistry 43 (2004) 3979-3986.

[67]   L.L. Kiefer, S.A. Paterno, C.A. Fierke, Hydrogen bond network in the metal binding site of carbonic anhydrase enhances zinc affinity and catalytic efficiency, Journal of the American Chemical Society 117 (1995) 6831-6837.

[68]   C.C. Huang, C.A. Lesburg, L.L. Kiefer, C.A. Fierke, D.W. Christianson, Reversal of the hydrogen bond to zinc ligand histidine-119 dramatically diminishes catalysis and enhances metal equilibration kinetics in carbonic anhydrase II, Biochemistry 35 (1996) 3439-3446.

[69]   C.A. DiTusa, K.A. McCall, T. Christensen, M. Mahapatro, C.A. Fierke, E.J. Toone, Thermodynamics of metal ion binding. 2. Metal ion binding by carbonic anhydrase variants, Biochemistry 40 (2001) 5345-5351.

[70]   J.A. Hunt, C.A. Fierke, Selection of carbonic anhydrase variants displayed on phage. Aromatic residues in zinc binding site enhance metal affinity and equilibration kinetics, J Biol Chem 272 (1997) 20364-20372.

[71]   J.A. Hunt, M. Ahmed, C.A. Fierke, Metal binding specificity in carbonic anhydrase is influenced by conserved hydrophobic core residues, Biochemistry 38 (1999) 9054-9062.

[72]   J.D. Cox, J.A. Hunt, K.M. Compher, C.A. Fierke, D.W. Christianson, Structural influence of hydrophobic core residues on metal binding and specificity in carbonic anhydrase II, Biochemistry 39 (2000) 13687 - 13694.

[73] R.W. Henkens, J.M. Sturtevant, The kinetics of the binding of Zn(II) by apocarbonic anhydrase, Journal of the American Chemical Society 90 (1968) 2669 - 2676.

[74] J.B. Hunt, M.J. Rhee, C.B. Storm, A rapid and convenient preparation of apocarbonic anhydrase, Anal Biochem 79 (1977) 614-617.

[75] Y. Pocker, C.T.O. Fong, Inactivation of bovine carbonic anhydrase by dipicolinate: Kinetic studies and mechanistic implications, Biochemistry 22 (1983) 813 - 818.

[76] C.E. Outten, T.V. O'Halloran, Femtomolar sensitivity of metalloregulatory proteins controlling zinc homeostasis, Science 292 (2001) 2488-2492.

[77] D.G. Nicholls, Mitochondria and calcium signaling, Cell Calcium 38 (2005) 311-317.

[78] J.T. Taylor, X.B. Zeng, J.E. Pottle, K. Lee, A.R. Wang, S.G. Yi, J.A.S. Scruggs, S.S. Sikka, M. Li, Calcium signaling and T-type calcium channels in cancer cell cycling, World Journal of Gastroenterology 14 (2008) 4984-4991.

[79] W. Breuer, S. Epsztejn, Z.I. Cabantchik, Iron acquired from transferrin by K562 cells is delivered into a cytoplasmic pool of chelatable iron(II), J Biol Chem 270 (1995) 24209-24215.

[80] G.J. Kress, K.E. Dineley, I.J. Reynolds, The relationship between intracellular free iron and cell injury in cultured neurons, astrocytes, and oligodendrocytes, J Neurosci 22 (2002) 5848-5855.

[81] F. Petrat, U. Rauen, H. de Groot, Determination of the chelatable iron pool of isolated rat hepatocytes by digital fluorescence microscopy using the fluorescent probe, phen green SK, Hepatology 29 (1999) 1171-1179.

[82] A.N. Woodmansee, J.A. Imlay, Quantitation of intracellular free iron by electron paramagnetic resonance spectroscopy, Methods Enzymol 349 (2002) 3-9.

[83] T.D. Rae, P.J. Schmidt, R.A. Pufahl, V.C. Culotta, T.V. O'Halloran, Undetectable intracellular free copper: the requirement of a copper chaperone for superoxide dismutase, Science 284 (1999) 805-808.

[84] S. Lindskog, P.O. Nyman, Metal-Binding Properties of Human Erythrocyte Carbonic Anhydrases, Biochim Biophys Acta 85 (1964) 462-474.

[85] K.A. McCall, C.A. Fierke, Colorimetric and fluorimetric assays to quantitate micromolar concentrations of transition metals, Anal Biochem 284 (2000) 307-315.

[86] L.A. Finney, T.V. O'Halloran, Transition metal speciation in the cell: insights from the chemistry of metal ion receptors, Science 300 (2003) 931-936.

[87] K. Hakansson, A. Wehnert, A. Liljas, X-ray analysis of metal-substituted human carbonic anhydrase II derivatives, Acta Crystallogr D Biol Crystallogr 50 (1994) 93-100.

[88] C.A. DiTusa, T. Christensen, K.A. McCall, C.A. Fierke, E.J. Toone, Thermodynamics of metal ion binding. 1. Metal ion binding by wild-type carbonic anhydrase, Biochemistry 40 (2001) 5338-5344.

[89] J.A. Hunt, C.A. Fierke, Selection of carbonic anhydrase variants displayed on phage: aromatic residues in zinc binding site enhance metal affinity and equilibration kinetics, Journal of Biological Chemistry 272 (1997) 20364-20372.

[90] T.H. Maren, Use of inhibitors in physiological studies of carbonic anhydrase, American Journal of Physiology 232 (1977) F291-F297.

[91] S.K. Nair, J.F. Krebs, D.W. Christianson, C.A. Fierke, Structural basis of inhibitor affinity to variants of human carbonic anhydrase II, Biochemistry 34 (1995) 3981-3989.

[92] R.F. Chen, J.C. Kernohan, Combination of bovine carbonic anhydrase with a fluorescent sulfonamide, J Biol Chem 242 (1967) 5813-5823.

[93] R.B. Thompson, E.R. Jones, Enzyme-based fiber optic zinc biosensor, Analytical Chemistry 65 (1993) 730-734.

[94] R.B. Thompson, W.O. Whetsell, Jr., B.P. Maliwal, C.A. Fierke, C.J. Frederickson, Fluorescence microscopy of stimulated Zn(II) release from organotypic cultures of mammalian hippocampus using a carbonic anhydrase-based biosensor system, J Neurosci Methods 96 (2000) 35-45.

[95] R.B. Thompson, B.P. Maliwal, C.A. Fierke, Selectivity and sensitivity of fluorescence lifetime-based metal ion biosensing using a carbonic anhydrase transducer, Anal Biochem 267 (1999) 185-195.

[96] R.B. Thompson, B.P. Maliwal, V. Feliccia, C.A. Fierke, High sensitivity determination of Zn(II) and Cu(II) *in vitro* by fluorescence polarization, in: G.E. Cohn (Ed.), Systems and Technologies for Clinical Diagnostics and Drug Discovery, vol. 3259, SPIE, San Jose, CA, 1998, pp. 40-47.

[97] R.B. Thompson, M.W. Patchan, Lifetime-based fluorescence energy transfer biosensing of zinc, Anal Biochem 227 (1995) 123-128.

[98] C.J. Frederickson, L.J. Giblin, 3rd, R.V. Balaji, R. Masalha, C.J. Frederickson, Y. Zeng, E.V. Lopez, J.Y. Koh, U. Chorin, L. Besser, M. Hershfinkel, Y. Li, R.B. Thompson, A. Krezel, Synaptic release of zinc from brain slices: factors governing release, imaging, and accurate calculation of concentration, J Neurosci Methods 154 (2006) 19-29.

[99] T. Forster, Intermolecular energy migration and fluorescence (Ger.), Annalen der Physik 2 (1948) 55 - 75.

[100] R.B. Thompson, M.L. Cramer, R. Bozym, Excitation ratiometric fluorescent biosensor for zinc ion at picomolar levels, J Biomed Opt 7 (2002) 555-560.

[101] J.S. Wadia, S.F. Dowdy, Transmembrane delivery of protein and peptide drugs by TAT-mediated transduction in the treatment of cancer, Adv Drug Deliv Rev 57 (2005) 579-596.

[102] L.L. Kiefer, S.A. Paterno, C.A. Fierke, Second shell hydrogen bonds to histidine ligands enhance zinc affinity and catalytic efficiency, Journal of the American Chemical Society 117 (1995) 6831 - 6837.

[103] C.J. Frederickson, J.-Y. Koh, A.I. Bush, The neurobiology of zinc in health and disease, Nature Reviews Neuroscience 6 (2005) 449 - 462.

[104] Y. Li, C.J. Hough, S.W. Suh, J.M. Sarvey, C.J. Frederickson, Rapid translocation of Zn(2+) from presynaptic terminals into postsynaptic

hippocampal neurons after physiological stimulation, J Neurophysiol 86 (2001) 2597-2604.

[105] C.A. Fierke, R.B. Thompson, Fluorescence-based biosensing of zinc using carbonic anhydrase, Biometals 14 (2001) 205-222.

[106] R.B. Thompson, B.P. Maliwal, V.L. Feliccia, C.A. Fierke, K. McCall, Determination of picomolar concentrations of metal ions using fluorescence anisotropy: biosensing with a "reagentless" enzyme transducer, Anal Chem 70 (1998) 4717-4723.

[107] R.B. Thompson, B.P. Maliwal, H.H. Zeng, Zinc biosensing with multiphoton excitation using carbonic anhydrase and improved fluorophores, J Biomed Opt 5 (2000) 17-22.

[108] D. Elbaum, S.K. Nair, M.W. Patchan, R.B. Thompson, D.W. Christianson, Structure-based design of a sulfonamide probe for fluorescence anisotropy detection of zinc with a carbonic anhydrase-based biosensor, Journal of the American Chemical Society 118 (1996) 8381-8387.

[109] R. Bozym, T.K. Hurst, N. Westerberg, A. Stoddard, C.A. Fierke, C.J. Frederickson, R.B. Thompson, Determination of Zinc Using Carbonic Anhydrase-Based Fluorescence Biosensors, Fluorescence Spectroscopy 450 (2008) 287-309.

[110] W. Stumm, J.J. Morgan, Aquatic Chemistry: Chemical Equilibria and Rates in Natural Waters, Third ed., Wiley-Interscience, New York, 1996.

[111] L.E. Brand, W.G. Sunda, Reduction of marine phytoplankton reproduction rates by copper and cadmium, Journal of Experimental Marine Biological Ecology 96 (1986) 225 - 250.

[112] M. Martin, K.E. Osborn, P. Billig, N. Glickstein, Toxicities of ten metals to Crassostrea gigas and Mytilus edulis embryos and Cancer magister larvae, Marine Pollution Bulletin 12 (1981) 305 - 308.

[113] J.W. Moffett, L.E. Brand, P.L. Croot, K.A. Barbeau, Cu speciation and cyanobacterial distribution in harbors subject to anthropogenic Cu inputs, Limnology and Oceanography 42 (1997) 789 - 799.

[114] R.B. Thompson, H.H. Zeng, C.A. Fierke, G. Fones, J. Moffett, Real-time *in situ* determination of free Cu(II) at picomolar levels in sea water using a fluorescence lifetime-based fiber optic biosensor, in: G.E. Cohn (Ed.), Clinical Diagnostic Systems: Technologies and Instrumentation, vol. 4625, Society of Photooptical Instrumentation Engineers, San Jose, CA, 2002, pp. 137 - 143.

[115] R.B. Thompson, Z.F. Ge, M. Patchan, C.C. Huang, C.A. Fierke, Fiber optic biosensor for Co(II) and Cu(II) based on fluorescence energy transfer with an enzyme transducer, Biosensors & Bioelectronics 11 (1996) 557-564.

[116] R.B. Thompson, Z. Ge, M.W. Patchan, C.A. Fierke, Energy transfer-based fiber optic metal ion biosensor, in: J.R. Lakowicz (Ed.), SPIE Conference on Advances in Fluorescence Sensing Technology II, vol. 2388, SPIE, San Jose, CA, 1995, pp. 138 - 147.

[117] C. van den Berg, Determining the copper complexing capacity and conditional stability constants of complexes of copper (II) with natural

organic ligands in seawater by cathodic stripping voltammetry of copper-catechol complex ions, Marine Chemistry 15 (1984) 1 - 18.

[118] S.L. Belli, A. Zirino, Behavior and calibration of the copper(II) ion-selective electrode in high chloride media and marine waters, Analytical Chemistry 65 (1993) 2583-2589.

[119] K.W. Bruland, E.L. Rue, J.R. Donat, S.A. Skrabal, J.W. Moffat, Intercomparison of voltammetric techniques to determine the chemical speciation of dissolved copper in a coastal seawater sample, Analytica Chimica Acta 405 (1999) 99 - 113.

[120] Y. Zheng, X. Cao, J. Orbulescu, V. Konka, F.M. Andreopoulos, S.M. Pham, R.M. Leblanc, Peptidyl fluorescent chemosensors for the detection of divalent copper, Anal Chem 75 (2003) 1706-1712.

[121] C. Palm, S. Netzereab, M. Hallbrink, Quantitatively determined uptake of cell-penetrating peptides in non-mammalian cells with an evaluation of degradation and antimicrobial effects, Peptides 27 (2006) 1710-1716.

[122] P.J. Dittmer, J.G. Miranda, J.A. Gorski, A.E. Palmer, Genetically encoded sensors to elucidate spatial distribution of cellular zinc, J Biol Chem 284 (2009) 16289-16297.

[123] J.L. Vinkenborg, T.J. Nicolson, E.A. Bellomo, M.S. Koay, G.A. Rutter, M. Merkx, Genetically encoded FRET sensors to monitor intracellular Zn(2+) homeostasis, Nat Methods (2009).

[124] N.C. Shaner, G.H. Patterson, M.W. Davidson, Advances in fluorescent protein technology, J Cell Sci 120 (2007) 4247-4260.

[125] B.J. Bevis, B.S. Glick, Rapidly maturing variants of the Discosoma red fluorescent protein (DsRed), Nat Biotechnol 20 (2002) 83-87.

[126] E.M. Merzlyak, J. Goedhart, D. Shcherbo, M.E. Bulina, A.S. Shcheglov, A.F. Fradkov, A. Gaintzeva, K.A. Lukyanov, S. Lukyanov, T.W. Gadella, D.M. Chudakov, Bright monomeric red fluorescent protein with an extended fluorescence lifetime, Nat Methods 4 (2007) 555-557.

[127] N.C. Shaner, R.E. Campbell, P.A. Steinbach, B.N. Giepmans, A.E. Palmer, R.Y. Tsien, Improved monomeric red, orange and yellow fluorescent proteins derived from Discosoma sp. red fluorescent protein, Nat Biotechnol 22 (2004) 1567-1572.

CHAPTER 2: Optimizing Metal Selectivity of the Metal Binding Motif in Human CA(II)

INTRODUCTION

Many proteins bind various transitional metals with high affinity. Furthermore, the affinity varies with the identity of the metal and the metal cofactor is usually critical to the biological function of the protein. The incorporation of the correct metal into metalloproteins, including Carbonic Anhydrase, is dependent on both the concentration of the metal ion *in vivo* and the affinity of the protein [66]. Even where metallochaperones transport the metal ion *in vivo*, selectivity is required [128]. Typically transition metal binding sites are comprised of 3-4 protein ligands that are embedded in a hydrogen bond network. These hydrogen bond interactions make structural and electrostatic contributions that orient the ligands for optimal metal coordination and reactivity [64]. For example, D124 in Cu, Zn superoxide dismutase plays a role in metal binding by forming hydrogen bonds with histidine ligands to zinc and copper [129]. Variants of this enzyme show that when these hydrogen bonds are disrupted, the ability to coordinate zinc is virtually lost. Substantial effort to create high-affinity transition metal proteins via *de novo* design and genetic engineering have advanced the understanding of the determinants of these sites and sensing technology.

Structure-function relationships in protein-zinc binding sites have been extensively delineated via studies of the active site structures in carbonic anhydrase. Carbonic anhydrase II (CA(II)) contains a conserved His_3H_2O zinc polyhedron which is essential for catalysis. The largest alterations in metal affinity in carbonic anhydrase have been obtained by altering the number and chemical nature of the His side chains that directly coordinate [130]. Removal of one ligand (His_2 sites) decreases Zn affinity $> 10^5$ fold. In contrast, CA(II) mutations that replace the solvent molecule with a fourth protein ligand enhance the zinc affinity up to 200-fold [61].

Additional features of metal ion binding sites that have been hypothesized to alter affinity and selectivity in CA(II) and other metalloproteins are polarizability of the coordinating atom, size of the binding site relative to size of the metal ion, and the binding site geometry. In wild-type CA(II), the hydrogen bond network that fully saturates the zinc ligands (H94, H96, H119) and the hydroxide ion of the tetrahedral metal coordination polyhedron are referred to as the second shell residues or the "indirect" zinc ligands (Figure 2.1). The direct histidine ligands His 94 and His 119 of carbonic anhydrase form hydrogen bonds with the side chains of the residues Q92 and E117, respectively. Mutation of any of these second shell ligands to alanine decreases zinc affinity 10-20-fold [131]. The loss of zinc affinity could arise from alterations in the thermodynamics of the His−Zn interaction in the bound versus unbound states or changes in the thermodynamics of solvation of the active site. In wild-type CA(II), one of the carboxylate oxygens of Glu-117 accepts a hydrogen bond from an imidazole N-H

of the direct ligand His-119 (Figure 2.1); this interaction is postulated to preorganize the binding site and thereby enhance the overall affinity for the active site zinc [132]. The crystallographically determined structure of E117A CA(II) is very similar to that of wild-type protein. In addition to decreasing the zinc affinity, removal of the Glu-117−His-119 hydrogen bond significantly enhances the zinc association rate constant. These data have led to a proposed mechanism for zinc binding that involves an initial complex formed by zinc coordination to His-94 and His-96, followed by slow ligand exchange

The zinc bound water ligand forms a hydrogen bond with the side chain of Thr-199.   Zinc binds to CA(II) in tetrahedral geometry with one bound water molecule while bound copper forms a trigonal bipyramidal geometry with two water molecules [133]. Therefore, we proposed that alteration of the hydrogen bonding network with the metal-water molecules and/or the volume of the active site near these molecules would alter the copper/zinc selectivity. Here we demonstrate that replacement of Thr199 with amino acids that cannot form a hydrogen bond decreases zinc affinity while substitution of amino acids capable of hydrogen bonding with the zinc-water ligand have little or no effect on zinc affinity. These results demonstrate that hydrogen bonding interactions with the zinc-water ligand stabilize the bound metal ion. In contrast, mutations that disrupt the hydrogen bond with the zinc-water ligand enhance the copper binding affinity. These data demonstrate that the hydrogen bond with the metal-water ligand is an important determinant of the zinc selectivity of CA(II).
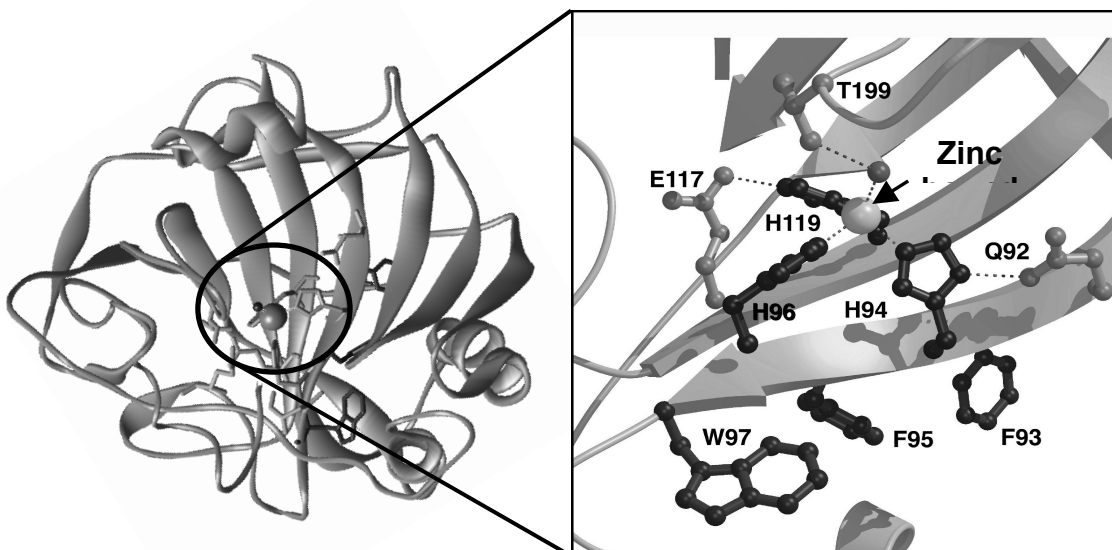
Figure 2:1: Ribbon diagram of human Carbonic Anhydrase II:

Metal binding site highlighting: the zinc ion as a sphere; the direct ligand histidines, H94, H96, H119; the second shell ligands Q92, E117, T199; and hydrophobic residues F93, F95, W97

The goal of the work presented in this chapter is to first construct, via protein engineering, CA(II) metal ion sensors with predictable structure and function-zinc and copper affinities. Secondly, in addition to preparing new CA(II) variants and analyzing their metal affinity, the fluorescent properties and stability for incorporation into sensors useful for measuring Cu(II) and Zn(II) at sea, were optimized. These studies provide insight into the design of CA(II) mutants with predictable zinc affinity and zinc/copper selectivity.

MATERIALS AND METHODS

Vector construction and mutagenesis:

The CA(II) variants with substitutions at threonine-199 and glutamine-92 were prepared using the pACA vector, encoding human CA(II) under the control of a T7 promoter (Fig 2.2), as the starting template [134]. The genes

ATGGCCCATCACTGGGGGTACGGCAAACACAACGGACCTGAGCACTGGCA
TAAGGACTTCCCCATTGCCAAGGGAGAGCGCCAGTCCCCTGTTGACATCGA
CACTCATACAGCCAAGTATGACCCTTCCCTGAAGCCCCTGTCTGTTTCCTAT
GATCAAGCAACTTCCCTGAGGATCCTCAACAATGGTCATGCTTTCAACGTGG
AGTTTGATGACTCTCAGGACAAAGCAGTGCTCAAGGGAGGACCCCTGGATG
GCACTTACAGATTGATT**CAG**TTTCACTTTCACTGGGGGTTCACTTGATGGACA
AGGTTCAGAGCATACTGTGGATAAAAAGAAATATGCTGCAGAACTTCACTTG
GTTCACTGGAACACCAAATATGGGGATTTTGGGAAAGCTGTGCAGCAACCT
GATGGACTGGCCGTTCTAGGTATTTTTTTGAAGGTTGGCAGCGCTAAACCG
GGCCTTCAGAAAGTTGTTGATGTGCTGGATTCCATTAAAACAAAGGGCAAGA
GTGCTGACTTCACTAACTTCGATCCTCGTGGCCTCCTTCCTGAATCCCTGGA
TTACTGGACCTACCCAGGCTCACTG**ACC**ACCCCTCCTCTTCTGGAATGTGT
GACCTGGATTGTGCTCAAGGAACCCATCAGCGTCAGCAGCGAGCAGGTGTT
GAAATTCCGTAAACTTAACTTCAATGGGGAGGGTGAACCCGAAGAACTGAT
GGTGGACAACTGGCGCCCAGCTCAGCCACTGAAGAACAGGCAAATCAAAG
CTTCCTTCAAATAA

Figure 2:2: Sequence of human CA(II):

DNA sequence encoding the gene for human carbonic anhydrase II. The highlighted nucleotides indicate the codons for glutamine-92 and threonine-199. The CA(II) variants listed in Table 2.1 were constructed using site directed mutagenesis

Carbonic Anhydrase (II) Variant	Position 92	Position 199
Wild Type	CAG	ACC
Q92A	GCA	ACC
Q92L	CUG	ACC
T199A	CAG	GCC
T199G	CAG	GGC
T199I	CAG	ATC
T199N	CAG	AAC
T199S	CAG	TCC
T199V	CAG	GTC

Table 2.1: Nucleotide mutations for site-directed amino acid mutagenesis:
For each amino acid mutation, the original codon in WT CA(II) and the mutated codon are shown

The Quik-Change site-directed mutagenesis methodology utilizes two completely complementary primers centered on the desired mutation to generate new plasmid DNA encoding the mutated protein [135]. In addition to altering the sequence of the second shell ligand, the asparagine at position 67 was mutated to cysteine (N67C) to allow labeling of protein with an extrinsic fluorophore. The resulting DNA was transformed into chemically competent Smart cells (Genlantis). The transformed cells were plated onto LB-agar plates with 100 µg/mL ampicillin and incubated at 37°C overnight. Single colonies were used to inoculate 50 mL LB-amp liquid cultures, and grown overnight at 37°C. The

plasmid DNA was isolated using the Qiagen Hi-Speed Midi Plasmid Kit and the DNA sequence of the CA(II) gene in the purified plasmids was determined using the dideoxy method of Sanger et al. (1977) [136].

Protein expression and purification:

Chemically competent BL21(DE3) *E. coli* were transformed with the appropriate plasmid and grown overnight on selective LB-amp agar plates. A single colony was selected from the LB-amp plates and grown overnight at 37°C in liquid LB-amp culture. A 1:200 dilution of the overnight culture was used to inoculate the expression culture of LB media with 0.5x M9 salts, 0.4% glucose, 100 μg/mL ampicillin, 0.42 mM $ZnSO_4$ and grown at 37°C to $OD_{600\ nm}$ = 0.8 – 1. CA(II) protein overexpression was induced by the addition of 0.25 mM isopropyl-β-D-thiogalactopyranoside (IPTG) and additional $ZnSO_4$. After 3 hours of growth at 30°C, protease inhibitors (7.4 μg/mL phenylmethanesulfonyl fluoride (PMSF) and 0.92 μg/mL tosyl-L-argininyl-methyl ester (TAME), final concentrations) were added. The cells were harvested 3 h later (6 h after induction) by centrifugation at 4°C for 15 min at 5,000 rpm. The cell pellet was resuspended in 25 mL per liter of culture of cold lysis buffer (50 mM TRIS-SO_4 pH 8.0, 50 mM NaCl, 10 mM EDTA, 200 μM $ZnSO_4$, 1 mM dithiothreitol (DTT), 10 μg/mL PMSF and 1 μg/mL TAME) prior to flash freezing.

After slow thawing, the cells were lyzed using a microfluidizer and the cellular debris removed by centrifugation (45 min, 12,000 rpm). Streptomycin

sulfate (10%) was added at 4 °C and precipitated ribosome and nucleic acids were removed by centrifugation (30 minutes, 10,000 rpm). The resulting protein solution was dialyzed against buffer A (30 mM HEPES, pH 8.0, 0.2 mM $ZnSO_4$, and 1 mM DTT) in preparation for anion exchange chromatography. For all dialysis steps, the protein solution was dialyzed against 4 L of buffer overnight at 4°C. In the first purification step, the protein mixture from 1 L of culture is incubated with 25 mL of DEAE Sephacel (Amersham Bioscience), equilibrated with buffer A, for at least 30 min at 4 °C. The resin is then put into a column. CA(II) does not bind to the resin under these conditions and is collected in the flow-through. The column is then washed with 1 column volume of buffer. Generally CA(II), at this stage, is >90% pure and can be used immediately. If further purification is needed, the protein is dialyzed against buffer B (10 mM MES, pH 7.0, 0.1 mM $ZnSO_4$ and 1 mM tris(2-carboxyethyl)phosphine hydrochloride (TCEP)), and then incubated with 30 mL SP Sepharose (Amersham Bioscience) per liter of culture equilibrated in buffer B and incubated for 30 min at 4°C. The resin is then washed and the bound CA(II) eluted using ammonium sulfate. Since this is a batch purification in each elution step the resin was washed with 1.5 times the resin volume using buffer B containing either 50, 100, 200, 300, 400 or 500 mM ammonium sulfate via vacuum filtration. A sample from each fraction was run on a SDS PAGE gel to analyze protein purity. CA(II) eluted at ammonium sulfate concentrations between 200 and 400 mM. The eluted CA(II) was dialyzed against buffer B to remove the ammonium sulfate before the protein was quantitated, aliquoted and stored at -20 °C.

Protein quantitation:

The concentration of CA(II) was determined by absorbance at 280 nm (ε = 50,700 $M^{-1}cm^{-1}$) and the concentration of active CA(II) was determined by a stoichiometric titration of the fluorescence of the CA(II)-dansylamide (DNSA) complex with the tight binding ligand, diamox (acetazolamide, Sigma A6011). This method accurately measures the number of sulfonamide binding sites, reflecting CA(II) active sites [92]. The titration was carried out using concentrations CA(II) of 0.5 – 1 μM in 10 mM MOPS, pH 7.0 buffer containing 1-2 μM $ZnSO_4$. The excess zinc is present to ensure that all of the CA(II) in the sample is zinc bound. The fluorescent sulfonamide DNSA is added to the protein solution. Intrinsically fluorescent residues in the protein (Tryptophan and Tyrosine) are excited at 290 nm [137]. The fluorescence emission from these residues at ~340 nm excite DNSA with an emission wavelength of 450 nm. Addition of a non-fluorescent competing ligand, Diamox, competes with DNSA for binding to CA(II) and decreases the observed FRET signal. Diamox is a non-fluorescent sulfonamide that has a nanomolar affinity for holo-CA(II). DNSA fluorescence as a function of added Diamox was measured. Under these conditions Diamox binding to CA(II) is essentially stoichiometric. Two linear fits were performed – the first line was fit to the initial fluorescence decrease (low Diamox concentrations) and the second line was fit to the plateau region (high Diamox concentrations). The intercept of the two linear fits yields the concentration of zinc bound to the active site of CA(II).

Dapoxyl sulfanomide synthesis (Optimized in collaboration with Da Wang):

Ten milligrams dapoxyl sulfonyl chloride (Molecular Probes) was dissolved in 2 mL dry acetonitrile and placed in a 10 mL pre-dried reaction flask. Anhydrous ammonia gas was bubbled through a dry ice acetone-cooled cold-trap condenser. Liquid ammonia was then slowly dripped into the flask containing the dissolved Dapoxyl sulfonyl chloride. The reaction was allowed to stir on ice. Upon completion of the reaction, the mixture exhibits a color change from brown to yellow-green. The flow of ammonia gas was stopped after 20 min. Excess ammonia was evaporated by stirring for ~45 min. To remove salt or unreacted contaminants, the mixture was filtered. The final product (dapoxyl sulfonamide) was dried using a SpeedVac® vacuum. The dry powder was dissolved in 1.5 mL of a 1:1 mixture of methanol and acetonitrile. The product was further purified by preparatory C18 reverse-phase HPLC (CH_3CN/H_2O-0.1% TFA, 5%-100% over 60 min, 5 mL/min, 350 nm detection (t_R=42 min)). Dapoxyl sulfonamide was confirmed by thin layer chromatography, mass spectrometry (a single peak at 344.0 Da), and fluorescence (emission spectrum peak at 535 nm when excited at 350 nm) when complexed to *holo*-wild type carbonic anhydrase.
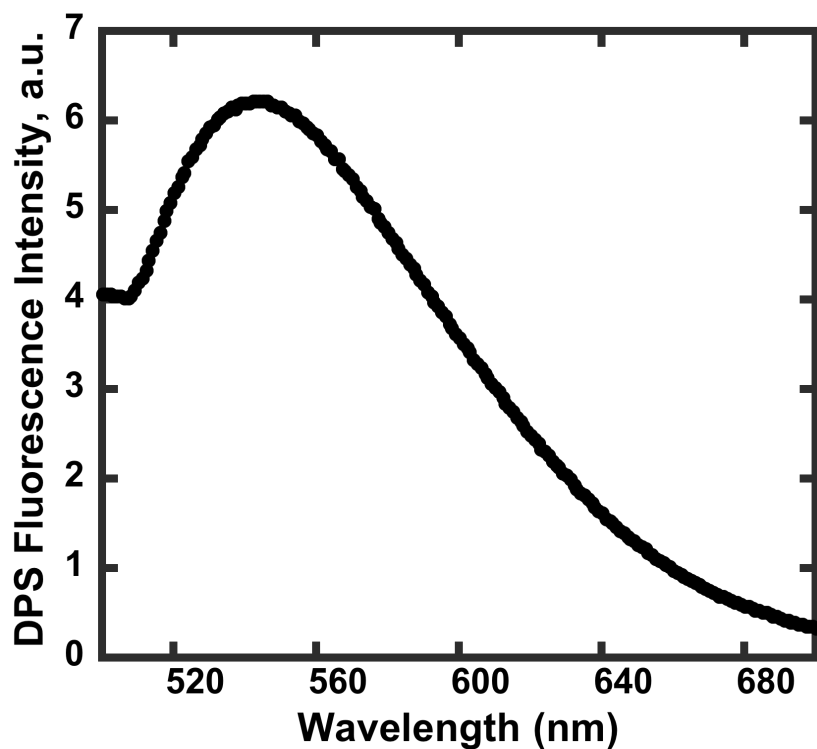
Figure 2:3: Fluorescence spectrum of dapoxyl sulfonamide bound to CA(II):

Emission spectrum (Ex = 365 nm) of 4 µM Dps in 10 mM MOPS, pH 7.0, 25°C in the presence of 1 µM WT CA(II)

The excitation and emission spectra of the product of the Dps synthesis were similar to those previously published (Figure 2.3). The final concentration of purified Dps was determined by measuring the absorbance at 365 nm (ε = 22,000 $M^{-1}cm^{-1}$) [107].

Measurement of CA(II) affinity for Dps:

The affinity of CA(II) for Dps was determined by monitoring the formation of the CA(II)-Dps complex from the increase in fluorescence (excitation = 280 nm

or 365 nm, emission 540 nm) upon stepwise addition of 0.2 μM Dps into a solution of 100 nm CA(II) in 10 mM MOPS (pH 7.0). These concentrations were 10-fold smaller than the reported K_d for Dps to holo-WT enzyme [130]. The fluorescence signal was measured 1-5 min after the addition of Dps. Binding constants and error estimates were determined using the Kaleidagraph curve-fitting program with Equation 2.1 when [Dps] < K_d or Equation 2.2 when [Dps] > K_d.

$$Fl_{obs} = \frac{Fl_{endpoint}}{(\frac{K_D}{[CA]} + 1)} \qquad \text{(Eq 2.1)}$$

$$[CA-Dps] = \frac{([CA]_{tot} + [Dps]_{tot} + K_D) - \sqrt{([CA]_{tot} + [Dps]_{tot} + K_D)^2 - 4[CA-Dps][CA]_{tot}}}{2} \qquad \text{(Eq 2.2)}$$

Conjugation of thiol-reactive fluorophores to CA(II) variants:

The CA(II) variants containing a unique cysteine at position 67 were conjugated with Oregon Green 488 C2-Iodoacetamide (Molecular Probes: Catalog No. O-6010; Figure 2.4) for measurement of metal affinity. The thiol-reactive Oregon Green dye and its conjugates exhibit bright fluorescence and have high photostability.   The N67C/C206S variant was labeled since this site is near the active site..

Figure 2:4: Thiol reactive dye Oregon Green:
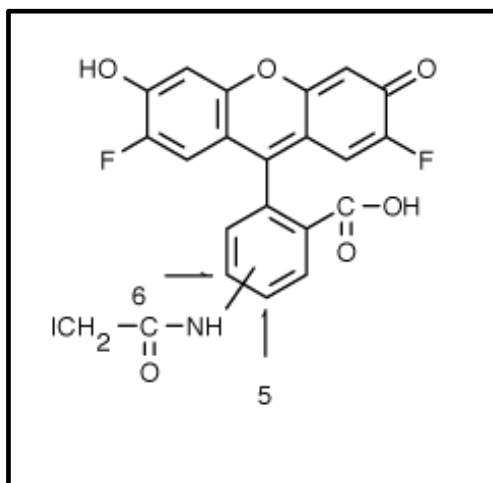
The key advantages of this fluorescent dye include greater photostability, water solubility, brighter emission intensities and pH insensitivity in the physiological pH range.

Before conjugation, the protein was thawed and dialyzed against 50 mM HEPES buffer pH 7.2 at 4 $^{\circ}$C. The cysteine in CA(II) was reduced with 1 mM DTT or tris(2-carboxyethyl)phosphine (TCEP) for 3 h at 4 $^{\circ}$C. Excess reductant was removed via dialysis against 50 mM HEPES buffer pH 7.2 at 4 $^{\circ}$C overnight. A 5-fold molar excess of the fluorescent Oregon Green 488-iodoacetamide dissolved in DMF (dried with ammonium sulfate) was added to <100 μM reduced CA(II) and allowed to react for 1-2 h at room temperature. The volume of DMF used should not exceed by more than 5% of the total volume of the labeling reaction mixture to ensure that the protein is not denatured. The reaction was stopped by adding 10-fold molar excess of β- mercaptoethanol (BME) over Oregon Green 488-iodoacetamide. BME reacts with the iodoacetamide moiety in the fluorphores, but not the thioether linkage of the protein. To remove fluorophore

that is not covalently attached, the labeled protein was dialyzed (100 mM bicine, pH 7.2) 2-3 times each for ~1-2 hours until the dialysate was colorless. Concentrations of the label and the protein were determined from absorbance at the peak fluorophore absorbance wavelength and extinction coefficient, as reported by Molecular Probes (see Table 2.2). The extent of labeling was estimated by comparison of the fluorophore concentration to the protein concentration, which was determined using the absorbance at 280 nm and the calculated protein extinction coefficient.

Dye Derivative	Absorbance	Emission	Extinction Coefficient
Oregon Green 488	491	516	68,000 $cm^{-1}M^{-1}$

Table 2.2: Spectral characteristics of selected reactive dye:

This thiol-reactive dye is excited with visible light. The absorption (Abs) and emission (Em) maxima are reported in nm

Preparation of *Apo*-enzyme:

All plasticware and pipette tips used for preparation of metal free solutions and *apo*-protein was purchased as "metal free" (Bio-Rad) to minimize metal ion contamination. All solutions were made using deionized, 18 MΩ water and were

stored in low metal, pre-treated plasticware. *Apo*-CA(II) was prepared by

overnight incubation with 25 mM dipicolinic acid (DPA) in 10 mM metal-free

(chelexed) MOPS buffer, pH 7.0, followed by chromatography on a PD-10

column (Sephadex G-25M, 5 cm X 15 cm, Pharmacia) pre-equilibrated with

10 mM metal- free MOPS buffer, pH 7.0. The resulting enzyme was

concentrated using an Amicon Ultra concentrator (Millipore) and the protein

concentration was determined from the absorbance at 280 nm using ε_{280}=

50,070 $M^{-1}cm^{-1}$ for all variants. The bound zinc ion concentration was

determined by ICP-MS. Further studies were continued only if the metal: protein

stoichiometry of the apo-enzyme was ≤ 0.1.

Zinc affinity measurements:

        500 nM apo-CA(II) (with or without an extrinsic fluorophore attached) was

incubated with Zn-NTA buffers that have a wide range of free zinc concentrations

(chelexed 10 mM MOPS, pH 7.0, 1 mM nitrilotriacetic acid (NTA), $0 - 9.6 \times 10^{-4}$

M added $ZnSO_4$, $0 - 5.1 \times 10^{-8}$ M free zinc). Total zinc content in each buffer was

measured by ICP-MS. Free metal concentrations in each buffer were calculated

using the MINEQL+ software package (Environmental Research Software,

Hallowell, ME) (Table 2.3). CA(II) was equilibrated in the metal ion buffer at 25

$^{\circ}$C for 8 to 14 h. Then, 4 µM Dps was added to the protein and buffer mixture

followed by centrifugation at 20,000 x*g* for 5 min. The Dps fluorescence (Ex =

340 nm, Em = 535 nm) was measured in a fluorimeter for each free zinc

concentration. The protein concentration was also determined from A_{280}. During

FRET analysis, the intrinsic protein fluorescence acts as a donor to the Dps

inhibitor. The Dps fluorescence was then monitored as a function of the free zinc

concentration. A single binding isotherm (Eq 2.3) was fit to the data to determine

the apparent zinc affinity of CA(II).

(Eq 2.3)

$$\left(\frac{FI}{Abs}\right)_{obs} = \frac{\left(\frac{FI}{Abs}\right)_{endpoint}}{\frac{K_{zn}}{[Zn]}+1}$$

	[Zn], total M	[Zn], Free M	2X [Zn], total M
Bufffer # Control	Control	Control	Control
1	1.00E-09	2.13E-15	2.00E-09
2	5.00E-09	1.06E-14	1.00E-08
3	1.00E-07	2.13E-13	2.00E-07
4	2.50E-07	5.32E-13	5.00E-07
5	5.00E-07	1.06E-12	1.00E-06
6	2.00E-06	4.26E-12	4.00E-06
7	5.00E-06	1.07E-11	1.00E-05
8	2.50E-05	5.46E-11	5.00E-05
9	5.00E-05	1.12E-10	1.00E-04
10	2.00E-04	5.32E-10	4.00E-04
11	5.00E-04	2.13E-09	1.00E-03
12	7.50E-04	6.39E-09	1.50E-03
13	9.00E-04	1.92E-08	1.80E-03
14	9.60E-04	5.10E-08	1.92E-03

Table 2.3: Zinc (II) Metal Buffer Series:

This is a set of free zinc (II) calibration buffers made with MOPS as the pH buffer
and NTA as the metal ion buffer. The final free zinc concentrations in 2 mM
NTA, 10 mM MOPS buffer, pH 7.0, 25 $^{\circ}$C is μM-pM. **Note: This is a 2X buffer:
for example, dilute with equal volume sample to make 1X final buffer**

Copper affinity measurement:

The CA(II) variants containing the N67C/C206S substitutions (50 nM) were labeled with Oregon Green and the apo-enzyme prepared as described above. Stoichiometric Cu(II) binding to Oregon Green-labeled CA(II) results in an 85% decrease in fluorescence intensity; this decrease in fluorescence was used to monitor the copper affinity. Green labeled CA(II) (0.5 µM) was incubated with Cu(II)-NTA buffers in 10 mM MOPS, pH 7.0, at room temperature. The free metal concentrations were calculated using the MINEQL+ software package (Environmental Research Software, Hallowell, ME) (see Table 2.4). Following equilibration at 25 °C, the Oregon Green 488 fluorescence (Ex = 491 nm, Em = 516 nm) intensity was monitored in a fluorimeter as a function of the free copper concentration. A single binding isotherm (Eq 2.4) was fit to the data to determine the apparent copper affinity of CA(II).

(Eq 2.4)

$$\left(\frac{Fl}{Abs}\right)_{obs} = \frac{\left(\frac{Fl}{Abs}\right)_{endpoint}}{\frac{K_{Cu}}{[Cu]}+1}$$

	[Cu] free, M	[Cu] total, M	2X [Cu] total, M
Buffer #:			
0	Control	Control	Control
1	3.76E-15	5.00E-07	1.00E-06
2	7.52E-15	1.00E-06	2.00E-06
3	1.88E-14	2.50E-06	5.00E-06
4	3.78E-14	5.00E-06	1.00E-05
5	5.68E-14	7.50E-06	1.50E-05
6	7.59E-14	1.00E-05	2.00E-05
7	1.93E-13	2.50E-05	5.00E-05
8	3.96E-13	5.00E-05	1.00E-04
9	6.10E-13	7.50E-05	1.50E-04
10	8.36E-13	1.00E-04	2.00E-04
11	1.07E-12	1.25E-04	2.50E-04
12	2.51E-12	2.50E-04	5.00E-04
13	4.52E-12	3.75E-04	7.50E-04
14	7.54E-12	5.00E-04	1.00E-03
15	1.26E-11	6.25E-04	1.25E-03
16	2.26E-11	7.50E-04	1.50E-03
17	4.28E-11	8.50E-04	1.70E-03

Table 2.4: Copper (II) Metal Buffer Series:
This is a set of free copper (II) calibration buffers made with MOPS as the pH
buffer and NTA as the metal ion buffer. The final free copper concentrations in 2
mM NTA, 10 mM MOPS buffer, pH 7.0, 25°C is fM-pM. **Note: This is a 2X
buffer: for example, dilute with equal volume sample to make 1X final buffer**

RESULTS

Sulfonamide inhibitors bind to CA(II) by coordinating to the zinc ion at the active site, replacing the metal water ligand. For many fluorescent aryl sulfonamides, including dapoxyl sulfonamide (Dps), binding to CA(II) leads to a significant increase and a blue shift in the fluorescence emission. Therefore, Dps binding to CA(II) can be monitored by changes in fluorescence (excitation = 365 nm, emission 540 nm).

Using the characteristic fluorescent intensity changes upon Dps binding to holo-enzyme, the affinity of the second shell variants of CA(II) for Dps (Figure 2.5) has been determined. In particular, mutations at T199 could alter the Dps affinity since crystal structures suggest a hydrogen bond between Dps and the hydroxyl of T199. A single binding isotherm was fit to the data for Dps binding to N67C/TI99N/C206S CA(II) and N67C/TI99G/C206S CA(II), but the quadratic form of the single binding isotherm yielded the best fit of the N67C/TI99V/C206S and N67C/TI99I/C206S data due to the high affinity. The results of those fits are shown in Table 2.5. The affinity of the N67C/C206S CA(II) variant is comparable to that of WT CA(II) implying that these mutations do not affect sulfonamide affinity. In this set of experiments, "WT" data refer to N67C/C206S CA(II). Furthermore, the TI99V/N67C/C206S and TI99I/N67C/C206S variants have an affinity for Dps that is comparable to "WT" CA(II), suggesting that a hydrogen bond with T199 is not necessary for high Dps affinity. However, substitution of T199 with glycine (T199G/N67C/C206S) or asparagine (T199N/ N67C/C206S) in

CA(II) decreases the Dps affinity by 5-fold and 35-fold, respectively compared to "WT" CA(II).
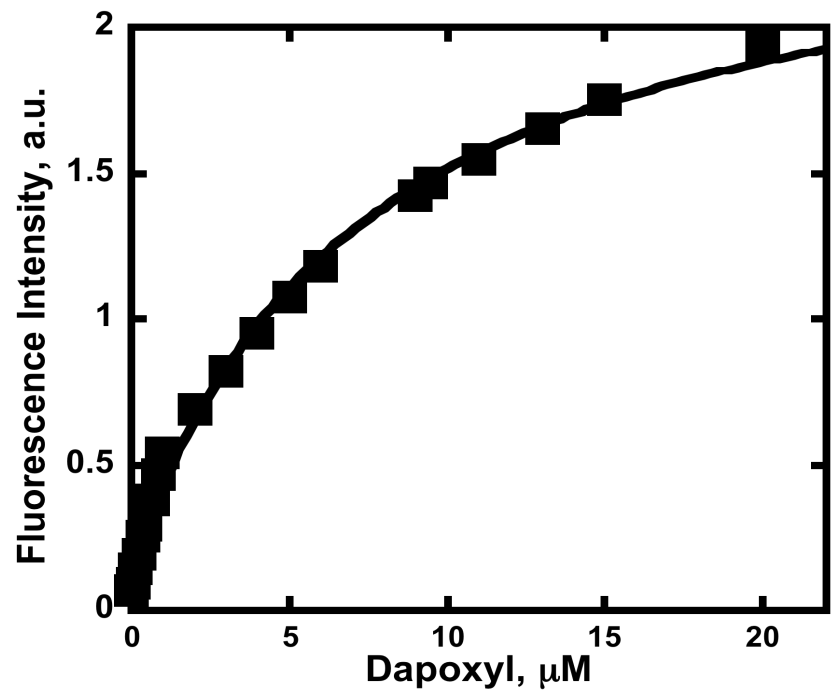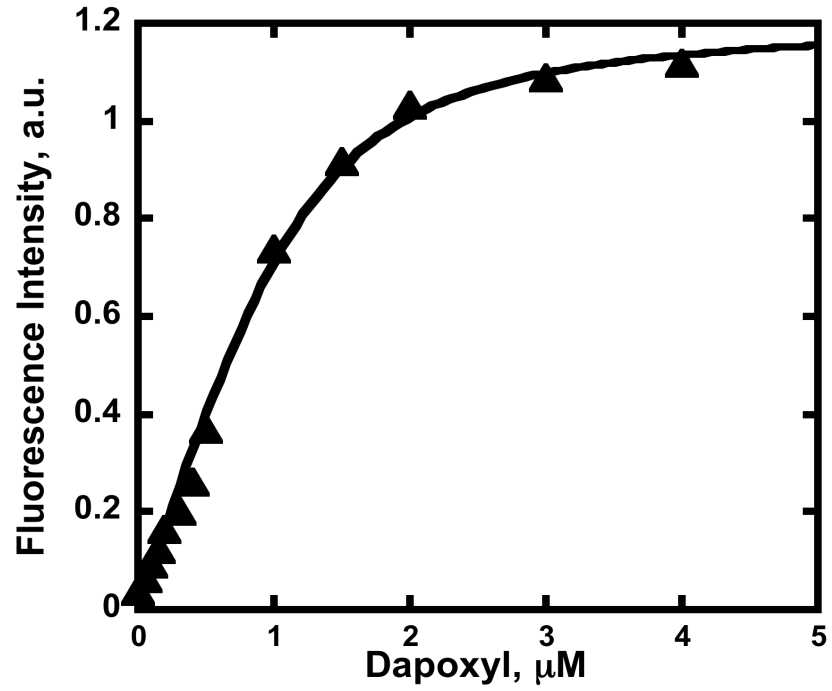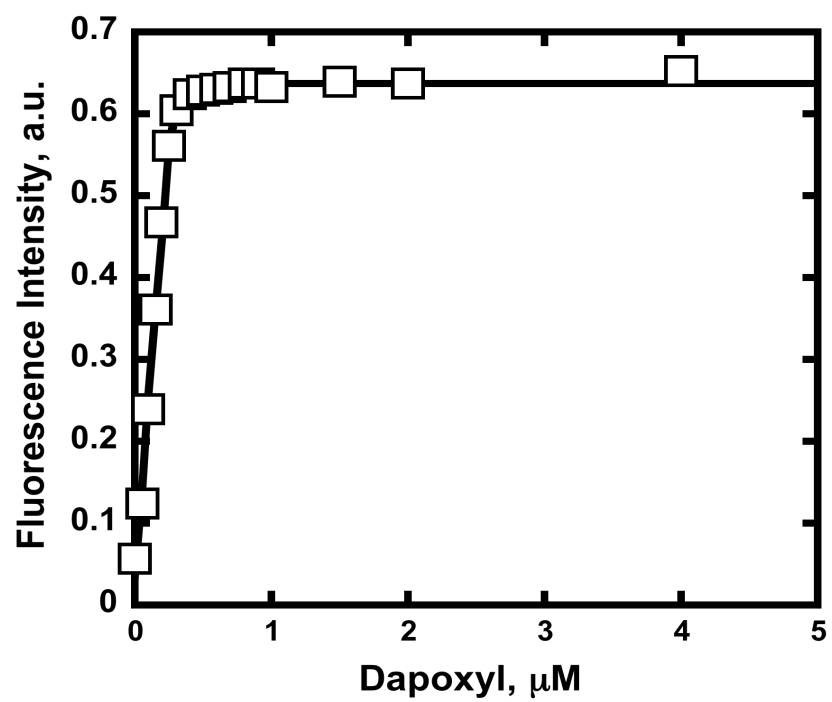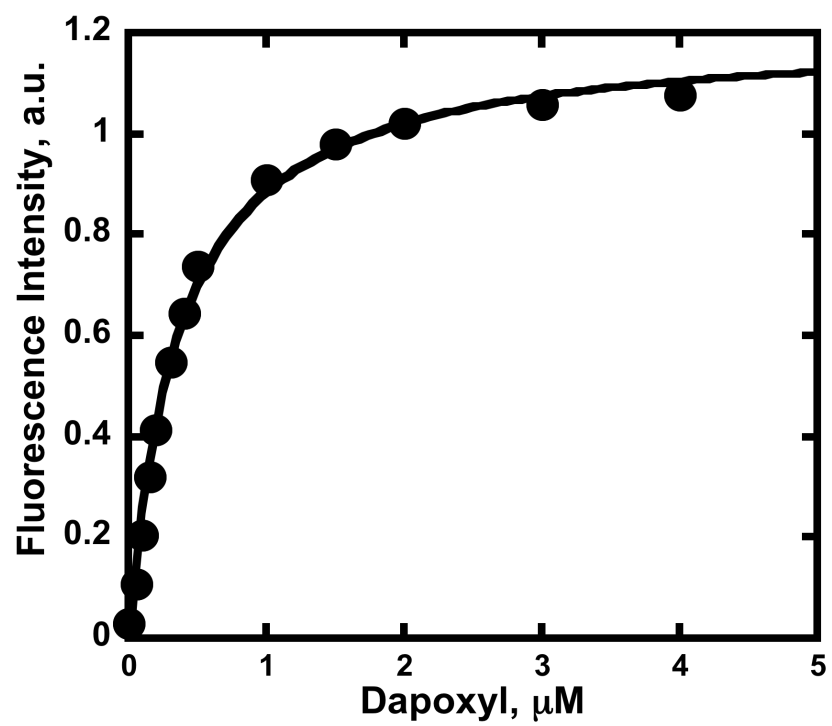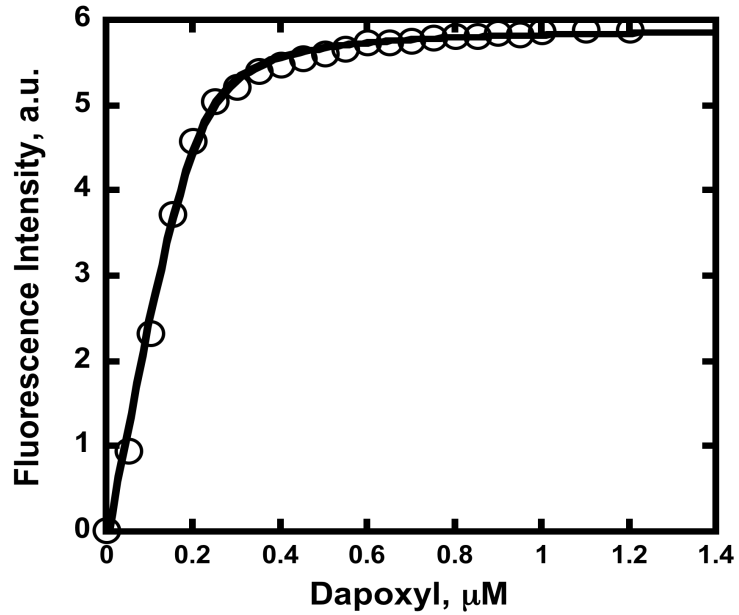
Figure 2:5: Dps affinity studies of 2nd shell mutants:

The measured affinities of protein for Dps as determined in 10 mM MOPS pH 7.0, 0.1 mM $ZnSO_4$, 100 nM CA(II) at room temperature. (▲): T199G; (■): T199N; (●): T199V; □: T199I; (○): WT-N67C/C206S

Protein	K_D^{Dps}, µM	Effect
N67C/C206S_CA(II)	0.21 ± 0.01	
T199G CA(II)	1.4 ± 0.09	7-fold weaker
T199I CA(II)	0.27 ± 0.01	Negligible
T199N CA(II)	7.2 ± 0.8	35-fold weaker
T199V CA(II)	0.35 ± 0.03	Negligible

Table 2.5: Dps affinity measurements of selected second shell variants:

The measured affinities of protein for Dps as determined in 10 mM MOPS, pH 7.0, 0.1 mM $ZnSO_4$, 25 °C. All of the listed mutations were made in human CA(II) and also contain the N67C and C206S mutations

The nature of the direct ligands and the structure of the hydrogen bond network are important for optimizing the metal affinity of CA(II) [58]. The hydrogen bond between the protein and the zinc ligands are proposed to orient the ligands in a tetrahedral geometry for optimal zinc coordination. Since Cu^{2+} binds to CA(II) with trigonal biypyramidal geometry with 2 coordinating water molecules, the second shell ligands are proposed to enhance the affinity of Zn^{2+} relative to Cu^{2+}. In particular, hydrogen binds to the zinc water ligand are hypothesized to influence Zn/Cu selectivity. The replacement of Thr199 with amino acids capable of forming a hydrogen bond with the zinc-water ligand is predicted to maintain high zinc affinity, while deletion of this hydrogen bond is predicted to decrease zinc affinity. On the other hand, mutations at Thr199 that

stabilize the metal coordination of multiple water molecules, perhaps by increasing the volume around the metal site, are predicted to enhance the copper affinity.

To test the importance of the second shell ligands in determining the Zn^{2+}/ Cu^{2+} selectivity, the following mutants were prepared using Quik-Change mutagenesis and characterized: T199A, T199G, T199I, T199N, T199S, T199V, Q92A, and Q92L. To measure the Zn^{2+} affinity, first apo-enzyme was prepared via dialysis against DPA. For all of the mutants, apo-enzyme was easily prepared using methods developed for the wild-type enzyme suggesting that the mutants do not bind Zn^{2+} significantly more tightly than WT CA(II).. The Zn^{2+}-bound CA(II) can be detected directly from the changes in fluorescence intensity upon binding Dps. However, the accuracy of the measurement increases by using a ratiometric method. Therefore, the fraction of CA(II) with bound Zn^{2+} was determined from FRET between Dps and the tryptophan and tyrosine residues in CA(II).

The Zn^{2+} affinity of CA(II) variants was evaluated by incubating apo-CA(II) with varying concentrations of free Zn^{2+} maintained using zinc-NTA buffers. The presence of metal-binding ligands together with zinc contamination from many sources generally makes it challenging to reproducibly prepare solutions with low concentrations of free zinc by simple addition of small amounts of zinc to ordinary pH buffers. For this reason we prepare zinc ion "buffers" to maintain fixed low zinc ion concentrations in a solution. These buffers contain moderate concentrations of zinc (mM) and a fairly tight-binding ligand, nitrilo-triacetic acid

(NTA). NTA chelates the majority of the zinc, and this composition resists

elevation of the free zinc concentration if contaminating zinc is present [138].

The zinc-bound CA(II) at each zinc concentration was detected by the addition of

Dps and measurement of the Dps fluorescence intensity (540 nm) ratioed to the

concentration of the protein in each sample (Figure 2.6). A single binding

isotherm was fit to these data and the calculated $K_{d,}{}^{Zn}$ values are listed in Table

2.6. The N67C/C206S mutations have little effect on the zinc affinity of CA(II).

However, mutations in the second shell ligands at Q92 and T199 uniformly

decrease the zinc affinity. Mutations at T199 have more variable effects on zinc

affinity. In this case, the side chains that retain a group that can form a hydrogen

bond (Asn and Ser) result in smaller decreases in affinity than side chains that

cannot form hydrogen bonds (Gly, Val, Ile). The T199V mutation has the largest

effect, decreasing zinc affinity almost 75-fold.
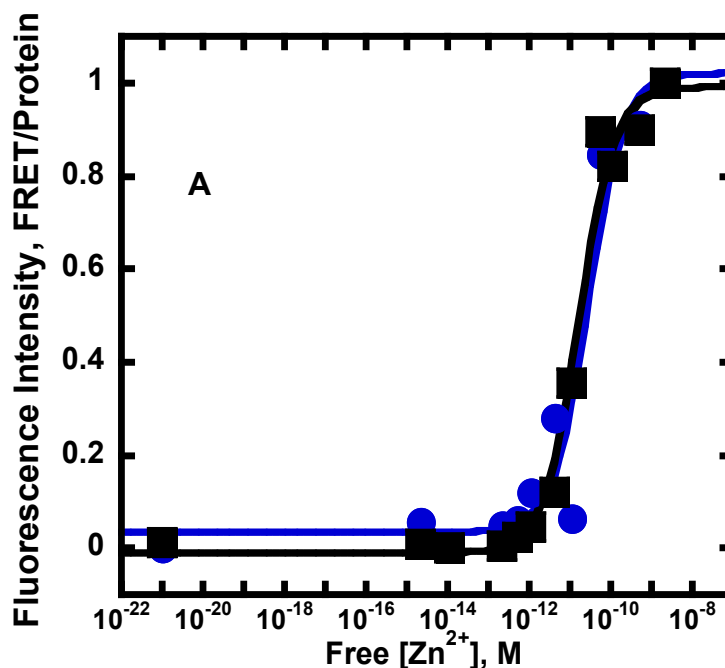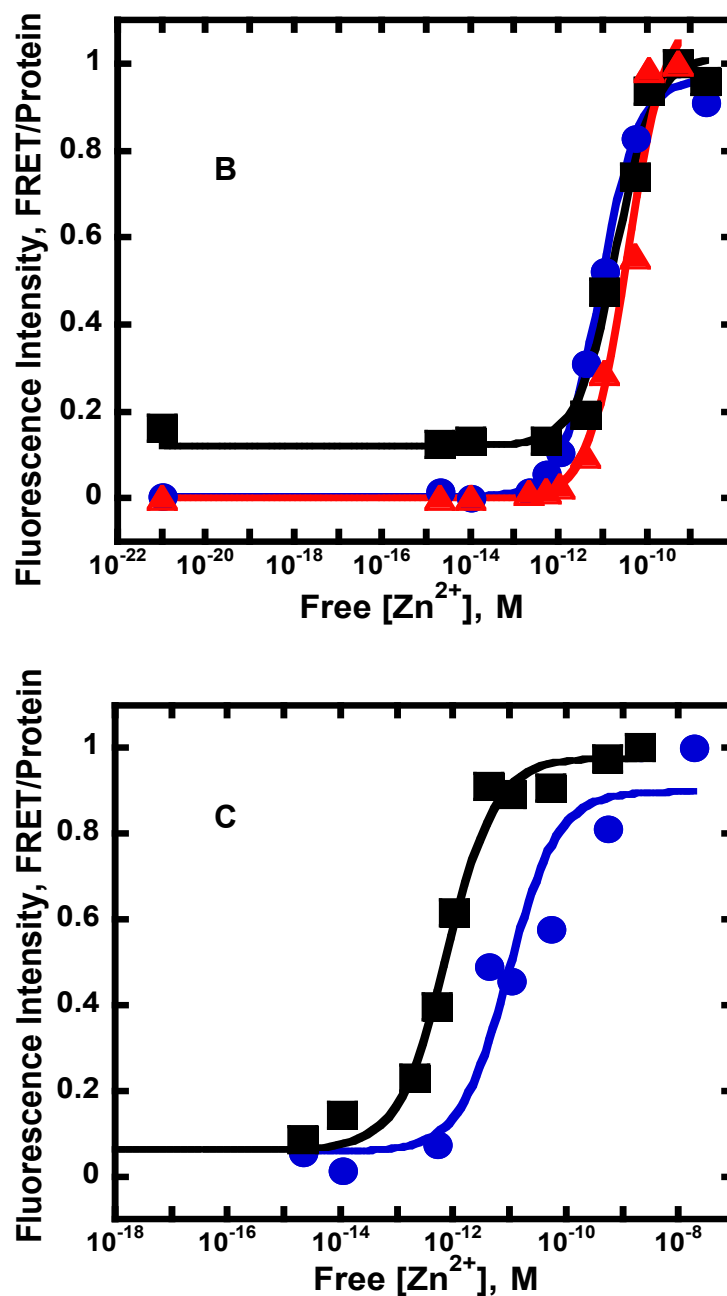
Figure 2:6: Zinc (II) affinity studies of second shell variants:

The fluorescence of 500 nM apo-CA(II)_Q92 and T199 mutants in 10 mM MOPS zinc-NTA buffers, pH 7.0, 4 mM Dps, with varying concentrations of free zinc at 25 $^{\circ}$C. The FRET emission (Ex = 290 nm, Em = 535 nm) was ratioed to the intrinsic protein fluorescence emission (Ex = 290 nm, Em = 340 nm). A single binding isotherm (Eq 2.3) was fit to the data and the values for K_D^{Zn} are listed in table 2.4. The FRET intensity ratio increases with zinc concentration as the fraction of zinc-bound CA(II) increases, producing a binding curve with picomolar affinity. A) (●) Q92L, (■) Q92A; B) (●) T199S, (■) T199N, (▲) T199I; C) (●) TI99V, (■) WT_N67C_C206S

To evaluate the role of second shell ligands in determining the Zn^{2+}/Cu^{2+} selectivity, we altered the size and hydrophobicity of the amino acids at positions 92 and 199 and measured the effect of these mutations on copper affinity. The copper affinity was monitored by quenching of a fluorophore conjugated to a single cysteine residue at position 67 (N67C/C206S) on the enzyme. Labeling efficiencies varied between 20-77% (data not shown). Oregon Green 488 was chosen as an optimal label for copper (II) determination due to its high extinction coefficient, quantum yield and photostability. Because the Oregon Green has high extinction coefficients and quantum yields, a measurable signal output upon metal binding was observable even at the low protein concentrations used for these measurements. Furthermore, copper binding significantly quenched (up to 70%) the fluorescence of Oregon Green conjugated to the Q92A and T199 mutants (Figure 2.7)

Fluorescently labeled apo-CA(II) was incubated with various concentrations of free Cu^{2+} maintained using MOPS, NTA-buffers, pH 7.0. The fluorescence Oregon Green (excitation = 496 nm, emission 524 nm) was measured at the various Cu^{2+} concentrations and the signal plotted against free Cu^{2+} in each sample. A single binding isotherm was fit to the data.

The second shell mutations have a modest effect on Cu^{2+} affinity. Substitution at Q92, which forms a hydrogen bond with the His-94 zinc ligand, has little affect on the copper affinity. Alterations in at T199 either cause little affect on Cu^{2+} affinity (TI99S, I, and N) or decrease affinity up to 3-fold (T199G

and T199V) (Figure 2.8). Therefore, the second shell hydrogen bonds are less important for the affinity of CA(II) for Cu^{2+} than for Zn^{2+} and suggest that these side chains do not form energetically important hydrogen bonds with the copper-water ligands. Nonetheless, these mutations do alter the Zn^{2+}/ Cu^{2+}.
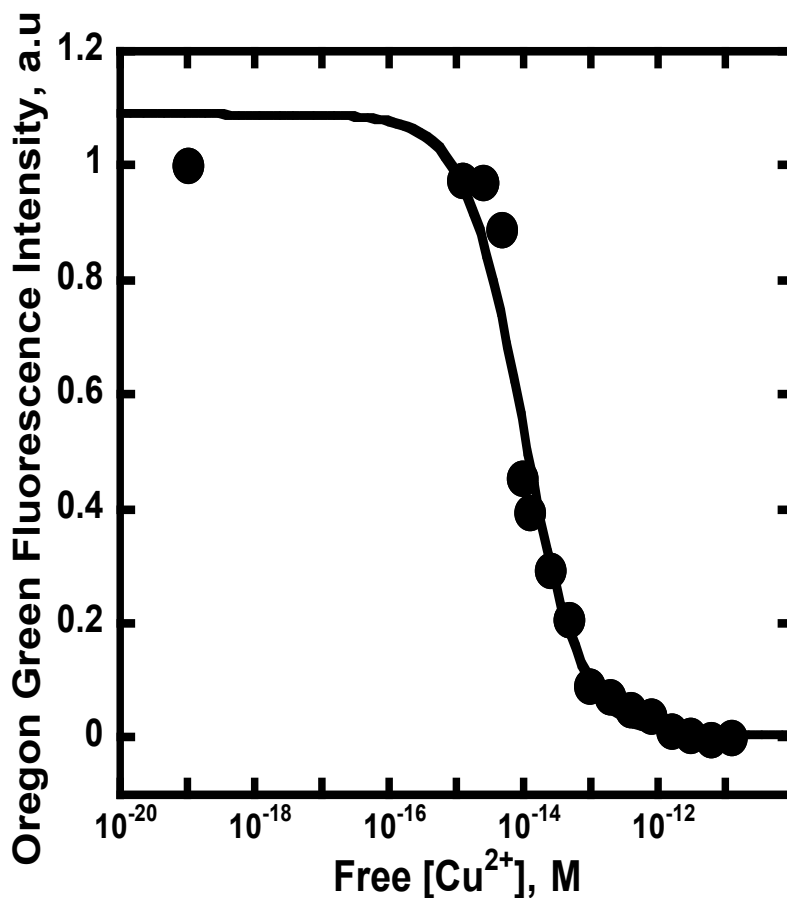
Figure 2:7: Fluorescence intensity of 100 nM-Oregon Green labeled WT-CA(II) as a function of free Cu^{2+}:
The fluorescence of 50 nM apo-OG-CA(II)_N67C/C206S in 10 mM MOPS copper-NTA buffers, pH 7.0 was monitored (Ex= 491 nm; Em= 520 nm). The wild-type enzyme binds copper more tightly than zinc with a K_d of 10 ± 2 fM. Quenching of the covalently attached fluorophore upon copper binding is more than >85%
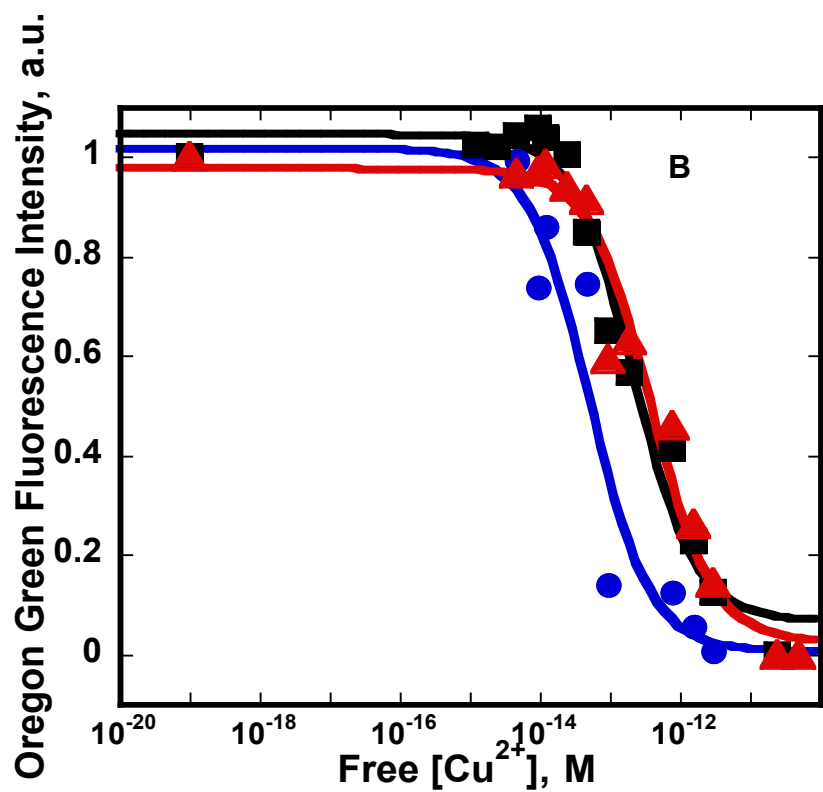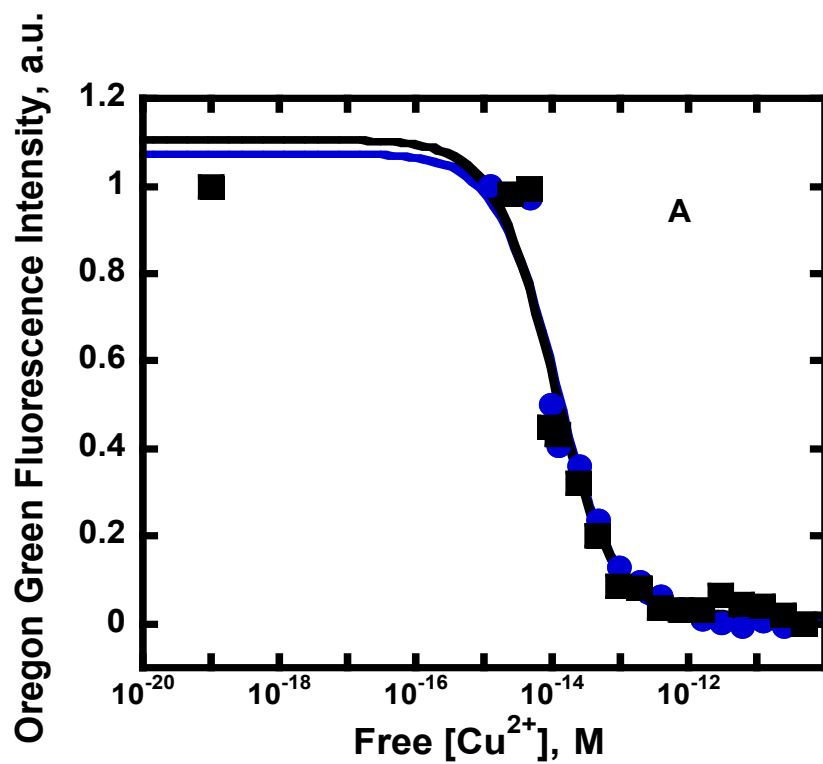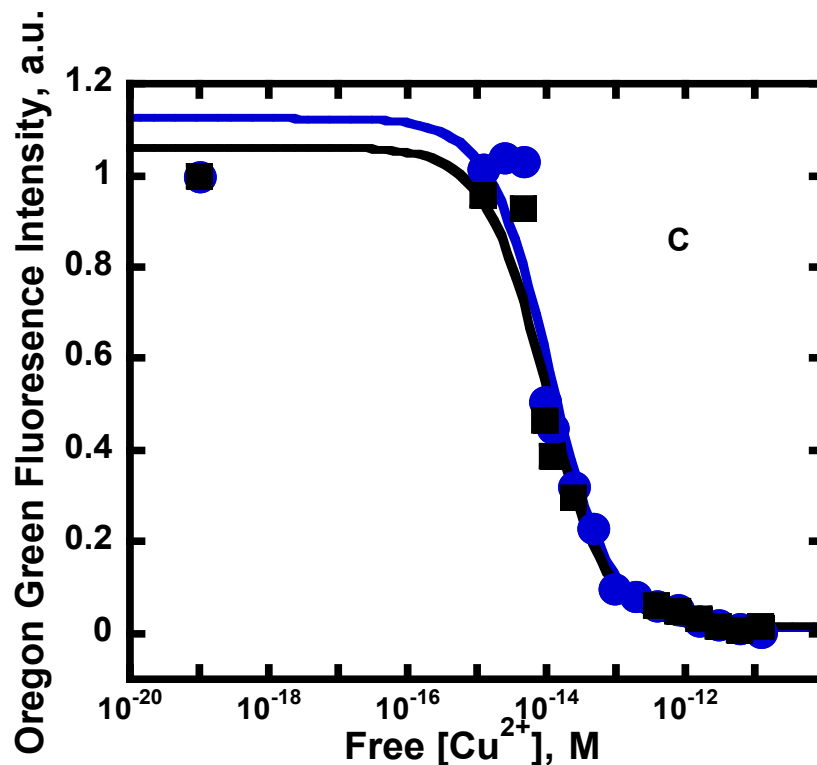
Figure 2:8: Fluorescence intensity of 100 nM-Oregon Green labeled T19and Q92 variants as a function of free Cu^{2+}:
The fluorescence of 100 nM apo-OG-CA(II)_Q92 and T199 mutants in 10 mM MOPS copper-NTA buffers, pH 7.0, with varying concentrations of free copper at 25 °C. Oregon Green emission is measured (Ex = 491 nm, Em = 516 nm). A single binding isotherm (Eq 2.4) was fit to the data and the values of K_{Dapp} are listed in table 2.4. Quenching of the covalently attached fluorophore upon copper binding is more than >70%. A) (●) Q92A, (■) Q92L; B) (●) T199G, (■) T199N, (▲) T199V; C) (●) TI99i, (■) T199S

CA(II) Mutant	K_D Cu (pM)	K_D Zn (pM)	$\underline{K_d(Zn)}$ $K_d(Cu)$
WT* N67C/C206S	0.012	0.8 ± .1	67
Q92A	0.01 ± 0.002	17 ± 4	1700
Q92L	0.012 ± 0.002	28 ± 16	2333
T199G	0.052 ± 0.028	38 ±	731
T199V	0.039 ± 0.011	59 ± 5	1513
T199I	0.010 ± 0.003	36 ± 10	3600
T199N	0.022 ± 0.011	20 ± 5	909
T199S	0.009 ± 0.002	9 ± 1	1000

Table 2.6: Zn^{2+}/Cu^{2+} specificity of second shell mutants

DISCUSSION

To demonstrate the utility of Dps as the donating fluorophore in our metal specificity studies, we first determined the binding affinity of the CA(II) mutants for Dps (Table 2.1). Amino acid substitutions at position 199 affect the binding of Dps differentially. These data suggest that the dissociation constants for Dps are related to the hydrophobicity of the active site cavity, rather than the ability of the side chain at T199 to form a hydrogen bond with Dps. Although these mutations decrease the Dps affinity compared to that of "WT" CA(II), changes in the Dps fluorescence can still be used to monitor zinc binding to CA(II).

To delineate the essential structural features that lead to Zn^{2+}/ Cu^{2+} specificity, we altered the size and hydrophobicity of the amino acids at positions 92 and 199 that form hydrogen bonds with the His94 and H_2O zinc ligand, respectively. The following section discusses the zinc and copper affinity of these CA(II) variants and their interactions with the zinc-water ligand.

T199A-The crystal structure of wild type CA(II) shows that the hydroxyl oxygen of T199 accepts a hydrogen bond from the zinc-bound water, one of the four direct zinc ligands [133]. A second hydrogen bond is formed between the hydroxyl hydrogen of T199 and a carboxylate oxygen of Glu-106. In previous work, mutation of T199 to Ala decreased the zinc affinity decreased by an order of magnitude [66] . Ippolito et al. have previously used X-ray crystallography to evaluate the T199A mutant structure [61]. These data show that the overall structure of this mutant is very similar to WT CA(II), however, the position of the

zinc-bound water shifts which allows the formation of a hydrogen bond with Glu-106 [139].

T199V-Substitution of valine for threonine at position 199 decreases the affinity for Zn^{2+} almost 75-fold compared to wild type CA(II). One interpretation of the decrease in affinity is that the hydrogen bond with the zinc-water ligand significantly stabilizes the bound metal ion. However, the crystal structure of T199V CA(II) indicates that Glu-106, which hydrogen bonds with the T199 side chain in WT, forms a novel hydrogen bond to the zinc ligand, His-96 [140]. Furthermore, the pK_a of the zinc-bound water increases to 8.7. Zinc affinity of WT CA(II) is dependent on pH due to the differential pK_a values of zinc-bound water in solution Zn-H_2O pK_a ~9-10) and bound to CA(II) (pK_a=6.8). Therefore, the observed decrease in Zn^{2+} affinity may be related to this change in pK_a. The pK_a of Cu^{2+}-bound water in CA(II) is unknown but is likely higher than Zn^{2+} due to the increased number of ligands. Therefore, effects on the pK_a of the metal-water ligand could lead to the observed alterations in the Zn^{2+}/ Cu^{2+} selectivity for the T199V variant.

T199G-Substitution of glycine for threonine at position 199 decreases the affinity for zinc almost 50-fold compared to wild type CA(II). The structure of copper bound to CA(II) demonstrates that copper forms a trigonal bipyramidal geometry common to copper binding sites by coordination of two water molecules. This mutation was proposed to stabilize the metal coordination of multiple water molecules, perhaps by the increased volume around the metal site.   Contrary to our prediction, copper affinity was not enhanced in the glycine

mutant, indicating that deletion of the Thr side chain modestly destabilizes, rather than stabilizes, Cu^{2+}-bound CAII.

T199I-Similar to T199G and T199V, substitution of isoleucine for threonine at position 199 decreases the affinity for zinc almost 50-fold compared to wild type CA(II). The observed decrease in Zn^{2+} affinity may be similarly related to an increase in the pK_a of the bound Zn-H_2O.

T199S and T199N-The T199S and T199N mutations retain a group that is capable of forming a hydrogen bond with the metal-water ligand. Both of these substitutions decrease zinc affinity (10-20-fold) but the decreases are smaller than those observed for mutations that cannot form hydrogen bonds. This observation is consistent with the suggestion that this hydrogen bond stabilizes zinc affinity. Copper binding affinities for these mutants are unchanged.

The the carboxamide side chain of Q92 is a hydrogen bond acceptor for the protonated nitrogen atom in the imidazole ring of H94. .Characterization of mutations at this residue allows evaluation of the role of second shell ligands in determining Zn^{2+}/Cu^{2+} selectivity. Structures of these mutants demonstrate that the hydrogen bond between zinc-bound hydroxide and the side chain of T199 is maintained and that zinc-protein ligand coordination distances do not differ significantly from those of wild type CA(II) [65].

Q92A and Q92L-Removal of the side chain that functions as a hydrogen bond acceptor for the His-94 zinc ligand and replacement by a hydrogen bond with a solvent molecule in the Q92A mutant decreases zinc affinity 20-fold. In

the variant Q92L the zinc affinity is decreased by 35-fold. The electron density

map of Q92L CA(II) shows that a solvent molecule cannot be recruited to

form a hydrogen bond to H94 [141]. These data demonstrate that the second

shell ligand stabilizes zinc affinity, perhaps by orienting the His side chain in the

apo-enzyme to the tetrahedral geometry observed in the zinc-bound enzyme.

Copper (II) binds to CA(II) with trigonal bypyramidal geometry, suggesting that

removal of a hydrogen bond might increase selectivity for copper relative to zinc.

Indeed, our metal affinity measurements show modest effects on the copper

affinity but zinc affinity is decreased 35-fold, leading to a change in the Zn^{2+}/Cu^{2+}

selectivity of the 2nd-shell variants of CA(II).

SUMMARY

The indirect ligands in metalloenzymes have been proposed to orient the ligands for optimal metal coordination based on a few key design characteristics: structure, composition and binding site environment. To examine the molecular determinants of the metal ion specificity, we measured the Zn^{2+}/Cu^{2+} binding ratios of 7 CA(II) mutants that differ with respect to the size and hydrophobicity at the positions 92 and 199. The general trend is that any change in the indirect ligands for the wild type polyhedron decreases metal ion affinity overall, but reduces Zn^{2+} affinity much more than the affinity for Cu^{2+}. The largest perturbations in the Zn^{2+}/Cu^{2+} ratio are observed for the Q92L and T199I variants where decreased zinc affinities relative to stabilized copper affinities increase the K_{Zn}/K_{Cu} by 30-f and 47-fold, respectively. One important success of this work was the development of a series of CA(II) variants with significantly improved properties for sensing copper in the presence of zinc.

One hypothesis for altering metal specificity is that the size of the metal ion binding site can influence the metal selectivity. The larger site "should" favor the binding of a large ion over that of a small ion. In addition, larger binding sites might stabilize the binding of metal-water ligands. However, as seen in Table 2.6 the size of the substituted side chain at position 199 does not influence the binding selectivity for Zn^{2+} versus Cu^{2+}. Nonetheless, the effect of mutations to the second shell ligands on metal binding is large and variable, suggesting that the second shell ligands play varied roles, including orientation of direct ligands and electrostatic effects transmitted through the direct ligands [106]. A clear

74

trend is presented suggesting that hydrogen bonding to second shell ligands influences metal ion selectivity in CA(II) by specifically enhancing zinc affinity. These data, support the proposal that the geometry of the direct ligands in the active site of the apo-enzyme is important for determining metal ion specificity in CA(II).

REFERENCES

[1]   K.A. McCall, C.A. Fierke, Probing determinants of the metal ion selectivity in carbonic anhydrase using mutagenesis, Biochemistry 43 (2004) 3979-3986.

[2]   D.J. Eide, Zinc transporters and the cellular trafficking of zinc, Biochim Biophys Acta 1763 (2006) 711-722.

[3]   L.L. Kiefer, C.A. Fierke, Functional characterization of human carbonic anhydrase II variants with altered zinc binding sites, Biochemistry 33 (1994) 15233-15240.

[4]   J.A. Tainer, E.D. Getzoff, K.M. Beem, J.S. Richardson, D.C. Richardson, Determination and analysis of the 2 A-structure of copper, zinc superoxide dismutase, J Mol Biol 160 (1982) 181-217.

[5]   C.A. Fierke, R.B. Thompson, Fluorescence-based biosensing of zinc using carbonic anhydrase, Biometals 14 (2001) 205-222.

[6]   J.A. Ippolito, T.T. Baird, Jr., S.A. McGee, D.W. Christianson, C.A. Fierke, Structure-assisted redesign of a protein-zinc-binding site with femtomolar affinity, Proc Natl Acad Sci U S A 92 (1995) 5017-5021.

[7]   L.L. Kiefer, S.A. Paterno, C.A. Fierek, Hydrogen Bond Network in the Metal Binding Site of Carbonic Anhydrase Enhances Zinc Affinity and Catalytic Efficiency, Journal of the American Chemical Society 117 (1995) 6831-6837.

[8]   K. Hakansson, M. Carlsson, L.A. Svensson, A. Liljas, Structure of Native and Apo Carbonic Anhydrase-Ii and Structure of Some of Its Anion Ligand Complexes, Journal of Molecular Biology 227 (1992) 1192-1204.

[9]   J.D. Cox, J.A. Hunt, K.M. Compher, C.A. Fierke, D.W. Christianson, Structural influence of hydrophobic core residues on metal binding and specificity in carbonic anhydrase II, Biochemistry 39 (2000) 13687-13694.

[10]   J.A. Hunt, M. Ahmed, C.A. Fierke, Metal binding specificity in carbonic anhydrase is influenced by conserved hydrophobic core residues, Biochemistry 38 (1999) 9054-9062.

[11]   S.K. Nair, T.L. Calderone, D.W. Christianson, C.A. Fierke, Altering the mouth of a hydrophobic pocket. Structure and kinetics of human carbonic anhydrase II mutants at residue Val-121, J Biol Chem 266 (1991) 17320-17325.

[12]   M.M. Ling, B.H. Robinson, Approaches to DNA mutagenesis: an overview, Anal Biochem 254 (1997) 157-178.

[13]   F. Sanger, G.M. Air, B.G. Barrell, N.L. Brown, A.R. Coulson, C.A. Fiddes, C.A. Hutchison, P.M. Slocombe, M. Smith, Nucleotide sequence of bacteriophage phi X174 DNA, Nature 265 (1977) 687-695.

[14]   R.F. Chen, J.C. Kernohan, Combination of bovine carbonic anhydrase with a fluorescent sulfonamide, J Biol Chem 242 (1967) 5813-5823.

[15]   H. Edelhoch, Spectroscopic determination of tryptophan and tyrosine in proteins, Biochemistry 6 (1967) 1948-1954.

[16]   R.B. Thompson, B.P. Maliwal, H.H. Zeng, Zinc biosensing with multiphoton excitation using carbonic anhydrase and improved fluorophores, J Biomed Opt 5 (2000) 17-22.

[17]   K.A. McCall, C. Huang, C.A. Fierke, Function and mechanism of zinc metalloenzymes, J Nutr 130 (2000) 1437S-1446S.

[18]   R. Bozym, T.K. Hurst, N. Westerberg, A. Stoddard, C.A. Fierke, C.J. Frederickson, R.B. Thompson, Determination of zinc using carbonic anhydrase-based fluorescence biosensors, Methods Enzymol 450 (2008) 287-309.

[19]   Y. Xue, A. Liljas, B.H. Jonsson, S. Lindskog, Structural analysis of the zinc hydroxide-Thr-199-Glu-106 hydrogen-bond network in human carbonic anhydrase II, Proteins 17 (1993) 93-106.

[20]   J.F. Krebs, C.A. Fierke, Determinants of Catalytic Activity and Stability of Carbonic Anhydrase II as Revealed by Random Mutagenesis, Journal of Biological Chemistry 268 (1993) 948-954.

[21]   C.A. Lesburg, C. Huang, D.W. Christianson, C.A. Fierke, Histidine --> carboxamide ligand substitutions in the zinc binding site of carbonic anhydrase II alter metal coordination geometry but retain catalytic activity, Biochemistry 36 (1997) 15780-15791.

[22]   C.A. Lesburg, M.D. Lloyd, D.E. Cane, D.W. Christianson, Crystallization and preliminary X-ray diffraction analysis of recombinant pentalenene synthase, Protein Sci 4 (1995) 2436-2438.

[23]   R.B. Thompson, B.P. Maliwal, V.L. Feliccia, C.A. Fierke, K. McCall, Determination of picomolar concentrations of metal ions using fluorescence anisotropy: biosensing with a "reagentless" enzyme transducer, Anal Chem 70 (1998) 4717-4723.

CHAPTER 3: Tuning Metal Sensitivity and Ratiometric Change with Design of an Expressible FRET-based Carbonic Anhydrase Zn(II) Sensor

INTRODUCTION

The physiological importance of Zn^{2+} demands that cells maintain control over the homeostasis of this metal ion. Although most of the intracellular Zn^{2+} is tightly bound, serving as a structural and catalytic cofactor for a number of cellular proteins, it is ubiquitous among the compartments of the cell [58]. Well-studied examples of the role of zinc in a number of human disorders and biochemical pathways have been outlined in the introduction of this work (see Chapter 1). Despite the acceptance of these phenomena, the mechanistic details surrounding intracellular Zn^{2+} storage, transport and function are poorly defined even in the simplest of organisms [142]. Several families of fluorescent Zn^{2+} probes have been designed to address the need to understand the spatial and temporal distribution of ionic zinc pools in living cells [143], [40]. However, these sensors typically lack selectivity between the cytosol and subcellular compartments. More importantly, these probes are limited in their ability to detect free Zn^{2+} concentrations below the nanomolar range [144],[145]. Likewise, the TAT-tag mediated delivery of ratiometric CA(II) sensors, which has been successfully applied to mammalian cell lines to detect pM levels of readily exchangeable zinc, cannot be taken up by other organisms in the cell without

detrimental effects. Also, the chemical labeling of this isolated protein with the AlexaFluor fluorophore is tedious, labor intensive, and does not always proceed in high yield.   Until recently, genetically encoded fluorescence based sensor proteins with higher binding affinity and full cell compatibility remained underdeveloped. Vinkenborg et al developed a FRET- based sensor that can ratiometrically monitor intercellular zinc fluctuations in the cytosol and subcellular organelles [146].

Here we describe an advancement in CA(II)-based zinc sensing that can be readily expressed in cells. The expressible sensor is constructed by fusing a fluorescent protein to CA(II) as a fluorescence acceptor and using a zinc-dependent FRET donor, dapoxyl sulfonamide; as used in our earlier generation sensors. The relatively small size of the fluorescent protein variants and CA(II) means that efficient energy transfer between the dapoxyl sulfonamide and the fluorescent protein acceptor is feasible. An ideal candidate fluorescent protein for an expressible CA(II) sensor should meet the following criteria: excitation spectrum overlaps with the emission of dapoxyl sulfonamide to ensure good FRET efficiency, high extinction coefficient and quantum yield, fast maturation, and monomeric state. Fluorescent proteins have been applied successfully as non-invasive labels to study protein localization, dynamics and interactions in living cells[48].

The first and most studied of this class is the Green Fluorescent Protein (GFP) that was originally isolated from the hydroid jellyfish Aequorea Victoria [147]. The fluorophore of GFP resides within an 11- stranded β-barrel and is

formed autocatalytically by spontaneous cyclization of three amino acids; serine,

tyrosine and glycine [148]. Mutagenesis of GFP has generated a variety of

fluorescent proteins with shifted wavelengths of excitation and emission, ranging

from blue to red [149]. Besides mutations that affect the spectral properties,

numerous modifications have been described that improve the photophysical

properties, environmental stabilities and protein folding properties [150], [151].

Directed evolution studies have generated a large pool of fluorescent proteins

that can be used for this purpose, such as variants of RFPs from Discosoma sp.

and Entacmaea quadricolor [127]. This great work creating fluorescent proteins

with far red shifted excitation and emission profiles that reduce the problem of

autofluorescence making them more suitable for imaging in whole tissues or

organisms has recently been published [152]. Furthermore, fluorescent proteins

with different spectra can be coupled to CA variants with different zinc affinities,

thus creating a multicolor measurement covering a wide dynamic range in a

single experiment. This chapter illustrates our initial experiments to prepare and

analyze mOrange and mCherry fusion proteins for use as an expressible zinc

sensor.

MATERIAL AND METHODS

DNA Cloning and Mutagenesis:

Bacterial Vector Design:

The construction of the fusion proteins of CA(II) and mCherry and

mOrange used the pACA1 vector, encoding CA and the pRSET-B vector (Figure

3.1) encoding the fluorescent proteins, both under the control of a T7 promoter,

as
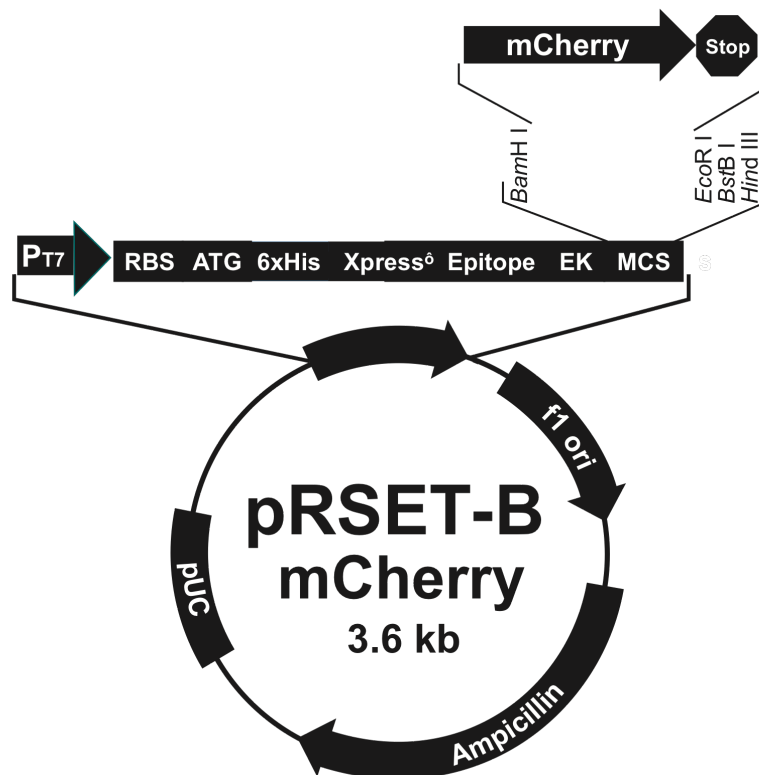
Figure 3:1: Map of pRSET-B:

The pRSET vectors are pUC-derived expression vectors designed for high-level protein expression and purification of cloned genes in *E. coli*. High levels of expression of genes cloned into the pRSET vectors are made possible by the presence of the T7 promoter

the starting template [134]. The Tsien group of the Howard Hughes Medical Institute at the University of California, San Diego (UCSD) donated the mCherry and mOrange plasmids. Extension of overlapping gene segments by PCR is a simple, versatile technique for site-directed mutagenesis. Initial PCR's generate overlapping gene segments that are then used as template DNA for another PCR to create a full-length product. Internal primers generate overlapping, complementary 3' ends on the intermediate segments and introduce nucleotide substitutions, insertions or deletions for site-directed mutagenesis, encode the nucleotides found at the junction of adjoining gene segments [153]. Overlapping strands of these intermediate products hybridize at this overlapping region in a subsequent PCR and are extended to generate the full-length product that can include restriction enzyme sites for inserting the product into an expression vector for cloning purposes.

To construct a vector encoding the CA_mCherry and CA_mOrange fusion proteins, PCR-amplified fragments encoding each individual protein were generated from the native plasmids with appropriate primers (Table 3.1).

Primer Name	Primer Sequence (5'------> 3')
A	GAA ATA ATT TTG TTT AAC TTT AAG AAG GAG ATA TAC CAT GG
B	CTC CTC GCC CTT GCT CAC TCC GCC ACC TTT GAA GGA AGC
C	GCT TCC TTC AAA GGT GGC GGA GTG AGC AAG GGC GAG GAG
D	GTC TCC TTT CGG GCT TTG TTA GCA GCC GGA TCA AGC TT

Table 3.1: Overlap Extension PCR PrimersTable

The sequence between CA(II) and mCherry(mOrange) is a three glycine (GGG) linker. In this method, first the CA(II) gene is amplified using a 3' primer that extends the 3' end of the gene and, separately, the mCherry gene is amplified using a 5' primer that adds the complementary sequence to the 5' end of this gene. Secondly, the two fragments are mixed, denatured and re-annealed. In the absence of added primers, the complementary region of the two fragments act as primers forming a full-length fusion gene (Figure 3.2). In the next step, the CA_mOrange and CA_mCherry are amplified using primers complimentary to the
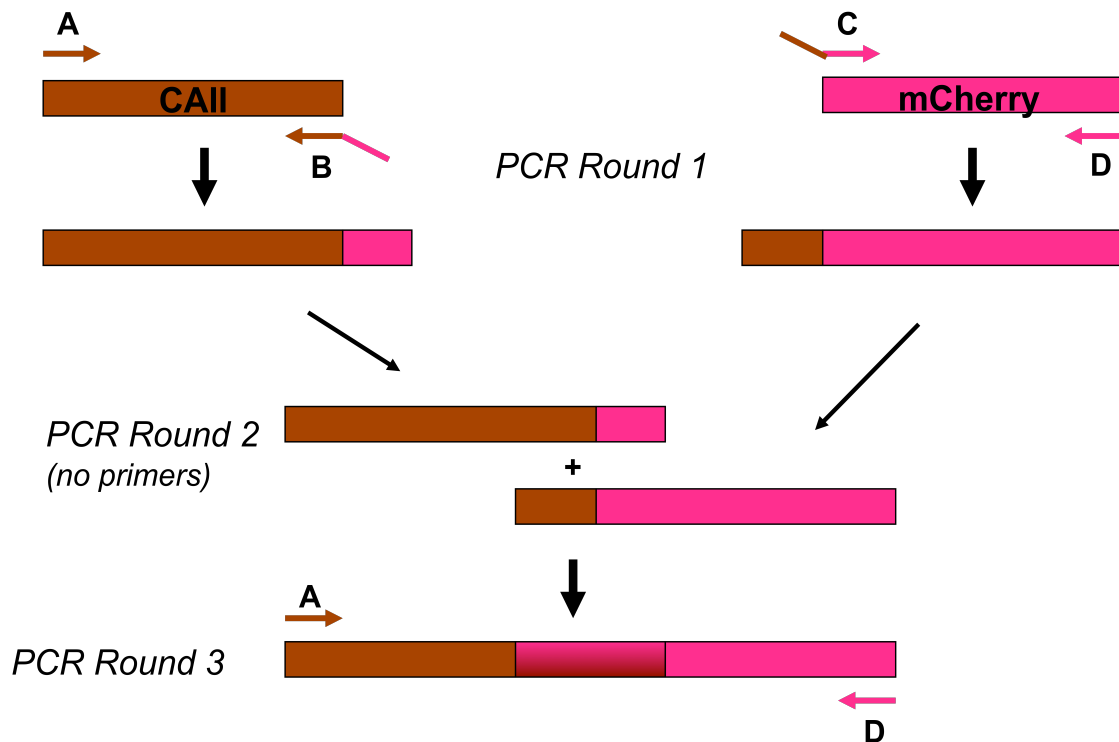
Figure 3:2: Fusion of CA(II) (brown) and mCherry (pink) sequences by overlap extension PCR:

The CA(II) region is amplified with primers A and B, and the mCherry region is amplified with primers C and D. Primers B and C are reverse complementary and are specific to the part of the fused region encoding the GGG-linker. When mixed together, the PCR products will hybridize and extend from the overlap site. The fusion product is amplified from primers A and D

5' end of CA and the 3' end of mCherry. These primers also included the following restriction sites: Nco1 (5' end of CA(II)) and HindIII (3' ends of the fluorescent proteins.

Finally, the DNA product encoding the CA_mCherry and CA_mOrange fusion protein, was PCR amplified for further optimization using TOPO Cloning Technology (Invitrogen, Life Technologies). Ligation of our fusion products into a multiple cloning vector allows us to manipulate our fusion product with higher

efficiency introduced. The CA_mCherry and CA_mOrange fragments were ligated into the TOPO vector at the Nco1 and HindIII restrictions sites. Finally, the DNA encoding the CA(II)_FP were PCR amplified using GGG**GAATTC**ATGGCCCATCACTGGGGGTA primers as a forward and GGG**CTCGAG**TCTTGTACAGCTCGTCCATGCC as a reverse primer, hereby introducing EcoR1 at the 5' end and Xho1 3' end along the gene via Zero Blunt® TOPO® PCR Cloning. The modified gene of the CA_mCherry protein was completely removed from the TOPO vector with alkaline phosphatase,CIP (from NEB, Beverly, MA). Calf intestinal alkaline phosphatase catalyzes the removal of the 5' phosphate from DNA, thus restricting re-ligation of the vector alone. A compatible modified CA_mOrange fragment was generated by digestion of the CA_mOrange TOPO vector with the same restriction enzymes. Resulting, CA_mOrange and CA_mCherry fragments were purified by separation on an agarose gel prepared with Molecular Biology grade agarose (Bio-Rad) and electrophoresed in modified TAE buffer (40 mM TRIS-acetate, 0.1 mM EDTA, pH 8.0). The appropriate bands were excised from the gel and the DNA was recovered using the Montage DNA Gel Extraction Kit (Millipore). The concentration of the DNA recovered from the gel was generally low ng/µL concentrations.

Ligation reactions of the fusion products, encoding the EcoR1 and Xho1 restriction sites, into the bacterial vectors pET23a and pET20b were performed in 1X T4 DNA ligase buffer (50 mM Tris-HCl, 10 mM $MgCl_2$, 10 mM Dithiothreitol 1 mM ATP, pH 7.5 @ 25°C. Supplied as a 10X concentrated stock) using 5 µL of

vector, 5 µL of insert DNA and 1 µL of T4 DNA Ligase (NEB) in a total volume of

50 µL. Vector-only control ligations were also prepared. The ligation mixes were

incubated overnight on ice. The following day, 5 µL of the ligation mix was

transformed into 50 µL of chemically competent SmartCells following the protocol

provided (Open Biosystems, Huntsville, AL). This protocol calls for mixing the

ligation mix and the competent cells on ice for 15 min, followed by 45 s at 42°C.

The heat shocked cells were added to 250 µL of media SOC media and

incubated at 37°C for 1 h in an air incubator.   All of the transformed cells were

plated out onto LB-agar plates with 100 µg/mL ampicillin and incubated at 37°C

overnight. Vector re-ligation was determined from the number of colonies

observed on the vector only control plates and all samples showed more colonies

on the vector plus insert plates. Unfortunately, the number of colonies were not

estimated and documented. Single colonies from the vector plus insert plate

were used to inoculate 50 mL LB-amp liquid cultures, and grown overnight at

37°C. The plasmid DNA was isolated using the Qiagen Hi-Speed Midi Plasmid

Kit and the purified plasmids were submitted for DNA sequencing. The resulting

DNA construct encoding CA_mOrange and CA_mCherry, named p23aCA_mO

or p23aCA_mC p20bCA_mO or p20bCA_mC contains a T7 promoter for over-

expression and the linker inserted between CA(II) and mCherry (Table 3.2). The

map of the CA(II)_mCherry fusion protein are shown in Figures 3.3-3.4.

In efforts to further optimize this sensor technology, a third bacterial

vector, pET24a encoding CA_mCherry was generated by Da Wang (Fierke Lab).

The protein was digested from the pAH_CA_mCh vector and PCR amplified. The

amplified CA_mCherry gene was inserted in the BamH1 and Xho I sites of the

pET24a vector, generating p24aHCA_mCh. Because the TAT tag is upstream of

BamHI it was not included in the final fusion product. This plasmid contains a

histidine tag on the C-terminus (3' end of mCherry).
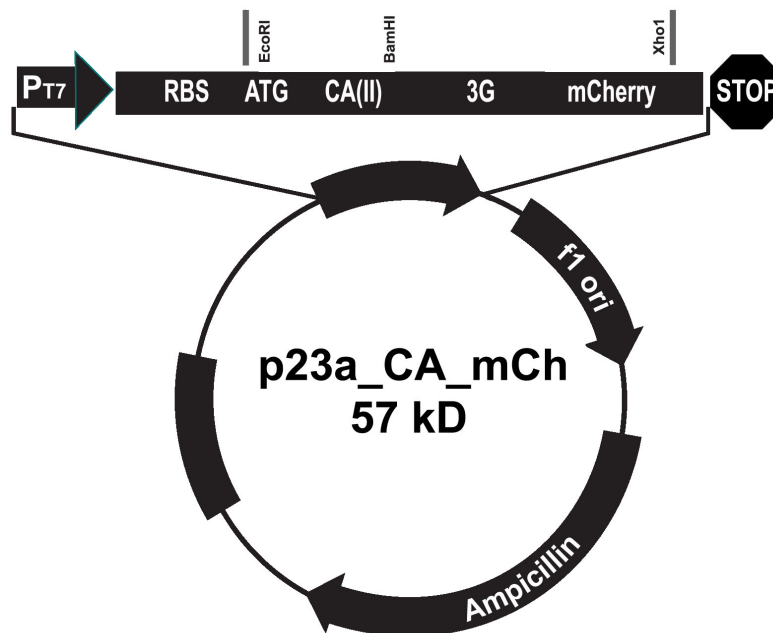
Figure 3:3: Map of pET23A_mCherry:

CA(II)_mCherry was inserted into the pET23a vector between the EcoRI and
Xho1 sites. "3G" represents the tri-glycine linker. The plasmid is expressed under
the control of the T7 promoter and is an Ampicillin-resistance gene

Vector Name	Encoded Protein	Linker Sequence	Parent Vector	Mutations
pACA1[a]	CA(II)			Xho1 site added→ 5'-CTCGAG-3'
pRSET-B[b]	mCherry/mOrange			
p23a_CA_mCh[c]	CA(II)_mCherry	GGG	pACA1 and pRSET-B	EcoR1 site added→ 5'-GAATTC-3' Xho1 site added
pAHT_CA_mCh[d]	CA(II)_mCherry	GGG	pAHT1 and p23a_CA_mCh	N-termini HIS_6 removed C-termini HIS_6 added
p20b_CA_mCh[c]	CA(II)_mCherry	GGG	pACA1 and pRSET-B	EcoR1 site added Xho1 site added
p24aH_CA_mCh[e]	CA(II)_mCherry	GGG	pAHT_CA_mCh	
pRS316-CA_mC[c]	CA(II)_mCherry	GGG	pACA1 and pRSET-B	Sal1 site added→ 5'-GTCGAC-3' Not1 site added→ 5'-GCGGCCGC-3'

Table 3.2: Summary of CA(II) and fluorescent protein vectors:

Summary of vectors used and constructed including the vector name, the encoded protein, linker sequence (if applicable), the parent vector and any mutations made. CA(II)_mOrange versions of these plasmids were also constructed. [a – from 16; b – Donated by the Tsien group; c – constructed by Tamiika Hurst; d – constructed by Andrea Stoddard ; e – constructed by Da Wang]

Mammalian vector design:

A TAT_CA_mCherry gene was generated using overlap extension using pAHT1 encoding His6-TAT-wtCA in pACA1 and the p23a_CA_mCh plasmid encoding CA_mCherry under the control of a T7 promoter, were used as the starting templates. The resulting fusion product, mCherry fused to the 3' end (C-termini) of CA(II) by a three glycine linker was re-ligated into the pET23a vector at the EcoRI and XhoI sites, creating pAHT_CA_mCh. The HIS-6 tag on the N-

termini was removed and added to the C-termini end by QuikChange

mutagenesis (Stratagene) (Figure 3.5).

Eucharyotic vector design:

For expression of CA(II)_mCherry and CA(II)_mOrange in *S. cerevisiae*,

the fused gene containing the tri-glycine linker was PCR amplified from the

TOPO vector using primers complimentary to the 5' end of CA and the 3' end of

mCherry. These primers also included the following restriction sites: Sal1 (5' end

of CA(II)) and Not1 (3' ends of the fluorescent proteins). Both mutations were

introduced at the same time using the quickchange multi-site directed

mutagenesis kit (stratagene) with forward and reverse primers

GGG**GTCGAC**ATGGCCCATCACTGGGGGTA and

GGCG**GCGGCCGC**TTACTTGTACAGCTCGTCCATG, respectively. All

restriction site changes were confirmed either by restriction enzyme digestion

and/or DNA sequencing. The molecular biology protocols used to subclone the

digested product encoding the fusion protein linked by a tri-glycine sequence into

the Sal1 and Not1 sites of pRS316 are the same as those detailed for the

construction of the bacterial vectors. The resulting vectors were named

pRS316_CA_mCh and pRS316_CA_mO (Table). The fusion proteins can be

expressed in yeast strains DY1457 and ZHY1 (provided by David Eide,

University of Missouri) by induction with galactose (Figure 3.6). The *in vivo*

concentration of the fusion protein can be estimated from the fluorescence of

intact cells and crude cellular lysates.
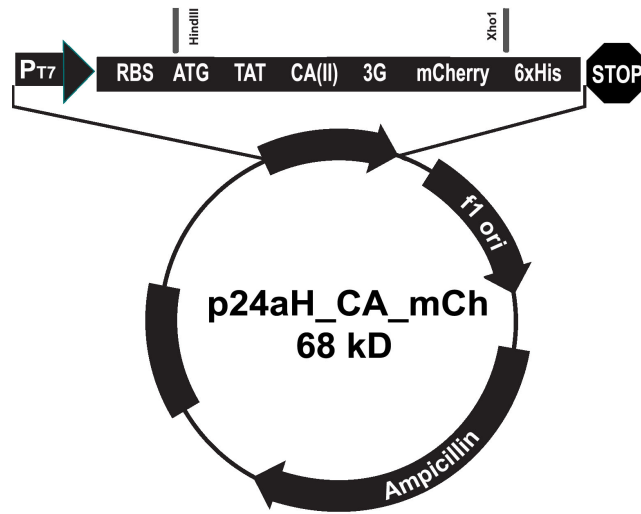
Figure 3:4: Map of pET24A_CA(II)_mCherry:

CA(II)_mCherry was inserted into the pET24a vector between the BamH1 and Xho1 sites. "3G" represents the tri-glycine linker. The plasmid is expressed under the control of the T7 promoter and is an Ampicillin-resistance gene. The plasmid contains a C-term His-Tag
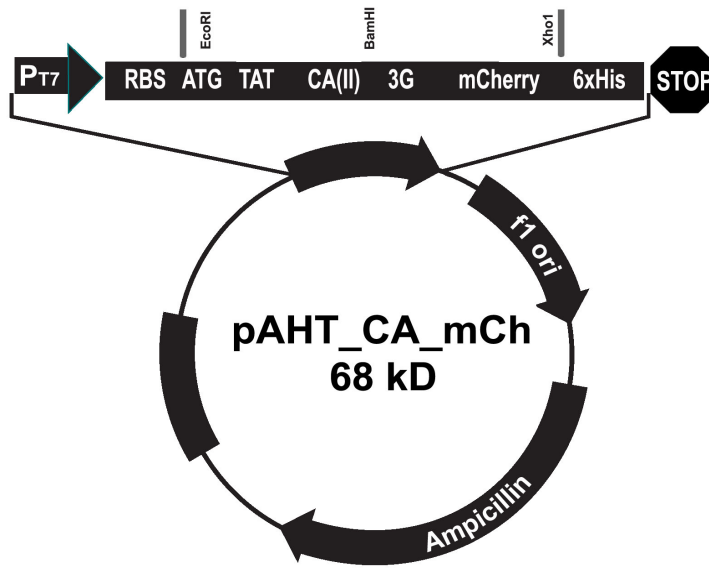
Figure 3:5: Map of pET23a_TAT_CA(II)_mCherry:

CA(II)_mCherry was inserted into the pET23a vector between the EcoR1 and Xho1 sites. "3G" represents the tri-glycine linker. The plasmid is expressed under the control of the T7 promoter and is an Ampicillin-resistance gene. The plasmid contains a C-term His-Tag with the TAT-tag can be expressed in mammalian cell lines
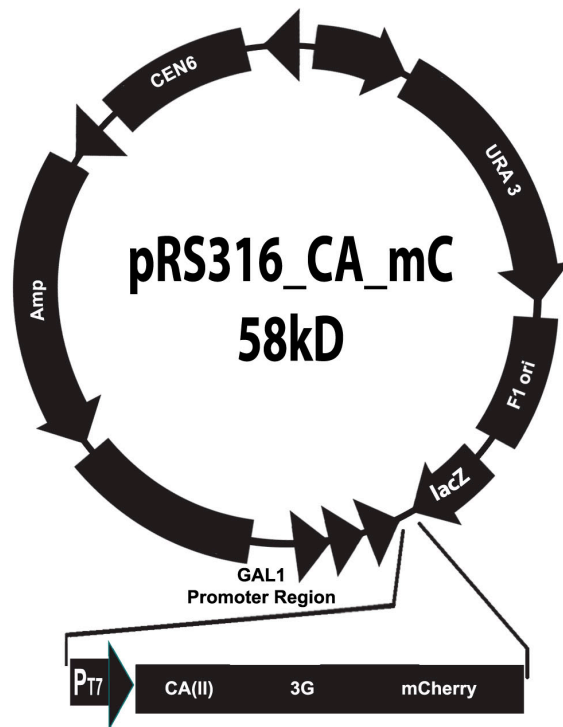
Figure 3:6: Map of pRS316_CA(II)_mCherry:

CA(II)_mCherry was inserted into the pRS316 yeast vector between the Sal1 and Not1 sites. "3G" represents the tri-glycine linker. The plasmid is expressed under the control of the T7 promoter and is an Ampicillin-resistance gene

Protein expression and purification in *E. coli*:

The protocol used for recombinant expression of the CA(II)-fluorescent

protein fusion in bacterial cells is modified from the methods used to overexpress

CA(II) [154], and used to purify the CA(II) only proteins. Chemically competent

BL21(DE3) *E. coli* were transformed with the appropriate plasmid encoding HIS-

tagged CA(II)_FP fusion and grown overnight on LB ampicillin agar plates. A single colony was selected from the LB-amp plates and grown overnight at 37°C in liquid 2XYT-amp culture. The cells were diluted 1:200 in 2XYT, grown at 37°C until OD_{600}= 0.7-0.75 and protein induced by the addition of 1 mM isopropyl β-D-thiogalactopyranoside (IPTG). After 6 h of incubation at 25°C, the cells were harvested by centrifugation at 4°C for 15 min at 6,000 xg. The cell pellet was resuspended in 10 mL per liter of culture of cold 50 mM TRIS-SO$_4$ pH 8.0, 50 mM NaCl, 200 μM ZnSO$_4$, 1 mM dithiothreitol (DTT), 10 μg/mL PMSF and 1 μg/mL TAME prior to flash freezing.

After thawing, the cells were lyzed using a microfluidizer and the cellular debris removed by centrifugation (45 min, 10,000 xg). A 1.0% streptomycin sulfate precipitation was performed and the debris removed by centrifugation (30 minutes, 10,000 xg). The resulting protein solution was dialyzed against buffer (30 mM Hepes, pH 8.0, 150 mM NaCl) in preparation for nickel affinity batch chromatography. Nickel (II) is bound to Sepharose fast flow resin (Amersham Biosciences) by chelation using nitriloacetic acid (NTA) [155]. Two milliliters of NTA beads are first washed thoroughly and rinsed with 20 mL of 50 mM EDTA to remove interfering trace metals. Next, the resin is rinsed with 20 mL 0.5 mM NaCl. Salt help promote optimal purification. The salts and EDTA are thoroughly diluted by washing the resin with 40 mL deionized water. To charge the resin with nickel, the resin is incubated with 40 mL of 0.1 M NiSO$_4$ for a minimum 15 min. After the nickel solution is removed the now Ni^{2+}- NTA- beads were rinsed with 40 mL of deionized water. 25 mL protein is added to the resin containing 15 mL

0.5 mM imidazole, 420 μL 5 mg/mL PMSF and 210 μL 1 mg/mL TAME protease

inhibitors. The resin slurry and protein are allowed to stir in a 250 mL beaker at

4°C for 1 h.   Low concentrations of imidazole are used to remove low affinity

bound proteins. The protein is eluted by washing with 1M Hepes buffer, pH 8.0,

continually increasing concentrations of 40 mL volumes of imidazole (50 mM,

100 mM, 150 mM, 250 mM, 300 mM) at room temperature using vacuum

filtration. The fusion protein normally elutes at 200 mM imidazole. The purity

and molecular mass of each fraction was assessed using SDS PAGE. Generally

the fusion protein is >90% pure. The protein is dialyzed against 4 L 30 mM

Hepes, 150 mM NaCl,, adjusted to pH 8.0 overnight at 4°C. After dialysis the

protein concentration was quantified, and the protein was aliquoted, frozen and

stored at 20°C.

Protein quantitation:

For the CA(II) fusion proteins, the protein concentration was estimated

using the absorption of the fluorescent protein (ε_{587nm} = 82620 $M^{-1}cm^{-1}$ for

CA(II)_mCherry and $\varepsilon_{548\,nm}$ = 82620 $M^{-1}cm^{-1}$ for CA(II)_mOrange). The

extinction coefficient for the fusion protein was determined using Vector NTI.

This is an integrated software program that aids in the creation and manipulation

of biological molecules based on sequences analysis.

The concentration of active CA(II) fusion protein was determined by an

active site titration. As previously discussed, this method accurately measures

the number of sulfonamide binding sites, ignoring any contaminating protein and

any CA(II) incapable of binding sulfonamide. An aliquot of purified fusion protein was diluted to a final concentration of 0.5 – 1 µM in 10 mM MOPS, pH 7.0 buffer containing 1-2 µM $ZnSO_4$. The excess zinc is present to insure that all of the CA in the sample is in the zinc bound form. The fluorescent sulfonamide (4 µM of either dansylamide, DNSA or Dps) is added to the protein solution. The concentration of the CA(II) bound fluorescent sulfonamide was monitored either by FRET between the intrinsic protein fluorescence and DNSA (excitation 290 nm, emission 450) or by the fluorescence enhancement of Dps (excitation 365 nm, emission 540 nm) . The CA(II)-fluorescent sulfonamide complex is then titrated with diamox (acetazolamide, Sigma A6011) which has a higher affinity for CA(II) (nanomolar) and binds essentially stoichiometrically. Under these conditions diamox binding to CA(II) is essentially stoichiometric (Figure 3.7). Two linear fits were performed – the first line was fitted to the initial fluorescence decrease (low damox concentrations) and the second line was fitted to the plateau region (high diamox concentrations). The intercept of the two linear fits yields the concentration of holo-CA(II)_Fusion protein active sites.

Dps affinity of CA(II)_mCherry and CA(II)_mOrange:

The fluorescence spectra of CA(II) fusion proteins in the apo-, zinc-bound and Dps-bound forms were measured on the AB2 fluorimeter in 10 mM MOPS, pH 7.0. The response of CA(II)_FP for Dps was measured by adding 2-4 µM Dps to 1 µM holo-CA(II)_FP in 10 mM MOPS, pH 7.0 by monitoring the change
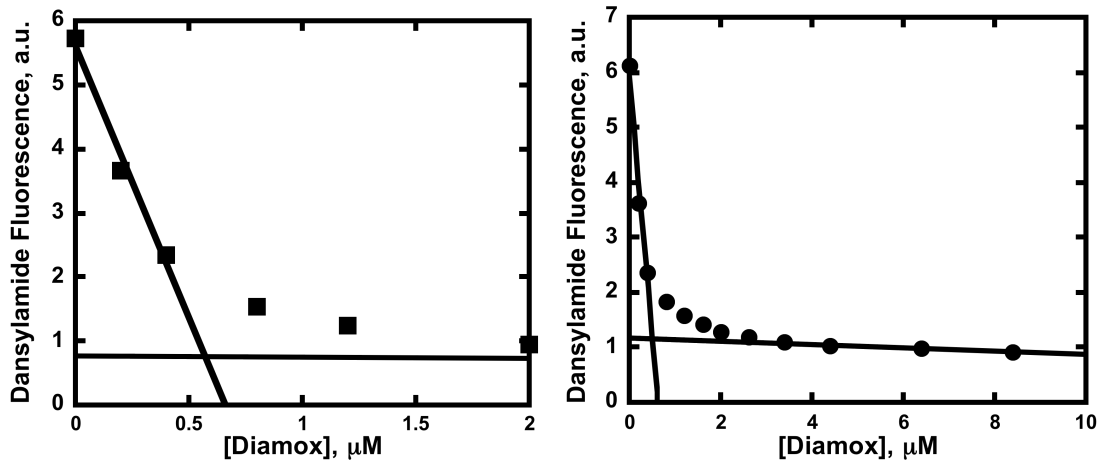
Figure 3:7: Measuring the concentration of active fusion protein:

DNSA fluorescence emission (Ex: 290 nm, Em: 450 nm) as a function of diamox concentration at 1 µM holo- (■) CA(II)_mOrange (●) CA(II)_mCherry with 4 µM DNSA, and 2 µM zinc in 10 mM MOPS, pH 7.0. Two linear fits were performed-The intercept of the two linear fits yields the concentration of holo-CA(II)_Fusion protein active sites

in fluorescence (excitation 365, emission 535 for Dps and excitation 365,

emission 562_mOrange or emission 617_mCherry) for Dps-bound CA(II)_FP and

FRET intensities.

Preparation of *Apo*-enzyme:

To remove the native metal from the purified fusion proteins, 1.5 mL of

sample was incubated in 25 mM DPA in 10 mM metal-free (chelaxed) MOPS

buffer, pH 7.0 overnight, followed by chromatography on a PD-10 column

(Sephadex G-25M, 5cm X 15 cm, Pharmacia) pre-equilibrated with 10 mM metal

free MOPS buffer, pH 7.0. Concentration of the resulting enzyme was done

using an Amicon Ultra concentrator (Millipore). All plasticware and pipette tips

used for preparation of metal free solutions and *apo*-protein was purchased as

"metal free" (Bio-Rad) to minimize metal ion contamination. All solutions were

made using deionized, 18 MΩ water and were stored in the low metal, pre-

treated plasticware. The enzyme concentration was then determined using

absorbance spectroscopy. The bound zinc ion concentration was determined by

ICP-MS. Zinc studies were performed on enzyme containing <10% bound zinc.

Zinc affinity measurements:

To measure the apparent zinc affinity, 100 nM *apo*-enzyme was incubated

with Zn-NTA buffers (See Table). After equilibration at 25°C for 8-12 h, 2 µM Dps

was added to the protein- buffer mixture and allowed to incubate for 30 min. The

ratio of the Dps fluorescence (Ex = 365 nm, Em = 535 nm) to the fluorescent

protein fluorescence (mOrange, Ex = 547 nm, Em= 562; mCherry, Ex = 587 nm,

Em =610) of each of each sample containing varying free zinc concentrations

was measured on an AB2 fluorimeter. A single binding isotherm was fit to the

data to determine the apparent zinc affinity of CA(II)_mOrange and

CA(II)_mCherry.

RESULTS

The expression of genes in mammalian cells has become increasingly important to study a number of biological questions and as a primary method for production of proteins for potential medicinal use. Mammalian cells are frequently used as a host for expression of foreign genes, because of their compatibility to human disorders. To measure zinc in mammalian cells, Andrea Stoddard (Fierke Lab) adapted the CA-based biosensor for uptake by mammalian cells by attaching a TAT (―transactivator of transcription‖) peptide to CA(II)_mCherry. The TAT peptide is encoded by HIV-1 and contains an 11 amino acid (G-Y-R-K-K-R-R-H-R-R-G) protein transduction domain (PTD) allowing the cell to carry the protein across the membrane and into the cytoplasm [156]. Previous studies report that TAT-fused fluorescent-labeled CA(II) was rapidly taken up by cells with no apparent ill effects in concentrations sufficient to permit fluorescence microscopy [157].

Much of our understanding of zinc transport and its regulation in eukaryotes comes from studies of the yeast Saccharomyces cerevisiae [158]. Yeast cells transport Zn with high affinity via a plasma membrane-associated transport proteins. Additionally, various compartments within the cells have zinc transporters that transport zinc into or out of a particular compartment. More specifically, the yeast *Saccharomyces cerevisiae* is a powerful model system for measuring homeostasis of intracellular zinc ions [159]. The use of an expressed CA fusion protein in yeast to detect *in vivo* free zinc has several advantages.

This is due to the biochemical similarity to human cells and ease of growth and genetic manipulation. The activity of these transporters is regulated at both transcriptional and posttranscriptional levels in response to zinc [128], [160]. These different mechanisms work together to precisely balance zinc uptake and its storage and utilization.

Although very reproducible, stoichiometric methods depend on accurate knowledge of the concentration of CA(II) and maintenance of an excess concentration of both CA(II) and sulfonamide. Therefore, stoichiometric methods do not work for *in vivo* measurements where the total zinc concentration is high (~0.2 mM) and well buffered by numerous ligands and consequently difficult to deplete. To address these issues, an excitation ratiometric method was developed based on Förster resonance energy transfer (FRET) between the cell-permeable sulfonamide, dapoxyl sulfonamide, and the fluorescent protein fused to CA(II) (Figure 3.8). mCherry or mOrange serves as a FRET acceptor for the bound sulfonamide, such that emission from the bound sulfonamide is efficiently transferred to fluorescent protein, which emits at much longer wavelengths.
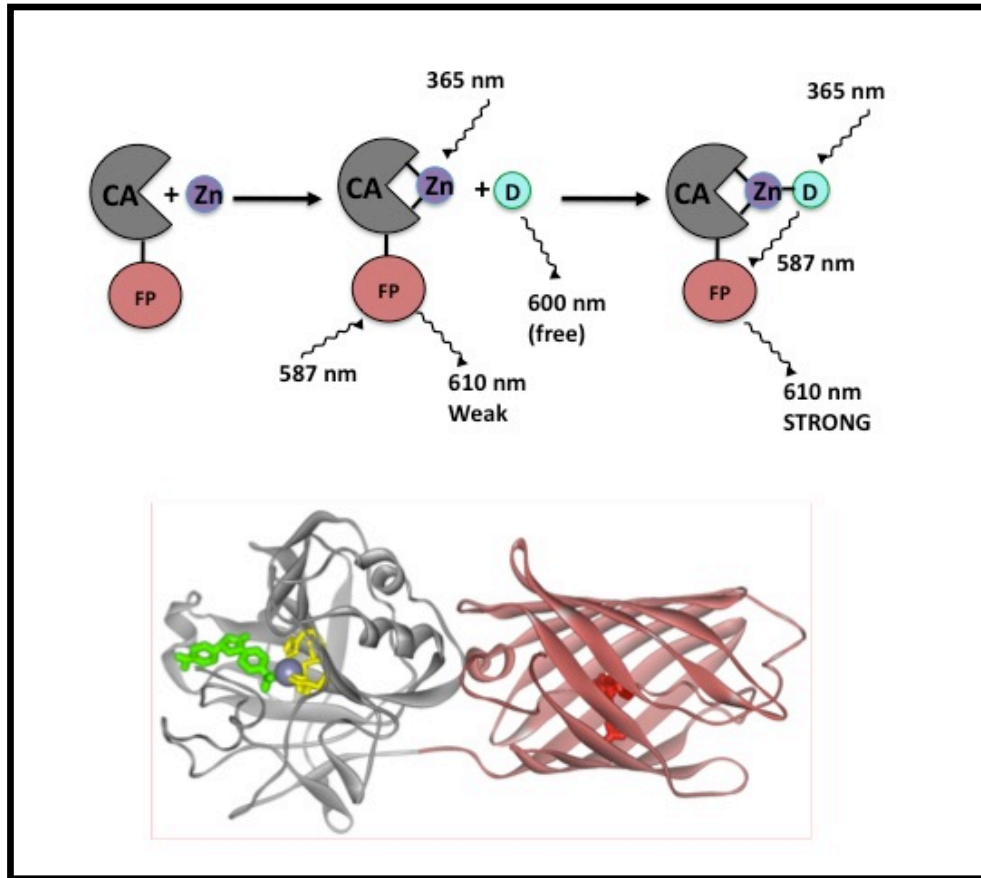
Figure 3:8: Schematic representation of ratiometric zinc sensing using CA(II)_mCherry:

Upon zinc binding to CA(II), Dps binds to the holo enzyme, accompanied by a large change in fluorescence of mCherry. In the absence of zinc, mCherry (Ex = 587 nm, Em = 610 nm) fluorescence is observed when excited at 587 nm. Upon zinc binding, Dps (Ex = 365 nm, Em = 610 nm (bound)) acts as the FRET donor to the acceptor, mCherry, leading to fluorescence emission at 610 nm

A series of vectors encoding CA(II)_mCherry and CA(II)_mOrange constructs have been successfully made. These different vectors are expected to be useful in bacteria and yeast. Initial characterization of the CA(II)_FP proteins encoded by the bacterial and mammalian plasmids, indicate that they have properties suggesting they will be useful for measuring *in vivo* "free" zinc levels.

Fluorescent Protein	Excitation Max (nm)	Emission Max (nm)	Extinction Coefficient $(M^{-1} cm^{-1})$	Quantum Yield	$t_{1/2}$ for maturation
mOrange	547	562	71,000	0.69	2.5h
mCherry	587	610	72,000	0.22	0.25h

Table 3.3: Spectral characteristics of selected monomeric fluorescent proteins:

The physical properties mOrange and mCherry are shown, including the emission wavelength, excitation wavelength, extinction coefficient at that wavelength, the quantum yield of the fluorescence, and the half time for chromophore maturation at 37°C

The spectral characteristics of the fusion protein are listed in Table 3.3 [127]. The excitation properties of mOrange and mCherry and the overlap of its absorbance with the emission of dapoxyl sulfonamide are chosen so that energy transfer between the two fluorophores is quantitative based on the concentration of bound zinc. To demonstrate the utility of Dps as the donating fluorophore to excite the fluorescent protein in our zinc binding studies, we first characterized the spectrum profiles of apo- and holo- forms of the fusion protein pre- and post addition of Dps. (Figure 3.9) The profile of Dps bound to holo-WT-CA(II) is also
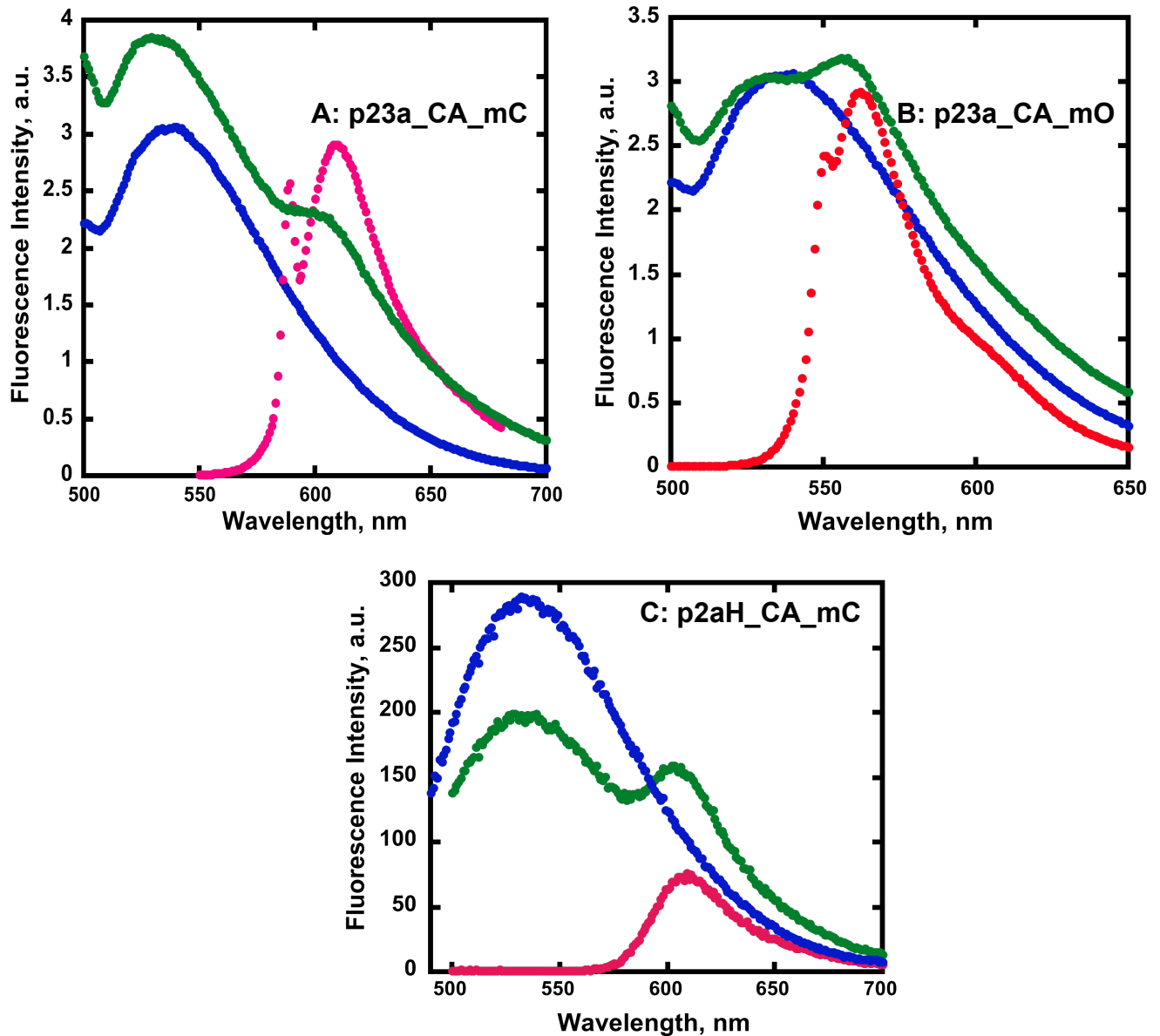
Figure 3:9: CA(II)_mCherry and CA(II)_mCherry emission spectra in the absence and presence of Dps:

A;C) Emission spectra of purified CA(II)_mCherry in 10 mM MOPS, 4 μM Dps, 1.0 μM ZnSO4, pH 7.0 in the absence (—) and presence (—) of Dps. The emission from the fluorescent protein increases upon binding of Dps to the holo-enzyme when excited at 365 nm. B) Emission spectra of CA(II)_mOrange in the absence (—) and presence (—) of Dps. Dps bound to holo-WT-CA(II) is also featured in each set (—)

shown for comparison purposes. Later, dissociation constants were determined by monitoring the increase in fluorescence (excitation = 365 nm, emission wavelength of the fluorescent protein) relative to the emission of the fluorescent protein only upon binding Dps to CA(II).

In particular, the spectral characteristics in the presence and absence of Dps with CA-mOrange and CA-mCherry are suited for zinc sensing under *in vivo* conditions. Upon addition of the Dps to CA_mOrange under *in vivo* conditions, an increase in the mOrange fluorescence is observed (Figure 3.9) at 562 nm when Dps is excited at 365 nm, demonstrating FRET. The FRET signal for mOrange (547 nm) is difficult to distinguish from the Dps emission (535 nm) because the spectral overlap emission is too large (Figure 3.9).

Similarly, with CA_mCherry, a shoulder is observed at 610 nm, at the right-hand side of the mCherry peak at approximately 610 nm when excited at 365 nm indicating FRET due to the large difference between the emission maximum for Dps (535 nm) and the excitation maximum of mCherry (587 nm) leading to poor spectral overlap and a smaller FRET signal upon Dps binding. The change in signal observed at 535 nm in the presence of Dps suggests that the binding of sulfonamides is not compromised.

Additionally, these ratiometric zinc sensors using CA(II) fused to a fluorescent protein with Dps bound were investigated in the presence of a increasing amounts of competing inhibitor, exthoxzolamide and diamox (See Figure 3.10). The decrease in Dps fluorescence was monitored over time until the
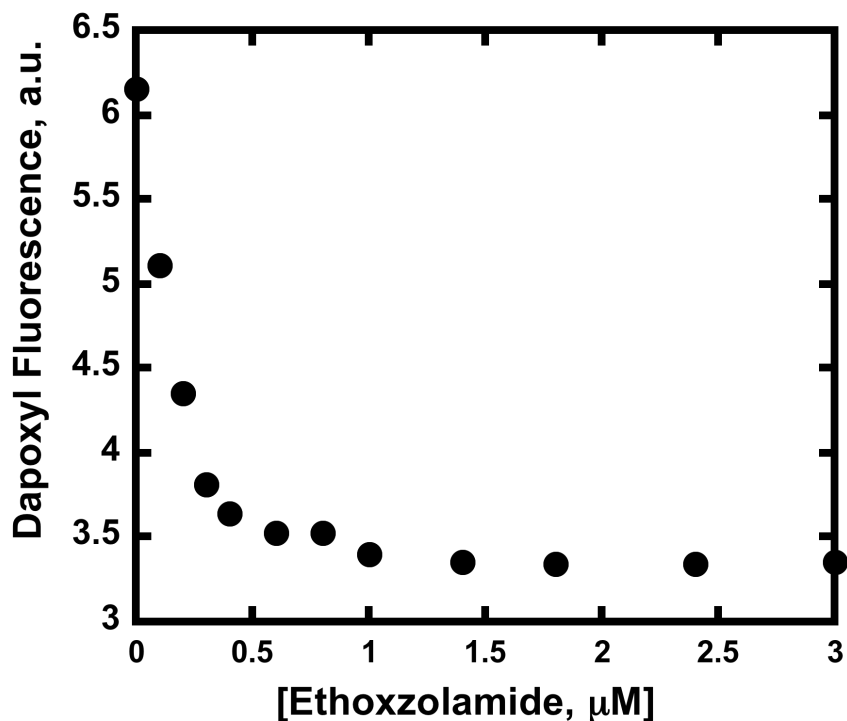
Figure 3:10: Emission spectra of Dps bound-CA(II)_mCherry in the presence of a non-fluorescent competitor inhibitor:

Dps fluorescence emission (Ex: 365 nm, Em: 535 nm) as a function of increasing concentrations of ethoxzolamide when added to 1 μM holo-(●) CA(II)_mCherry, 4 μM Dps, and 2 μM zinc in 10 mM MOPS, pH 7.0. Comparable profiles were observed for CA(II)_mOrange when treated under similar conditions. (data not shown)

fluorescence at 535 nm was extinguished. Both of these aryl sulfonamides can displace CA(II)-Zn^{2+}-Dps complexes-time of signal loss being dependent on competitor concentrations. This method proves that Dps is bound to the active site of CA(II)-non-specific binding of Dps to the protein is not occurring.

Further characterization of the fusion proteins required us to determine the apparent zinc affinity of the CA(II)_mCherry and CA(II)_mOrange sensors. The inherent affinity of zinc to CA(II) will not change, but it is hypothesized that in the presence of the bulky fluorescent protein, the apparent affinity will be altered.

The measurement of the binding constants in the nanomolar and less regime will call for the maintenance of "free" metal ion concentrations well below the concentration of total metal concentration of the ion of interests as well below the limit of detection when interfering metal ions may be present intracellularly. The well-designed buffer system as discussed in Chapter 2 is useful here as well. (See Table 3.4) In this approach, also considering future *in vivo* studies, we assume that the quantity of the zinc complexed to NTA will be much larger the total of zinc sequestered by other molecules (inorganic salts, proteins) will be negligible. Basically, NTA acts as the chelator so that the small losses of metal ions from solution that occur upon binding to a protein or surface are compensated for by re-equilibration of the chelator bound metal with the bulk solution [66]. It should be noted that the free metal ion concentration range of our buffer series is compatible with the expected dissociation constant of the fusion protein for that zinc. Like WT-CA(II) and its previously discussed mutants, the binding studies of the fusion proteins were performed at free zinc ion concentrations in the picomolar range.

Zinc (II) binding to CA(II) is observed as a fluorescence resonance energy transfer (FRET) signal between the membrane-soluble fluorophore, dapoxyl sulfonamide, that binds specifically to the CA(II)-Zn fusion protein and not to apo-CA(II) fusion protein. The K_d values for Zn^{2+} binding to mCherry and mOrange carbonic anhydrase sensors were determined from changes in excitation ratiometric fluorescent measurements to be 5.3 ± 0.9 pM, and 1.8 ± 0.3 pM, respectively (Figure 3.11).

	[Zn], total M	[Zn], Free M	2X [Zn], total M
Bufffer # Control	Control	Control	Control
1	1.00E-09	2.13E-15	2.00E-09
2	5.00E-09	1.06E-14	1.00E-08
3	1.00E-07	2.13E-13	2.00E-07
4	2.50E-07	5.32E-13	5.00E-07
5	5.00E-07	1.06E-12	1.00E-06
6	2.00E-06	4.26E-12	4.00E-06
7	5.00E-06	1.07E-11	1.00E-05
8	2.50E-05	5.46E-11	5.00E-05
9	5.00E-05	1.12E-10	1.00E-04
10	2.00E-04	5.32E-10	4.00E-04
11	5.00E-04	2.13E-09	1.00E-03
12	7.50E-04	6.39E-09	1.50E-03
13	9.00E-04	1.92E-08	1.80E-03
14	9.60E-04	5.10E-08	1.92E-03

Table 3.4: Zinc(II) metal buffer series:

This is a set of free zinc (II) calibration buffers made with MOPS as the pH buffer and NTA as the metal ion buffer. The final free zinc concentrations in 2 mM NTA, 10 mM MOPS buffer, pH 7.0, 25°C is μM-pM. **Note: This is a 2X buffer: for example, dilute with equal volume sample to make 1X final buffer**
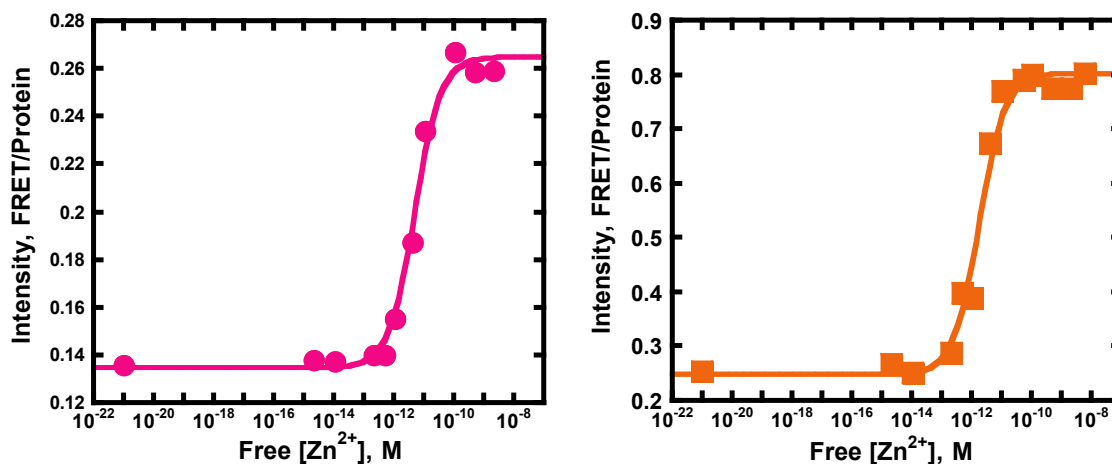
Figure 3:11: Fluorescence of apo-CA(II)_mVariant as a function of the free zinc concentration:

The fluorescence of 100 nM apo-CA(II)_ (●)m_Cherry and (■)m_Orange in 10 mM MOPS zinc-NTA buffer with varying concentrations of free zinc, pH 7.0. The ratio of FRET emission (Ex = 365 nm, Em = 610 nm (●) or 562nm (■)) to the fluorescent protein (Ex = 587 nm, Em = 610 nm (●) or Ex = 547 nm, Em = 562 nm (■)). A single binding isotherm (Eq 2.3) was fit to the data and a K_D^{App} of 5.3 ± 0.9 pM, and 1.8 ± 0.3 pM, respectively were determined

DISCUSSION

In the last decade, several genetically encoded fluorescent sensors have been developed based on variants of Green Fluorescent Protein (GFP) and fluorescence resonance energy transfer (FRET), a concept that was pioneered by Roger Tsien [161]. Early applications of genetically encoded sensors used Blue Fluorescent Protein (BFP) as the donor and GFP as the acceptor, but the low quantum yield and photostability of BFP soon led to the use of Cyan and Yellow Fluorescent Proteins (CFP and YFP, respectively) as donor and acceptor proteins in FRET-based sensors. For CFP and YFP an R_0 of 48 Å has been determined[162]. Since FRET efficiency depends on the distance and orientation of the fluorophores, it also can be an effective way to detect conformational changes on the scale of individual proteins or small molecules.

Intracellular imaging of sensors have been applied in imaging a variety of small molecules including calcium [48], cAmp [163], maltose [164], nitric oxide [165], and glucose [166]. In these sensors, fluorescent proteins are fused to proteins that naturally bind the target, combining the advantages of a genetically-encoded with a high affinity for target of interest.

The major intent of this work was to construct and optimize the CA(II) based sensor for zinc using an expressible and ratiometric approach. The advantages of a ratiometric approach for quantitative imaging free metal ion concentrations allow freedom from variations in excitation intensities, specimen thickness and fluorophore concentrations due to photobleaching [157].

Considering the FRET efficiencies, zinc affinities and stability of the sensor at physiological pH conditions, it was promising from the *in vitro* characterization experiments that the fusion proteins were ideal for *in vivo* imaging.   In efforts to elucidate the biology of zinc and its role in disease, we have designed an expressible, ratiometric sensor with CA(II) as the receptor molecule fused to the engineered intrinsically fluorescent proteins, mCherry and mOrange. These sensors can be expressed in bacteria, yeast or mammalian tissue culture cells.

The novelty of this sensor design, establishes a convenient means for utilizing the fusion protein to test a variety of biological conditions that may alter free zinc in the cells. These *in vitro* experiments suggest that this CA(II)-fluorescent protein fusion is a novel candidate as an expressible, *in vivo* sensor for ratiometric fluorescence imaging of intracellular Zn^{2+}. Because the chromophore of the fluorescent protein forms *in vivo* and Dps and the non-fluorescent sulfonamides are membrane permeable, this ratiometric zinc sensor can be expressed and analyzed *in situ*, dismissing the need to purify and/or label the sensor protein. However, the hydrophobic nature of Dps is something of a disadvantage for FRET based zinc sensing *in vivo*. Dps might bind to phospholipid bilayers such as that in the cell membrane mimicking the emission bound to CA(II). Because Dps partitions into membranes reversibly, we hypothesize that it will desorb from the membrane to bind to holo CA(II)_FP [167]. In addition, the method presented definitely saves money and time spent during protein preparations. The most recent application, investigations to test the readily exchangeable zinc concentration in *E. coli*, is discussed in Chapter 4.

REFERENCES

[1]   K.A. McCall, C. Huang, C.A. Fierke, Function and mechanism of zinc metalloenzymes, J Nutr 130 (2000) 1437S-1446S.

[2]   D.J. Eide, Multiple regulatory mechanisms maintain zinc homeostasis in Saccharomyces cerevisiae, J Nutr 133 (2003) 1532S-1535S.

[3]   C.J. Chang, E.M. Nolan, J. Jaworski, K. Okamoto, Y. Hayashi, M. Sheng, S.J. Lippard, ZP8, a neuronal zinc sensor with improved dynamic range; imaging zinc in hippocampal slices with two-photon microscopy, Inorg Chem 43 (2004) 6774-6779.

[4]   S.C. Burdette, G.K. Walkup, B. Spingler, R.Y. Tsien, S.J. Lippard, Fluorescent sensors for Zn2+ based on a fluorescein platform: Synthesis, properties and intracellular distribution, Journal of the American Chemical Society 123 (2001) 7831-7841.

[5]   C.J. Chang, J. Jaworski, E.M. Nolan, M. Sheng, S.J. Lippard, A tautomeric zinc sensor for ratiometric fluorescence imaging: application to nitric oxide-induced release of intracellular zinc, Proc Natl Acad Sci U S A 101 (2004) 1129-1134.

[6]   N.C. Lim, H.C. Freake, C. Bruckner, Illuminating zinc in biological systems, Chemistry 11 (2004) 38-49.

[7]   J.L. Vinkenborg, T.J. Nicolson, E.A. Bellomo, M.S. Koay, G.A. Rutter, M. Merkx, Genetically encoded FRET sensors to monitor intracellular Zn2+ homeostasis, Nat Methods 6 (2009) 737-740.

[8]   A. Miyawaki, J. Llopis, R. Heim, J.M. McCaffery, J.A. Adams, M. Ikura, R.Y. Tsien, Fluorescent indicators for Ca2+ based on green fluorescent proteins and calmodulin, Nature 388 (1997) 882-887.

[9]   O. Shimomura, F.H. Johnson, Y. Saiga, Extraction, purification and properties of aequorin, a bioluminescent protein from the luminous hydromedusan, Aequorea, J Cell Comp Physiol 59 (1962) 223-239.

[10]   M. Ormo, A.B. Cubitt, K. Kallio, L.A. Gross, R.Y. Tsien, S.J. Remington, Crystal structure of the Aequorea victoria green fluorescent protein, Science 273 (1996) 1392-1395.

[11]   R. Heim, D.C. Prasher, R.Y. Tsien, Wavelength mutations and posttranslational autoxidation of green fluorescent protein, Proc Natl Acad Sci U S A 91 (1994) 12501-12504.

[12]   R. Heim, Green fluorescent protein forms for energy transfer, Methods Enzymol 302 (1999) 408-423.

[13]   G.H. Patterson, J. Lippincott-Schwartz, A photoactivatable GFP for selective photolabeling of proteins and cells, Science 297 (2002) 1873-1877.

[14]   N.C. Shaner, R.E. Campbell, P.A. Steinbach, B.N. Giepmans, A.E. Palmer, R.Y. Tsien, Improved monomeric red, orange and yellow fluorescent proteins derived from Discosoma sp. red fluorescent protein, Nat Biotechnol 22 (2004) 1567-1572.

[15] X. Shu, N.C. Shaner, C.A. Yarbrough, R.Y. Tsien, S.J. Remington, Novel chromophores and buried charges control color in mFruits, Biochemistry 45 (2006) 9639-9647.

[16] S.K. Nair, T.L. Calderone, D.W. Christianson, C.A. Fierke, Altering the mouth of a hydrophobic pocket. Structure and kinetics of human carbonic anhydrase II mutants at residue Val-121, J Biol Chem 266 (1991) 17320-17325.

[17] S.N. Ho, H.D. Hunt, R.M. Horton, J.K. Pullen, L.R. Pease, Site-directed mutagenesis by overlap extension using the polymerase chain reaction, Gene 77 (1989) 51-59.

[18] L.L. Kiefer, C.A. Fierke, Functional-Characterization of Human Carbonic-Anhydrase-Ii Variants With Altered Zinc-Binding Sites, Biochemistry 33 (1994) 15233-15240.

[19] A.G. Aslamkhan, A. Aslamkhan, G.A. Ahearn, Preparation of metal ion buffers for biological experimentation: a methods approach with emphasis on iron and zinc, J Exp Zool 292 (2002) 507-522.

[20] Y. Yang, J. Ma, Z. Song, M. Wu, HIV-1 TAT-mediated protein transduction and subcellular localization using novel expression vectors, FEBS Lett 532 (2002) 36-44.

[21] R.A. Bozym, R.B. Thompson, A.K. Stoddard, C.A. Fierke, Measuring picomolar intracellular exchangeable zinc in PC-12 cells using a ratiometric fluorescence biosensor, ACS Chem Biol 1 (2006) 103-111.

[22] D.J. Eide, The molecular biology of metal ion transport in Saccharomyces cerevisiae, Annual Review of Nutrition 18 (1998) 441-469.

[23] A.C. Ward, Single-step purification of shuttle vectors from yeast for high frequency back-transformation into *E. coli*, Nucleic Acids Res 18 (1990) 5319.

[24] D.J. Eide, Zinc transporters and the cellular trafficking of zinc, Biochim Biophys Acta 1763 (2006) 711-722.

[25] H. Zhao, D. Eide, The yeast ZRT1 gene encodes the zinc transporter protein of a high-affinity uptake system induced by zinc limitation, Proc Natl Acad Sci U S A 93 (1996) 2454-2458.

[26] K.A. McCall, C.A. Fierke, Probing determinants of the metal ion selectivity in carbonic anhydrase using mutagenesis, Biochemistry 43 (2004) 3979-3986.

[27] A. Miyawaki, O. Griesbeck, R. Heim, R.Y. Tsien, Dynamic and quantitative Ca2+ measurements using improved cameleons, Proc Natl Acad Sci U S A 96 (1999) 2135-2140.

[28] M. Tramier, M. Zahid, J.C. Mevel, M.J. Masse, M. Coppey-Moisan, Sensitivity of CFP/YFP and GFP/mCherry pairs to donor photobleaching on FRET determination by fluorescence lifetime imaging microscopy in living cells, Microsc Res Tech 69 (2006) 933-939.

[29] L.M. DiPilato, X. Cheng, J. Zhang, Fluorescent indicators of cAMP and Epac activation reveal differential dynamics of cAMP signaling within discrete subcellular compartments, Proc Natl Acad Sci U S A 101 (2004) 16513-16518.

[30]   M. Fehr, W.B. Frommer, S. Lalonde, Visualization of maltose uptake in living yeast cells by fluorescent nanosensors, Proc Natl Acad Sci U S A 99 (2002) 9846-9851.

[31]   M. Sato, N. Hida, Y. Umezawa, Imaging the nanomolar range of nitric oxide with an amplifier-coupled fluorescent indicator in living cells, Proc Natl Acad Sci U S A 102 (2005) 14515-14520.

[32]   M. Fehr, S. Lalonde, I. Lager, M.W. Wolff, W.B. Frommer, *In vivo* imaging of the dynamics of glucose uptake in the cytosol of COS-7 cells by fluorescent nanosensors, J Biol Chem 278 (2003) 19127-19133.

[33]   R.B. Thompson, B.P. Maliwal, H.H. Zeng, Zinc biosensing with multiphoton excitation using carbonic anhydrase and improved fluorophores, J. Biomed. Opt. 5 (2000) 17-22.

CHAPTER 4: Reporting Intracellular Zinc in Escherichia coli

INTRODUCTION

An important prerequisite for further understanding the mechanism of zinc homeostasis and its involvement in diseases is the ability to image the concentration of these metals in living cells in real time. To study intracellular processes, it is necessary to have a detection system that allows sensitive, non-invasive, real-time imaging of metal ions in single living cells with high spatial resolution. Fluorescence microscopy is well suited for this purpose and the development of fluorescent probes that bind transition metal ions with high affinity and selectivity is an area of active research [106], [100], [168]. A variety of Zn(II)-specific fluorescent dyes have been developed [169], [170], [171] and recently the first two versions of Cu(I)-specific fluorescent chemosensors were reported [172], [173]. Although several of these sensors have already been used for intracellular imaging [174], small molecule sensors with physiologically relevant binding constants have been challenging to develop. Additionally, a major disadvantage of chemosensors or biosensors conjugated with synthetic dyes is the challenge of inserting them into cells. In efforts to develop biosensor for metal ions that could be adapted for *in vivo* purposes, several groups have developed fluorescent sensors based on natural metal binding proteins.   Protein-

113

based fluorescent Zn(II) sensors include fluorescently labeled peptides based on Zn-finger domains [168], the carbonic anhydrase-based sensors in combination with a Zn^{2+}- specific fluorescent substrate inhibitor [175] and green fluorescent protein (GFP) variants with Zn(II) binding sites introduced by protein engineering [50]. The latter have the important advantage of being genetically-encoded (i.e., no synthetic fluorescent groups are used. However, the GFP and zinc finger peptides do not have sufficient affinity to report on intracellular zinc concentrations.

A key advantage of genetically encoded sensor proteins is that these sensors consist entirely of amino acids and can be produced intracellularly. In addition, attachment of signal sequences and regulation of transcription allows control over their subcellular localization and over the intracellular sensor concentration [176], [177]. Finally, these sensors can be optimized for metal selectivity and affinity using mutagenesis and selection methods [178], [179]. As described in Chapter 3, we have chosen to prepare fusion proteins with mCherry and mOrange, two of the latest red versions of fluorescent proteins derived from the *Discosoma sp.* (DsRed) that have faster maturing chromophores in the monomeric form [127].

To analyze intracellular concentrations of metal ions or other ligands, a ratiometric fluorescent method is essential since this eliminates many artifacts [157]. Our ratiometric approach for imaging metal ions is based on the change in the efficiency of fluorescence resonance energy transfer (FRET) between a donor molecule and acceptor fluorescent protein [180].

An important benefit of FRET-based sensors is the generation of a ratiometric signal. Ratiometric detection provides a measure of the binding state that can be made independent of the absolute concentration of the sensor, which is important to obtain reliable and quantitative results in biological samples. Tsien and coworkers pioneered this concept by constructing the calcium sensor Cameleon in which the calcium binding protein calmodulin was fused to two spectral variants of GFP [161]. Calcium binding to calmodulin induces a conformational change in these fusion proteins that brings the donor and acceptor domains closer together which results in increased FRET. Unlike synthetic fluorescent probes which need to be introduced inside the cell via microinjection or passive diffusion, genetically- encoded sensors consist entirely of amino acids and can be produced inside cells by transcription and translation of their corresponding genes.

In this chapter, to the goal is to demonstrate the measurement of free cytosolic Zn^{2+} levels in E.coli, using fluorescence microscopy, with the ratiometric, genetically encoded CA(II)_mCherry sensor described in Chapter 3. This signal is not dependent on the sensor concentration. To determine the readily exchangeable or "free" zinc concentration, for the observed signal, the intracellular FRET signal was measured *in situ* as zinc concentration was equilibrated with a series of Zn^{2+} buffers.

MATERIALS AND METHODS

Expression and purification of CA(II) fusion proteins:

For *in vitro* measurements, the CA(II)_FP (CA_mCherry and CA_mOrange were expressed and purified as described in detail in Chapter 3. In short, expression plasmids (p23a_CA_mOrange, p23a_CA_mCherry, pAHT_CA_mCherry and p24aH_CA_mCherry) were transformed into *E. coli* BL21(DE3). Protein expression was induced in 0.5 L culture by addition of 1 mM IPTG at OD_{600} = 0.6-0.8, after which cells were grown at 25 °C and 220 rpm for six h and then harvested by centrifugation at 6000g at 4°C for 15 min. The cell pellet was disrupted using a microfluidizer in buffers supplemented with protease inhibitors. The fusion proteins were purified using nickel affinity column chromatography. Apo-enzyme was prepared by incubation with DPA as described in Chapter 3.

Growth of cells for imaging:

A single colony of BL21(DE3) in 5 mL of (1X A medium (7.6 mM $(NH_4)_2SO_4$, 33 mM KH_2PO_4, 60 mM K_2HPO_4, and 1.7 mM sodium citrate) (ref) supplemented with 40 mg/ml of all 20 essential L-amino acids (Sigma), 0.2% glucose, 1 mM $MgSO_4$, and $5E^{-5}$ % thiamine) and 100 mg/mL ampicillin and incubated at 37°C overnight. All media components except thiamine and MgSO4 were incubated overnight with 50 g/liter Chelex 100 resin (Bio- Rad) prior to mixing to remove trace metals, mixed and sterile-filtered before use. The

following procedure was used to prepare *E. coli* expressing Ca(II)_mCherry
fusion where the fluorescent chromophore in the protein is fully mature. This
media provides a low total zinc and reproducible concentrations. Media recipes
prepared from tryptone and yeast extract have variable higher total zinc
concentrations.

Overnight cultures were diluted 1:50 into fresh minimal medium and
incubated at 25 °C until the OD_{600} reached 0.2-0.3. Expression of the
CA_mCherry fusion protein was induced by addition of 0.2 mM IPTG and
incubated at 25 °C 12-14 h. 1 mL of induced sensor cells were spun down,
washed with fresh medium to rid any residual IPTG, resuspended in 5 mL
medium and incubated for 2-3 h at 30 °C. This strategy allows sufficient time for
the sensor to mature prior to imaging. Achieving a slower rate of expression has
been attempted by reducing incubation temperatures to 25 °C and using a series
of IPTG concentrations between 5-500 mM. The multiples of samples were
expressed and prepared for imaging accordingly the protocol described above.

FRET microscopy:

Fluorescent images were acquired using a Nikon Eclipse TE2000-U
epifluorescence microscope through a Nikon Plan Fluor 100×/1.3 NA oil
immersion objective with a Photometrics CoolSNAP HQ cooled CCD camera.
For FRET measurements, a 400DCLP dichroic mirror (Chroma Technology)
and two filters (Chroma; D350/50X, HQ575_50x and HQ625_30m) alternated
by a Lambda filter wheel. All filters and dichroic mirrors were purchased from

Chroma Technology Corp. The complete filter sets for fluorescence imaging are summarized in Table 4.1. Live cell images and solution measuremnts were acquired using a 50-ms exposure time for the FRET channel and using a 500-ms exposure time for the acceptor channel. After acquisition, the images were manipulated using MetaMorph software package (Molecular Devices). Background values were subtracted from the images collected in each channel. These adjusted values also took into consideration interference by background fluorescence from the cells. This also corrected for fluorescence from membrane-bound Dps. Final data analysis of the collected images were completed using the software Image J.

	Channel FRET (Excitation Filter)	Exposure Time	Channel FP (Excitation Filter)	Exposure Time	Dichroic Mirror	(Emission Filter)
CA(II)_mOrange	D350/50x	500ms	HQ530_30x	50ms	550 dcxru	HQ580_40m_2p
CA(II)_mCherry	D350/50X	500ms	HQ575_50x	50ms	605 lpxru	HQ625_30m
Dapoxyl	D350/50x	50ms	N/A	500ms	400 dclp	HQ535_30m

Table 4.1: Fluorescence imaging filter sets for different CA(II)_FP and DpsT

Imaging live *E. coli* cells:

To immobilize bacteria on a glass bottom 96-well plate (MatriCal Bioscience), the glass was derivatized with poly-L-lysine in accordance to the following method [181]. In preparation of imaging, 2 mL of cells were plated on poly-*L*-lysine-coated glass 96-well plates and equilibrated with the appropriate solutions. Each plate was rinsed in 18 MΩ water, soaked in ethanol containing 5% (w/v) potassium hydroxide for 10 min, rinsed with water and then soaked in a solution of 0.05% poly-L-lysine in water (Sigma P8920) for 5 min. After a final rinse with water, the slides were allowed to dry at 37°C for 1 – 2 h.

Before imaging, 2 mL of cell culture (prepared as described above) was added to a single well and incubated until dry. The media was removed and incubated with inhibitor for 20 min at room temperature. Dps and ethoxzolamide were prepared fresh on the day of use as 200 mM and 100 mM stock solutions in DMSO, respectively. Concentrations of 50 mM, 200 mM, 500 mM $ZnSO_4$ diluted in 100 μL fresh MOPS medium, were added to the 96-well plate containing immobilized *E. coli* cells. The cells were allowed to equilibrate with Zn^{2+} for 5-10 min and then imaged. Zinc depletion studies were performed by adding 1 mM EDTA dissolved in MOPS medium to the cells that were treated with Dps. Images were acquired as above. The signal in the FRET and acceptor channels were taken sequentially and measured only once at each concentration point.

The inhibitor solution was then replaced with fresh MOPS media and the cells were imaged immediately in both the FRET and FP channels. A

ratio image of FRET/FP was then created, and the average intensity in each cell calculated. The free Zn^{2+} concentration was determined from the *in situ* calibration curve.

In vitro calibration of CA(II) fusion sensors:

The apparent zinc affinities of the CA(II)_fusion protein sensors were measured by microscopy in MOPS NTA-chelated zinc buffers with known free zinc concentrations (described in Chapter 3). Homogeneous solutions of 100 nM purified apo- CA(II)_mOrange and CA(II)_mCherry sensors were equilibrated with a series of zinc buffers plus 2 mM dapoxyl sulfonamide for 30-270 min at room temperature. Fluorescent images were taken in the two channels, FRET and FP, as described in Table using the Nikon Eclipse microscope. The ratio FRET/FP was plotted against the free zinc concentrations, and a single binding curve was fit to the data.

In situ calibration of CA(II)_mCherry:

Da Wang, a graduate student in the Fierke Lab, developed a method to calibrate the dependence of the FRET/FP CA(II) fusion proteins on the Zn^{2+} concentration *in situ*. The *E. coli* cells are treated with 100 mL of 1 mM EDTA in 10 mM metal free MOPS buffer for 15 min followed by a wash with 100 μL fresh MOPS buffer. Then 100 µL MOPS-NTA-Zn buffers (pH 7.6) containing 30 µM digitonin (made fresh from 30mM stock in DMSO) and 2 µM

Dps (made fresh from 200 µM stock in DMSO) were added to each well containing cells and incubated for 20 min at room temperature. The cells were then washed once with a MOPS-NTA-Zn buffer and incubated for 40 min. Finally, the cells were images using the CA_mCherry and FRET channels as described above. The FRET/FP ratio was plotted against the free zinc concentration in the buffers.

RESULTS

Calibration of CA(II)_Fluorescent Protein in microscope:

The long-range goal of the development of a CA(II)-based zinc biosensor is to prepare an easily usable, fluorescent sensor to measure intracellular zinc concentrations. Drawbacks of using the TAT-tagged, Alexa-Fluor-labeled CA(II) biosensor to measure intracellular zinc are that it is complicated to use not applicable to all cell lines and types and the apparent zinc affinity is not well matched to the intracellular zinc concentration. A genetically encoded sensor overcomes many of these challenges.

The preparation of genes and expression plasmids encoding CA(II)_FP as well as a zinc-dependent calibration curve of this sensor measured in a fluorimeter were described in Chapter 3. To demonstrate that a similar zinc-dependent change in the fluorescence (FRET/FP) ratio (emission at 625 nm, excitation at either 350 nm (FRET) or 575 nm (FP), we measured a calibration curve using purified CA_mCherry or CA_mOrange in a 96-well glass bottom plate on the microscope. ''Apo-CA(II)_FP was equilibrated with zinc-NTA buffers that varied the zinc concentration and the FRET/FP ratio was measured after addition of Dps. The $K_{d,app}$ for zinc measured from these data are 5.0± 3 pM and 2.8± 0.8 pM for CA(II)_mCherry and CA(II)_mOrange, respectively. These values are comparable to the values of 5.0± 1 pM and 1.8± 0.4 pM for CA(II)_mCherry and CA(II)_mOrange measured in the fluorimeter (Fig 3.11 , Chapter 3). Da Wang performed the same procedure on CA(II)_mCherry purified

from the plasmid pET24aH_CA_mCh. The zinc affinity of this construct is 23± 3

pM.
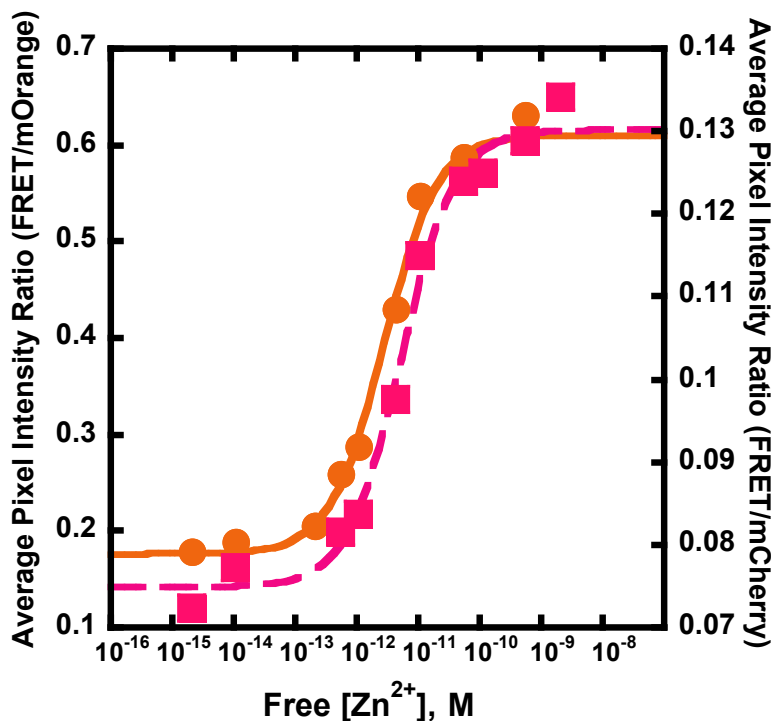
Figure 4:1: ***In vitro* caiibration curve of CA_mOrange and CA_mCherry encoded in p23a_CA_mCh or p23a_CA_mOr:**

100 nM apo-CA_FP sensor was pre-equilibrated with MOPS NTA-chelated zinc buffers (pH = 7.0) and 2 µM Dps at room temperature. FRET/FP excitation intensity ratios were taken in 96-well glass bottom plates using the fluorescence microscope. (●) *in vitro* calibration curve of CA_mOrange with 3-Gly linker (■) *in vitro* calibration curve of CA_mCherry sensor with 3-Gly linker. A single binding isotherm is fit to the data

For the calibration, total zinc levels were in excess of the sensor

concentration allowing the free zinc concentration to be buffered at fixed low

levels. A measurable increase of the FRET/FP ratio was observed, indicating that

the ratiometric change was large enough to be detected using a fluorescence microscope. The binding curves at pH 7.0 for the sensors are shown in Figure 4.1 and the *in vitro* data is summarized in Table 4.2. The variability of the K_d measurements of CA(II)_mCherry can be attributed to the sequences differences (addition of the HIS tag) between the parent vectors. Also, FRET/FP ratio measured for the zinc-response curves are in the same range as those measured in the fluorescence spectrophotometer.

Calibration Curve Conditions: Sensor Type:	*In vitro*, fluorimeter $K_{D,app}^{Zn}$ pH 7.0 (Chapter 3)	*In vitro*, microsocpe $K_{D,app}^{Zn}$ pH 7.0 (Figs. 1-2)	*In situ*, microscope $K_{D,app}^{Zn}$ pH 7.58 (Fig.)
CA_mCherry	5± 1 pM	5±3 pM	Not determined
CA_mCherry_pET24A	Not determined	23± 3 pM[a]	68± 34 pM
TAT_CA_mCherry	Not determined	Not determined	46± 26 pM
CA_mOrange	1.8±0.4 pM	2.8±0.8 pM	Not determined

Table 4.2: Binding data for CA(II) fused to fluorescent proteins comparing *in vivo* and *in situ* responses to free zinc:

Dissociation constants (Kd, apparent) were calculated using a single binding isotherm. Data are represented as K_d ± error. –[a] Data generated by Da Wang

Preparation of cells for zinc measurements:

Our observation that Zn(II) can mediate an interaction between Dps and mCherry by causing the energy transfer *in vivo*, prompted us to investigate the metal ion dependency by first considering growth conditions. Data suggests that higher concentrations of zinc and the types of growth medium have significant effect on how fast the protein expresses relative to how complete the chromophore matures. As a control, the effect of Zn^{2+} was determined without external metal dependent interactions between the donor and acceptor proteins by imaging cells grown in LB, 2XYT and minimal media. Using ICP-MS to compare total zinc levels across the media types, minimal media exhibit 5-10-fold lower zinc levels than those reported for rich media types. The results show that the intracellular level of free zinc is indeed total zinc-dependent and validate our sensing results obtained in the FRET experiments in the previous chapter.

Cells grown in medium with higher zinc levels normally exhibited higher intracellular free zinc concentrations, with less measurable signal changes, however without significant growth abnormalities (data not shown). These results suggest that the rate of expression versus chromophore maturation is disproportionate. This also implies, that *E. coli* cells, in order to conserve energy necessary to maintain intracellular free zinc concentrations, can develop greater tolerances to higher total zinc concentrations over time.

It is difficult to predict the presence of intramolecular Zn^{2+} mediated complexes intracellularly when no values of association constants have been determined. The acquirement, distribution, delivery and excretion of metals is a

tightly regulated process, which results in very low free metal concentrations in cells. The motivation driving this work yields the assumption that there is an exchangeable zinc pool in the cell that will not be challenged by the binding of zinc to carbonic anhydrase. Under this assumption, elevated sensor levels should not alter this zinc homeostasis.

Perhaps the easiest method for generating desired amounts of soluble protein in *E. coli* is to create conditions that reduce the rate of expression. Theoretically, as we hypothesized, in efforts to optimize growth conditions, lowering the expression rate allows the protein to fold properly and remain in solution. The Zn^{2+} affinities of the CA_mCherry protein constructs (5 to 68 pM) are well suited to probe free Zn^{2+} concentration in the low to mid- picomolar range in cells. Previous data suggest that an expressible sensor that is present in the nM-μM range can probe these low concentrations without significant perturbation of zinc homeostasis because the total cellular zinc is 0.2-0.5 mM and the sensor can equilibrate with this total pool [182]. Therefore, the cellular milieu acts as an efficient buffering system for metals such as Zn^{2+} [76]. However, to minimize the perturbation of metal homeostasis, the sensor concentration should be as low as possible.

On the other hand, expression of CA_mCherry must be sufficient to reliably measure changes in FRET emission upon Dps binding over the background fluorescence due to Dps binding to the membrane. To measure the intracellular zinc concentration of *E. coli*, we surveyed the effect of growth environment in order to determine optimal conditions for protein expression in *E.*

coli that will produce measurable signals when illuminated using the microscope. When expressing this protein in bacteria for purification purposes, chromophore maturation lifetimes were less of a concern as the chromophore matures prior to harvesting cells and continues to mature during purification. For *in vivo* studies, however, a fully matured chromophore is critical. mCherry is the fastest-maturing red monomeric fluorescent protein known to date. Unfortunately, our signal outputs are less than optimal because mCherry when fused to CA(II) is less bright, and it's near far-red excitation spectrum does not pair well with Dps emission, resulting in lower FRET efficiencies than we expected. mOrange on the other hand is the brightest monomeric protein derived from dsRed, but it is more pH sensitive, when fused to CA takes 2.5 times longer to reach full maturation and the extent of FRET overlap creates interfering background signals that can not be distinquished in our current zinc sensing approach. The *in vivo* work presented in this chapter was therefore limited to results generated using the CA_mCherry sensor.

FRET Signal Depends on CA(II)_mCherry Binding Dps and Zinc:

The imaging experiments that show CA(II)_mCherry is well expressed in *E. coli*. Furthermore, this signal is dependent on both Dps and zinc binding to CA(II)_mCherry. To evaluate the amount of background energy transfer, the spectral bleed-through parameters were determined. The donor bleed-through was determined in cells that do not express CA(II)_mCherry (BL21(DE3)_pET23a). Addition of Dps causes little increase in fluorescence in

the FRET channel (Figure 4.2), indicating the membrane-bound Dps does not interfere. In contrast, in cells expressing CA(II)_mCherry (BL21(DE3)_pET23a), a large increase in signal in the FRET channel is observed upon addition of Dps (Figure 4.2). Also Dps does not bind free zinc in the media or any sulfonamide bound to the membrane did not generate interfering signals.

To further confirm that the observed signal is due to Dps binding specifically to CA(II), the FRET/FP ratio in the zinc-bound state of cells expressing CA(II)_mCherry (BL21(DE3)_pET23a) that were equilibrated and saturated with ethoxzolamide was measured. The ideal condition was to show that the observed ratio is generated from specific binding of Dps to holo-enzyme. Recall, ethoxzolamide is a non-fluorescent sulfonamide inhibitor that acts as a competing ligand to dapoxyl. Once bound forms of the sulfonamide were determined according the protocols discussed, the free zinc concentration can be calculated in the same manner as for the wavelength ratiometric approaches baseline. Upon addition of 30 mM ethoxzolamide to cells treated with 2 mM Dps, fluorescence intensities of the FRET/FP ratio were quenched to levels as low as those observed for the CA(II)_FP minus Dps excited in the FRET channel (Figure 4.2). This experiment proved the specificity of the signal that originates from the zinc-bound CA(II)_mCherry sensor.

Furthermore, we examined whether the FRET/FP ratio is sensitive to changes in extracellular zinc. Incubation of BL21(DE3)_pET23a cells expressing

CA(II)_mCherry with 1 mM EDTA prior to addition of Dps was corrected out. *E. coli* is a gram-
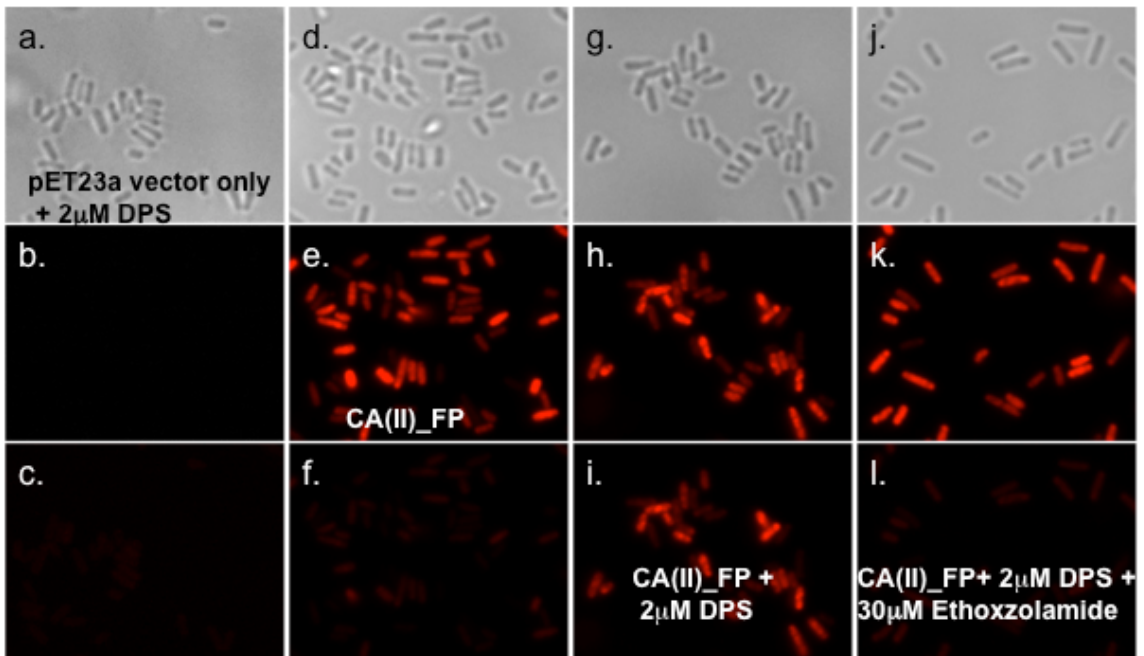
Figure 4:2: Fluorescence signal of the pET23A vector transformed in BL21(DE3) cells treated with inhibitor:

A-C) *E. coli* expressing pET24a vector void CA(II)_FP gene incubated with 100 mL 2 mM Dps. D-F) *E. coli* expressing pET23a vector with CA(II)_mCherry gene incubated with 100 mL 2 μM Dps. A single image was acquired with the FRET channel: Ex350/ Em625, exposure time 500ms.   Undetectable levels of background fluorescence from the FP channel was observed from membrane bound Dps; G-I) CA(II)_mCherry +/- Dps J-L) CA(II)_mCherry after addition of 100 mL 2 μM Dps and 100 mL 30 mM ethoxzolamide. Images were similarly acquired using exposure times 50 ms in the FP channel and 500 ms in the FRET channel

negative bacterium that has an outer membrane to act as an extra barrier against the perfusion of divalent ions. Lipopolysacchride (LPS) is an important structural component of the outer member and it is stabilized by divalent ions. Short incubation of the cells with the EDTA can disrupt the structure of outer membrane by destabilizing LPS, leading to a significant decrease in the FRET/FP ratio (Figure 4.3) within a 15-minute time frame [183]. This result demonstrates both that the zinc bound to CA(II) is labile and that the chelation of extracellular zinc leads to a net efflux of zinc from the cells.

In contrast, incubation of the *E. coli* cells with high extracellular zinc leads to an increase in the FRET/FP ratio (Figure 4.3). This result also demonstrates that intracellular zinc is affected by the extracellular concentration and that CA(II) equilibrates with the zinc pool. In response to zinc, these cells can modulate zinc via membrane receptors or channels. Binding of zinc resulted in a minimum ten-fold increase in fluorescence. These experiments show that the sensor reflects the intracellular zinc concentration.

FRET signal does not depend on sensor concentration:

To examine whether the FRET/FP ratio, and therefore the apparent zinc concentration depends on the sensor concentration, CA(II)_mCherry expression was altered by varying the IPTG at induction concentrations up to 1 mM. This alteration in IPTG concentration led to an non-proportional change in sensor concentration (Figure 4.4), while the FRET/FP ratio remained stable. The best fluorescent signal is observed at higher sensor concentrations. However, at very
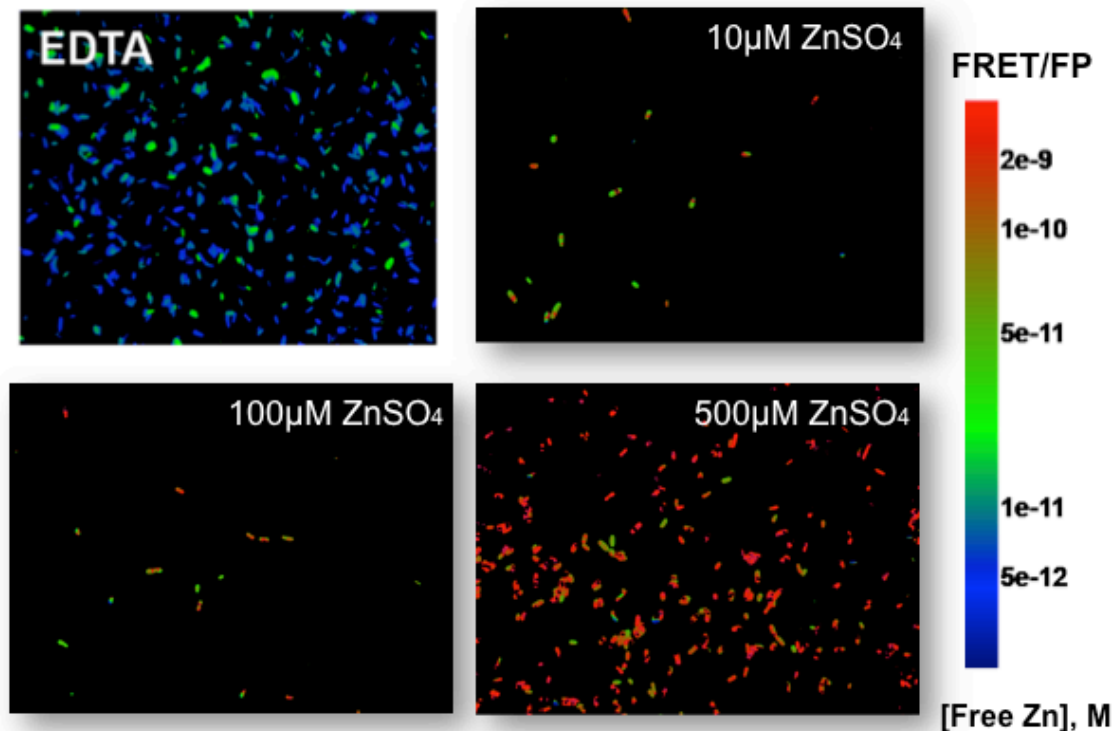
Figure 4:3: Altering extracellular Zn^{2+} affects the FRET/FP ratio and intracellular free Zn^{2+} concentration:

E. coli expressing CA(II)_mCherry (BL21(DE3)) were incubated with 2 µM Dps for 10 min, then 1-500 µM of zinc sulfate (or 1 mM EDTA) diluted in fresh MOPS media for 5 min. The FP signals (ex= 575; em= 625) and FRET (ex= 350; em= 625) signals were imaged in the microscope. plotted against total zinc concentrations. The FRET/FP ratio is calculated. Extrapolation of the image intensities is false colored (RGB) using the values generated from the *in situ* calibration data

high expression levels, chromophore maturation is limited and protein

aggregation observed. Therefore, the CA(II)_mCherry expression at 50-200 mM

IPTG was optimal for sensing. Future studies will also use this protocol to track

stages of growth, image and quantitate free zinc concentrations at desirable points along the cell's life cycle.

Quantification of "free" zinc in *E. coli*:

The intracellular free zinc concentration of *E. coli* cultured in minimal medium at log phase was measured using CA(II)_mCherry. In summary, expression plasmids were transformed into chemically competent *E. coli* BL21(DE3). Minimal medium used for culturing cells was supplemented with 100 µg/mL ampicillin to select for cells expressing CA(II)_mCherry protein. To quantify the concentration of zinc designated by a given FRET/FP ratio image in *E. coli*, an *in situ* calibration curve was determined. A main challenge to this experiment was the development of a method to equilibrate intracellular zinc with extracellular zinc buffers to set the "free" concentration. Since the zinc affinity of CA(II) is dependent on the pH, the calibration curves were carried out at pH 7.6, the likely cytosolic pH of *E. coli* [183]. As shown in Figure 4.5, the FRET/FP ratio of *E. coli* cells expressings CA(II)_mCherry varies with the "free" zinc concentration of the Zn-NTA buffers. This calibration curve varies from the *in vitro* calibration curves both in terms of an increase in the $K_{d, app}$ and the terms of the actual values of the FRET/FP ratios. This is due to the differences in the intensity of the emission signals generated (based on the efficiency of expression and chromophore maturation) from the FP. Therefore, the *in situ* calibration is essential for estimating the intracellular zinc concentration. Measurement of the FRET/FP

ratio of reproducibility for many cells expressing the fusion sensor, grown in minimal media gives a value of ~0.3. The *in situ* calibration curve indicates that histogram number extrapolates to an intracellular "free" or readily exchangeable zinc concentration of 10-50 pM.
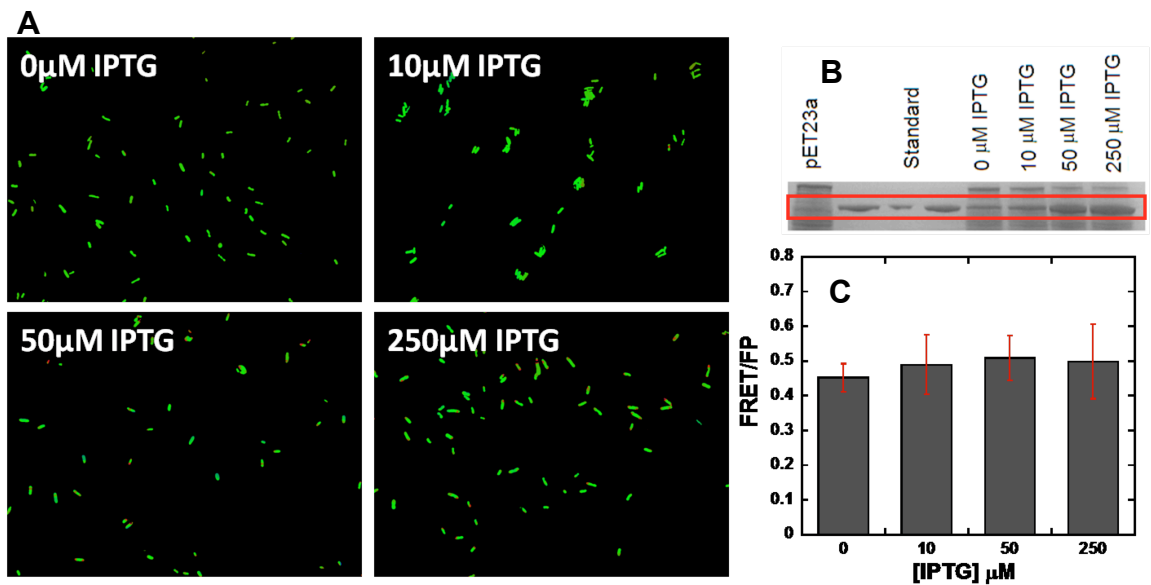
Figure 4:4: Expression levels of the CA(II)_mCherry sensor in BL21 (DE3) cells do not affect FRET/FP ratio:

A) Fluorescence imaging of *E.coli* expressing BL21(DE3) p23a_CA_mC cells grown as described in materials and methods with CA(II)_mCherry expression varied by addition of increasing concentrations of IPTG. B) The *E. coli* cells induced with varying concentrations of IPTG were lysed by sonication and the cell lysate was fractionated on a 12% SDS-PAGE gel. The CA(II)_mCherry band is shown at each IPTG concentration tested. C) The FRET/FP ratio from imaging BL21(DE3) p23a_CA_mC cells induced with varying IPTG concentrations was measured from imaging the cells and is not dependent on sensor concentration. Error bars are calculated based on standard deviation
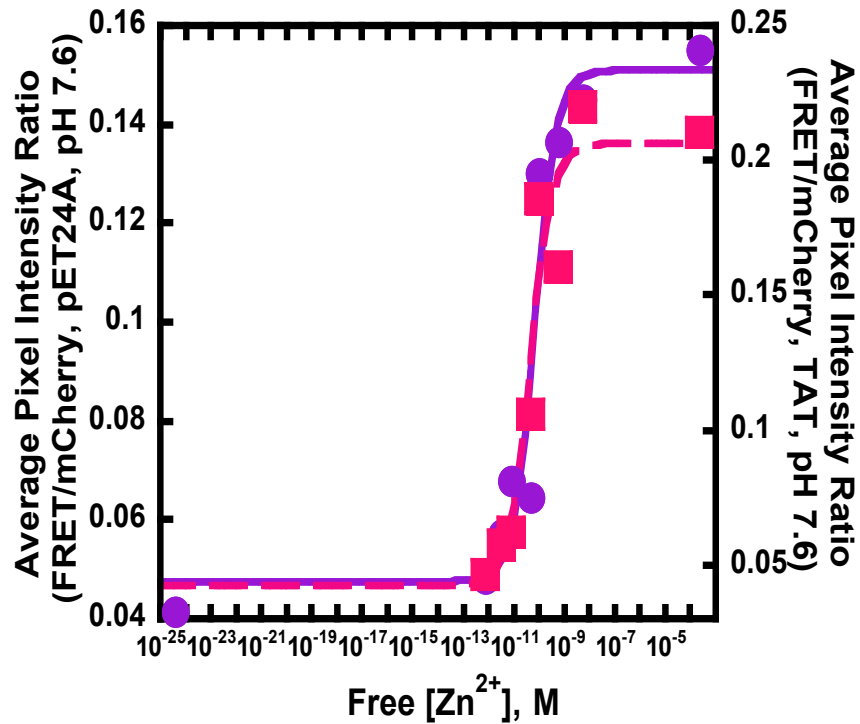
Figure 4:5: *In situ* calibration curve of the modified versions of

CA(II)_mCherry:

2mL *E. coli* cells expressing CA(II)_mCherry were treated with 100 µL 1 mM
EDTA in MOPS media. The cells were equilibrated with 100 µL MOPS NTA-
chelated zinc buffers (pH = 7.6) with 2 µM Dps and 30 µM digitonin for 40 min at
room temperature. FRET/FP excitation intensity ratios were taken in 96-well
glass bottom plates using the fluorescence microscope. (●) *in vitro* calibration
curve of BL21(DE3)_p24aH_mCherry encoding the CA(II)_mCherry_His sensor
with 3-Gly linker. (■) *in vitro* calibration curve of BL21(DE3)_pAHT_CA(II)_mCh
encoding the TAT_CA(II)_mCherry sensor with 3-Gly linker. Each data point
represents a single (2-channel) acquisition taken at the known free zinc
concentration. A binding isotherm are fit to these data

DISCUSSION

In the current study, CA(II)_mCherry was tested as a protein based sensor to probe free zinc concentrations in *E. coli* via intracellular imaging. We have shown that fusing CA(II) to mCherry via a short flexible tri-glycine linker does not disrupt important sensor properties. Having established the correct expression of CA(II)_mCherry, fluorescence microscopy experiments were performed on *E. coli* BL21(DE3) cells expressing CA(II)_mCherry. In order to accurately quantitate free cytosolic zinc, the differences in cellular environment and fluorescence instrumentation optics were voided. Calibrating the FRET/FP ratio in the presence of cells allowed us to determine the cells' response to zinc in real time. These *in situ* or quantitative calibrations were used to discern the numerical value for the resting, readily exchangeable zinc concentration in *E. coli*. These data clearly shows an increase in FRET signals between Dps and mCherry upon titration of Zn^{2+}, as expected, and this increase reflects the zinc concentration.

More importantly, the fact that zinc is able to form a stable complex with CA(II)_mCherry expressed in *E. coli* with an apparent dissociation constant consistent with reported cysolic free zinc concentrations in bacteria raises interesting biological questions concerning Zn^{2+} transport and storage *in vivo*. A fundamental assumption calculating the intracellular zinc concentration for the FRET/FP ratio and the calibration curve is that CA(II) is at thermodynamic equilibration with intracellular zinc. For CA(II)_mCherry, the zinc binding kinetics imaged in the cell occur within 20-40 min. To examine this assumption, Bozym et

al. tested two versions of the TAT-tagged, Alexa Fluor labeled carbonic anhydrase-based zinc sensors in PC-12 cells: one with a slow association rate constant of 10^5 M^{-1} s^{-1} and the other with a single site mutation (E117A) that increases the association rate constant by 800-fold [157]. They found that in these cells both sensors reach equilibrium in ~5 min. This rapid equilibration suggests that zinc binding processes are catalyzed by chaperones or small molecule-zinc complexes such as glutathione. This translates to CA(II) binding as a zinc complex which is at higher concentration than pM, therefore, CA(II)_mCherry, which concentration estimates are near mM, likely also binds zinc rapidly in cells.

In conclusion, we have developed a new generation of divalent metal sensors that can be utilized to measure low levels of free Zn^{2+} in various cell types. Optimization of the brightness and maturation lifetimes of this sensor will provide better visualization at lower expression levels. Furthermore, the current sensor system can be optimized by improving the relatively small difference in energy transfer that is observed upon binding of the metal. Lastly, by altering metal selectivity via mutagenesis this sensor can be used to probe physiologically relevant Zn^{2+} transport and storage pathways.

REFERENCES

[1]   R.B. Thompson, B.P. Maliwal, V.L. Feliccia, C.A. Fierke, K. McCall, Determination of picomolar concentrations of metal ions using fluorescence anisotropy: biosensing with a "reagentless" enzyme transducer, Anal Chem 70 (1998) 4717-4723.

[2]   R.B. Thompson, M.L. Cramer, R. Bozym, Excitation ratiometric fluorescent biosensor for zinc ion at picomolar levels, J Biomed Opt 7 (2002) 555-560.

[3]   G.K. Walkup, B. Imperiali, Design and evaluation of a peptidyl fluorescent chemosensor for divalent zinc, J. Am. Chem. Soc. 118 (1996) 3053-3054.

[4]   E.M. Nolan, S.C. Burdette, J.H. Harvey, S.A. Hilderbrand, S.J. Lippard, Synthesis and characterization of zinc sensors based on a monosubstituted fluorescein platform, Inorg Chem 43 (2004) 2624-2635.

[5]   C.C. Woodroofe, R. Masalha, K.R. Barnes, C.J. Frederickson, S.J. Lippard, Membrane-permeable and -impermeable sensors of the Zinpyr family and their application to imaging of hippocampal zinc *in vivo*, Chem Biol 11 (2004) 1659-1666.

[6]   K. Komatsu, K. Kikuchi, H. Kojima, Y. Urano, T. Nagano, Selective zinc sensor molecules with various affinities for Zn2+, revealing dynamics and regional distribution of synaptically released Zn2+ in hippocampal slices, J Am Chem Soc 127 (2005) 10197-10204.

[7]   H.H. Zeng, R.B. Thompson, B.P. Maliwal, G.R. Fones, J.W. Moffett, C.A. Fierke, Real-time determination of picomolar free Cu(II) in seawater using a fluorescence-based fiber optic biosensor, Anal Chem 75 (2003) 6807-6812.

[8]   L. Yang, R. McRae, M.M. Henary, R. Patel, B. Lai, S. Vogt, C.J. Fahrni, Imaging of the intracellular topography of copper with a fluorescent sensor and by synchrotron x-ray fluorescence microscopy, Proc Natl Acad Sci U S A 102 (2005) 11179-11184.

[9]   P. Chen, C. He, A general strategy to convert the MerR family proteins into highly sensitive and selective fluorescent biosensors for metal ions, J Am Chem Soc 126 (2004) 728-729.

[10]   R.B. Thompson, D. Peterson, W. Mahoney, M. Cramer, B.P. Maliwal, S.W. Suh, C. Frederickson, C. Fierke, P. Herman, Fluorescent zinc indicators for neurobiology, J Neurosci Methods 118 (2002) 63-75.

[11]   K.K. Jensen, L. Martini, T.W. Schwartz, Enhanced fluorescence resonance energy transfer between spectral variants of green fluorescent protein through zinc-site engineering, Biochemistry 40 (2001) 938-945.

[12]   S.J. Lin, R.A. Pufahl, A. Dancis, T.V. O'Halloran, V.C. Culotta, A role for the Saccharomyces cerevisiae ATX1 gene in copper trafficking and iron transport, J Biol Chem 272 (1997) 9215-9220.

[13]   D. Larin, C. Mekios, K. Das, B. Ross, A.S. Yang, T.C. Gilliam, Characterization of the interaction between the Wilson and Menkes disease proteins and the cytoplasmic copper chaperone, HAH1p, J Biol Chem 274 (1999) 28497-28504.

[14] E.M. van Dongen, T.H. Evers, L.M. Dekkers, E.W. Meijer, L.W. Klomp, M. Merkx, Variation of linker length in ratiometric fluorescent sensor proteins allows rational tuning of Zn(II) affinity in the picomolar to femtomolar range, J Am Chem Soc 129 (2007) 3494-3495.

[15] J.L. Vinkenborg, M.S. Koay, M. Merkx, Fluorescent imaging of transition metal homeostasis using genetically encoded sensors, Curr Opin Chem Biol 14 (2010) 231-237.

[16] N.C. Shaner, R.E. Campbell, P.A. Steinbach, B.N. Giepmans, A.E. Palmer, R.Y. Tsien, Improved monomeric red, orange and yellow fluorescent proteins derived from Discosoma sp. red fluorescent protein, Nat Biotechnol 22 (2004) 1567-1572.

[17] R.A. Bozym, R.B. Thompson, A.K. Stoddard, C.A. Fierke, Measuring picomolar intracellular exchangeable zinc in PC-12 cells using a ratiometric fluorescence biosensor, ACS Chem Biol 1 (2006) 103-111.

[18] L. Stryer, Fluorescence energy transfer as a spectroscopic ruler, Annu Rev Biochem 47 (1978) 819-846.

[19] A. Miyawaki, O. Griesbeck, R. Heim, R.Y. Tsien, Dynamic and quantitative Ca2+ measurements using improved cameleons, Proc Natl Acad Sci U S A 96 (1999) 2135-2140.

[20] W. Maret, Molecular aspects of human cellular zinc homeostasis: redox control of zinc potentials and zinc signals, Biometals 22 (2009) 149-157.

[21] C.E. Outten, T.V. O'Halloran, Femtomolar sensitivity of metalloregulatory proteins controlling zinc homeostasis, Science 292 (2001) 2488-2492.

[22] H.L. Alakomi, A. Paananen, M.L. Suihko, I.M. Helander, M. Saarela, Weakening effect of cell permeabilizers on gram-negative bacteria causing biodeterioration, Appl Environ Microbiol 72 (2006) 4695-4703.

CHAPTER 5: CONCLUSIONS AND FUTURE DIRECTIONS

Carbonic anhydrases are archetypical zinc metalloenzymes and as such, they have been developed as the recognition element of a family of fluorescent indicators (sensors) to detect metal ions, particularly Zn^{2+} and Cu^{2+}. WT CA(II) having a high affinity for both copper and zinc (Chapter 2) is known for its unmatched selectivity. Inherent limitations of selectivity still can present a problem for the application of these proteins in the studies of metal distribution in seawater and potentially cellular imaging of either of these metals. The original aim of this study was to elucidate the selectivity for either Cu^{2+} or Zn^{2+} by site directed mutagenesis of residues in the active site of CA(II) [132]. In an effort to develop a more copper specific sensor, single mutations were made at positions 92 and 199 in human CA(II). It was shown that the affinity for zinc in all tested mutant proteins was significantly decreased, as Zn(II) needs at least four coordinating ligands for binding. Subtle differences in coordination geometry can have major effects on metal specificity. More research is necessary to establish whether a more copper specific active site can be further optimized to enhance the specificity for copper over zinc when in contaminating metal environments. Nevertheless, the question of metal specificity is also important to consider for proteins that can be used to better understand metal homeostasis [184].

Fluorescent probes for imaging Zn^{2+} are known to and will continue to have

a major technical impact on biomedical research and related diseases for decades to come [41], [25]. Consequently, the major focus of this thesis was to develop a method to measure intracellular zinc via a ratiometric FRET-based sensor protein. Until recently, no examples of other ratiometric sensor proteins for zinc with pM sensitiviy that can be applied to live-cell imaging had been reported. The expressible sensors described in this thesis were based on the carbonic anhydrase platform. To create a FRET system, a series of red fluorescent proteins were fused to CA(II) via a tri-glycine linker. Energy transfer is observed when, in the presence of Zn^{2+} bound to the active site of CA(II) Dps acts as a donor to excite the fluorescent proteins, mOrange and mCherry. The Zn(II) affinity of the single protein sensor was found to depend on the gene's sequence, FRET overlap and chromophore maturation half lives, ranging from 2 pM to 60 pM. Zinc binding resulted in the formation of a stable tertiary complex that was insensitive to changes in the intracellular metal concentrations. Mutagenesis studies of the metal binding sites were attempted to probe the selectivity for Zn^{2+} in the fusion protein, but the preliminary work will be further developed.

Our cell imaging experiments with CA_mCherry and TAT_CA_mCherry have been optimized showing that the sensor is well expressed in bacteria. In addition, energy transfer was clearly observed with great response upon addition or depletion of zinc. Further improvements to our system will be to optimize protocols for expressing the fusion sensors in yeast and mammalian cell types.

The protein concentration of CA(II)_mCherry when expressed in BL21(DE3)

cells is not well established, concentrations studies suggest values in the range of 20-50 mM. This protein concentration and the measured free zinc concentration in the cytosol of *E. coli* is not unrealistic, suggesting that CA(II)_mCherry-Zn-Dps complexes could be formed in other cell types. A second important indication that this complex can be formed *in vivo* came from our zinc repletion and deletion studies which we observed a steady increase in FRET/FP ratios upon addition of Zn(II) to the extracellular millieu. More pronounced is our manipulation of FRET/FP ratios by the chelation of Zn with   EDTA. All signal outputs were confirmed via our *in vivo* exthoxzolamide studies-proving changes in emission intensities are zinc dependent.

Determination of the intracellular concentration of free Zn inside living cells is a major step forward as the exact concentration of these metals in mammalian cells is better understood, but still remains an unsolved issue. Our expressible sensor which has a zinc affinity in the pM range can probe these low concentrations, because cells act as an efficient buffering system for metals such as Zn(II) [76]. The free Zn(II) concentration could therefore be very low, but at the same time the total zinc concentration inside cells is much higher (µM), which is more than sufficient to saturate the sensor.

The CA(II)_mCherry (and CA(II))_mOrange) sensors described in this thesis have many attractive features for application as intracellular imaging tools for Zn. However, higher levels of expression of sensor might be necessary for reliable visualization in mammalian and yeast cells, which may interfere with normal functions of the cells. In our current yeast vector series, protein

141

expression is under the control of the galactose inducible, glucose repressed GAL1 promoter. Because these vectors do not result in adequate protein expression for fluorescence imaging, the constitutive PMA1 promoter is an even stronger yeast promoter [185]. PMA1 was not selected for the initial work because constitutive expression of a metalloproteins such as CA(II) were thought to may have a potential detrimental effect on the cells.

Furthermore, the current sensor system can be tweaked by improving the relatively small difference in energy transfer that is observed upon binding of the metal and by probing the metal selectivity for other biological relevant metals. Alternative sensor designs employing different fluorescent proteins variants are being studied [186]. These variants were selected because of excitation and emission spectra, enhanced brightness, and improved pH resistance. The enhanced brightness of these proteins is determined by several factors, including the faster maturation speed and efficiency, higher extinction coefficients, improved quantum yields and photostability. Replacement of the fluorescent proteins with these new variants in our expressible sensor design also allows more effective quantitative FRET imaging due to the close spectral overlap of the donor emission and acceptor absorption, resulting in a larger Förster distance. CA(II)_mCherry and CA(II)_mOrange are reported to have dissociations constants that are ideal, but exhibit a relatively small change in FRET/FP ratio of ~ 30% upon zinc binding. Varying linker length may prove to be as reasonable aapproach to increase the ratiometric change without sacrificing the lower apparent affinity for zinc.

The ability to image the concentration of transition metals in living cells in real time at a high resolution is considered a huge success for our lab. The research described in this thesis yielded new insights into the mechanism of metal homeostasis and metal specificity. Furthermore, this work provides important lessons for the rational design of a FRET-based sensors in general. The current sensor design can be employed to address more specific zinc dependent responses that result from more extreme growth and environmental conditions (i.e oxidative and nitrosative stress) and ultimately metals and their involvement in diseases [187].

REFERENCES

[1]   C. Andreini, L. Banci, I. Bertini, A. Rosato, Counting the zinc-proteins encoded in the human genome, J Proteome Res 5 (2006) 196-201.

[2]   J.E. Coleman, Zinc proteins: Enzymes, storage proteins, transcription factors, and replication proteins, Annual Review of Biochemistry 61 (1992) 897-946.

[3]   D.W. Christianson, Structural biology of zinc, Advances in Protein Chemistry 42 (1991) 281-355.

[4]   B.L. Vallee, D.S. Auld, Zinc coordination, function, and structure of zinc enzymes and other proteins, Biochemistry 29 (1990) 5647-5659.

[5]   D. Keilin, T. Mann, Carbonic anhydrase. Purification and nature of the enzyme, Biochem J 34 (1940) 1163-1176.

[6]   J.M. Matthews, M. Sunde, Zinc fingers--folds for many occasions, IUBMB Life 54 (2002) 351-355.

[7]   W. Maret, H.H. Sandstead, Zinc requirements and the risks and benefits of zinc supplementation, J Trace Elem Med Biol 20 (2006) 3-18.

[8]   B.L. Vallee, K.H. Falchuk, The biochemical basis of zinc physiology, Physiological Reviews 73 (1993) 79-118.

[9]   J.P. Liuzzi, R.J. Cousins, Mammalian zinc transporters, Annu Rev Nutr 24 (2004) 151-172.

[10]   M.J. Tuerk, N. Fazel, Zinc deficiency, Curr Opin Gastroenterol 25 (2009) 136-143.

[11]   N. Bhandari, R. Bahl, S. Taneja, T. Strand, K. Molbak, R.J. Ulvik, H. Sommerfelt, M.K. Bhan, Substantial reduction in severe diarrheal morbidity by daily zinc supplementation in young north Indian children, Pediatrics 109 (2002) e86.

[12]   C. Devirgiliis, P.D. Zalewski, G. Perozzi, C. Murgia, Zinc fluxes and zinc transporter genes in chronic diseases, Mutat Res 622 (2007) 84-93.

[13]   A.I. Bush, W.H. Pettingell, G. Multhaup, M.d. Paradis, J.-P. Vonsattel, J.F. Gusella, K. Beyreuther, C.L. Masters, R.E. Tanzi, Rapid induction of Alzheimer AB amyloid formation by zinc, Science 265 (1994) 1464-1467.

[14]   R.A. Cherny, C.S. Atwood, M.E. Xilinas, D.N. Gray, W.D. Jones, C.A. McLean, K.J. Barnham, I. Volitakis, F.W. Fraser, Y.S. Kim, X. Huang, L.E. Goldstein, R.D. Moir, J.T. Lim, K. Beyreuther, H. Zheng, R.E. Tanzi, C. Masters, A.I. Bush, Treatment with a copper-zinc chelator markedly and rapidly inhibits beta-amyloid accumulation in Alzheimer's disease transgenic mice, Neuron 30 (2001) 665 - 676.

[15]   C.G. Taylor, Zinc, the pancreas, and diabetes: insights from rodent studies and future directions, Biometals 18 (2005) 305-312.

[16]   R. Sladek, G. Rocheleau, J. Rung, C. Dina, L. Shen, D. Serre, P. Boutin, D. Vincent, A. Belisle, S. Hadjadj, B. Balkau, B. Heude, G. Charpentier, T.J. Hudson, A. Monpetit, A.V. Psheszhetsky, M. Prentki, B.I. Posner, D.J. Balding, D. Meyre, C. Polychronakos, P. Froguel, A genome-wide association study identifies novel risk loci for type 2 diabetes, Nature 445 (2007) 881 - 885.

[17] J. Szpunar, Bio-inorganic speciation analysis by hyphenated techniques, Analyst 125 (2000) 963-988.

[18] A. Sanz-Medel, M. Montes-Bayon, M. Luisa Fernandez Sanchez, Trace element speciation by ICP-MS in large biomolecules and its potential for proteomics, Anal Bioanal Chem 377 (2003) 236-247.

[19] T. Paunesku, S. Vogt, J. Maser, B. Lai, G. Woloschak, X-ray fluorescence microprobe imaging in biology and medicine, J Cell Biochem 99 (2006) 1489-1502.

[20] M. Ralle, S. Lutsenko, Quantitative imaging of metals in tissues, Biometals 22 (2009) 197-205.

[21] R.M. Rousseau, Detection limit and estimate of uncertainty of analytical XRF results, Rigaku 18 (2001) 33-47.

[22] C.J. Fahrni, Biological applications of X-ray fluorescence microscopy: exploring the subcellular topography and speciation of transition metals, Curr Opin Chem Biol 11 (2007) 121-127.

[23] P. Jiang, Z. Guo, Fluorescent detection of zinc in biological systems: recent development on the design of chemosensors and biosensors, Coordination Chemistry Reviews 248 (2004) 205 - 229.

[24] D.W. Domaille, E.L. Que, C.J. Chang, Synthetic fluorescent sensors for studying the cell biology of metals, Nat Chem Biol 4 (2008) 168-175.

[25] T. Hirano, K. Kikuchi, T. Nagano, zinc fluorescent probes for biological applications, in: C.D. Geddes, J.R. Lakowicz (Eds.), Reviews in Fluorescence 2004, Kluwer Academic / Plenum Publishers, New York, 2004, pp. 55 - 73.

[26] R.B. Thompson, Studying zinc biology with fluorescence: Ain't we got fun?, Current Opinion in Chemical Biology 9 (2005) 526 - 532.

[27] B. Morelle, J.M. Salmon, J. Vigo, P. Viallet, Measurement of intracellular magnesium concentration in 3T3 fibroblasts with the fluorescent indicator Mag-indo-1, Analytical Biochemistry 218 (1994) 170-176.

[28] L. Missiaen, W. Robberecht, L. Van Den Bosch, G. Callewaert, J.B. Parys, F. Wuytack, L. Raeymaekers, B. Nilius, J. Eggermont, H. De Smedt, Abnormal intracellular Ca^{2+} homeostasis and disease, Cell Calcium 28 (2000) 1-21.

[29] R.A. Bozym, R.B. Thompson, A.K. Stoddard, C.A. Fierke, Measuring picomolar intracellular exchangeable zinc in PC-12 cells using a ratiometric fluorescence biosensor, ACS Chemical Biology 1 (2006) 103 - 111.

[30] G. Grynkiewicz, M. Poenie, R.Y. Tsien, A new generation of calcium indicators with greatly improved fluorescence properties, Journal of Biological Chemistry 260 (1985) 3440-3450.

[31] M.E. Lippitsch, J. Pusterhofer, M.J.P. Leiner, O.S. Wolfbeis, Fibre-optic oxygen sensor with the fluorescence decay time as the information carrier, Analytica Chimica Acta 205 (1988) 1.

[32] J.R. Lakowicz, Principles of Fluorescence Spectroscopy, Second ed., Kluwer Academic / Plenum Publishers, New York, 1999.

[33] W.B. Dandliker, R.J. Kelly, J. Dandliker, J. Farquhar, J. Levin, Fluorescence polarization immunoassay. Theory and experimental method, Immunochemistry 10 (1973) 219-227.

[34] C.E. White, R.J. Argauer, Fluorescence Analysis: A Practical Approach, Marcel Dekker, Inc., New York, 1970.

[35] A. Fernandez-Gutierrez, A. Munoz de la Pena, Determinations of inorganic substances by luminescence methods, in: S.G. Schulman (Ed.), Molecular Luminescence Spectroscopy, Part I: Methods and Applications, vol. 77, Wiley-Interscience, New York, 1985, pp. 371-546.

[36] J.R. Lakowicz, I. Gryczynski, Z. Gryczynski, J.D. Dattelbaum, Anisotropy-based sensing with reference fluorophores, Analytical Biochemistry 267 (1999) 397 - 405.

[37] C.J. Frederickson, E.J. Kasarskis, D. Ringo, R.E. Frederickson, A quinoline fluorescence method for visualizing and assaying histochemically reactive zinc (bouton zinc) in the brain, Journal of Neuroscience Methods 20 (1987) 91-103.

[38] P.D. Zalewski, I.J. Forbes, W.H. Betts, Correlation of apoptosis with change in intracellular labile Zn(II) using Zinquin [(2-methyl-8-p-toluenesulphonamido-6-quinolyloxy)acetic acid], a new specific fluorescent probe for Zn(II), Biochemical Journal 296 (1993) 403-408.

[39] M.E. Huston, K.W. Haider, A.W. Czarnik, Chelation-enhanced fluorescence in 9, 10-bis(TMEDA) anthracene, Journal of the American Chemical Society 110 (1988) 4460 - 4462.

[40] S.C. Burdette, G.K. Walkup, B. Spingler, R.Y. Tsien, S.J. Lippard, Fluorescent sensors for Zn2+ based on a fluorescein platform: Synthesis, properties and intracellular distribution, Journal of the American Chemical Society 123 (2001) 7831-7841.

[41] K.R. Gee, Z.L. Zhou, D. Ton-That, S.L. Sensi, J.H. Weiss, Measuring zinc in living cells. A new generation of sensitive and selective fluorescent probes, Cell Calcium 31 (2002) 245 - 251.

[42] S.L. Sensi, D. Ton-That, P.G. Sullivan, E.A. Jonas, K.R. Gee, L.K. Kaczmarek, J.H. Weiss, Modulation of mitochondrial function by endogenous Zn2+ pools, Proceedings of the National Academy of Sciences 100 (2003) 6157 - 6162.

[43] M.M. Henary, Y. Wu, C.J. Fahrni, Zinc(II)-selective ratiometric fluorescent sensors based on inhibition of excited state intramolecular proton transfer, Chemistry in Europe Journal 10 (2004) 3015 - 3025.

[44] S. Aoki, D. Kagata, M. Shiro, K. Takeda, E. Kimura, Metal chelation-controlled twisted intramolecular charge transfer and its application to fluorescent sensing of metal ions and anions, Journal of the American Chemical Society 126 (2004) 13377 - 13390.

[45] H.A. Godwin, J.M. Berg, A fluorescent zinc probe based on metal induced peptide folding, Journal of the American Chemical Society 118 (1996) 6514-6515.

[46] G.K. Walkup, B. Imperiali, Fluorescent chemosensors for divalent zinc based on zinc finger domains. Enhanced oxidative stability, metal binding

affinity, and structural and functional characterization, Journal of the American Chemical Society 119 (1997) 3443-3450.

[47] J.S. Marvin, H.W. Hellinga, Conversion of a maltose receptor into a zinc biosensor by computational design, Proceedings of the National Academy of Sciences 98 (2001) 4955 - 4960.

[48] A. Miyawaki, J. Llopis, R. Heim, J.M. McCaffery, J.A. Adams, M. Ikura, R.Y. Tsien, Fluorescent indicators for Ca2+ based on green fluorescent proteins and calmodulin, Nature 388 (1997) 882-887.

[49] L.L. Pearce, R.E. Gandley, W. Han, K. Wasserloos, M. Stitt, A.J. Kanai, M.K. McLaughlin, B.R. Pitt, E.S. Levitan, Role of metallothionein in nitric oxide signaling as revealed by a green fluorescent fusion protein, Proceedings of the National Academy of Sciences 97 (2000) 477 - 482.

[50] K.K. Jensen, L. Martini, T.W. Schwartz, Enhanced fluorescence resonance energy transfer between spectral variants of green fluorescent protein through zinc-site engineering, Biochemistry 40 (2001) 938-945.

[51] W. Qiao, M. Mooney, A.J. Bird, D.R. Winge, D.J. Eide, Zinc binding to a regulatory zinc-sensing domain monitored *in vivo* by using FRET, Proc Natl Acad Sci U S A 103 (2006) 8674-8679.

[52] E.M.W.M.v. Dongen, T.H. Evers, L.M. Dekkers, E.W. Meijer, L.W.J. Klomp, M. Merkx, Variation of linker length in ratiometric fluorescent sensor proteins allows rational tuning of Zn(II) affinity in the picomolar to femtomolar range, Journal of the American Chemical Society 129 (2007) 3494 - 3495.

[53] N.U. Meldrum, F.J. Roughton, Carbonic anhydrase. Its preparation and properties, J Physiol 80 (1933) 113-142.

[54] H. Stadie W.C. and O'Brien, The catalysis of the hydration of carbon dioxide and the dehydration of carbonic acid by an enzyme isolated from red blood cells. , The Journal of Biological Chemistry
103 (1933) 521-529.

[55] A. Liljas, K.K. Kannan, P.C. Bergsten, I. Waara, K. Fridborg, B. Strandberg, U. Carlbom, L. Jarup, S. Lovgren, M. Petef, Crystal structure of human carbonic anhydrase C, Nat New Biol 235 (1972) 131-137.

[56] K. Hakansson, M. Carlsson, L.A. Svensson, A. Liljas, Structure of native and apo carbonic anhydrase II and structure of some of its anion-ligand complexes, Journal of Molecular Biology 227 (1992) 1192-1204.

[57] D.W. Christianson, C.A. Fierke, Carbonic anhydrase - Evolution of the zinc binding site by nature and by design, Accounts of Chemical Research 29 (1996) 331 - 339.

[58] K.A. McCall, C. Huang, C.A. Fierke, Function and mechanism of zinc metalloenzymes, J Nutr 130 (2000) 1437S-1446S.

[59] M.S. Kimber, E.F. Pai, The active site architecture of Pisum sativum beta-carbonic anhydrase is a mirror image of that of alpha-carbonic anhydrases, EMBO Journal 19 (2000) 1407 - 1418.

[60] L.L. Kiefer, J.F. Krebs, S.A. Paterno, C.A. Fierke, Engineering a cysteine ligand into the zinc binding site of human carbonic anhydrase II, Biochemistry 32 (1993) 9896-9900.

[61]   J.A. Ippolito, T.T. Baird, Jr., S.A. McGee, D.W. Christianson, C.A. Fierke, Structure-assisted redesign of a protein-zinc-binding site with femtomolar affinity, Proc Natl Acad Sci U S A 92 (1995) 5017-5021.

[62]   L.L. Kiefer, J.A. Ippolito, C.A. Fierke, D.W. Christianson, Redesigning the zinc binding siteof human carbonic anhydrase II: Structure of a His2Asp-Zn2+ metal coordination polyhedron, Journal of the American Chemical Society 115 (1993) 12581 - 12582.

[63]   R.S. Alexander, L.L. Kiefer, C.A. Fierke, D.W. Christianson, Engineering the zinc binding site of human carbonic anhydrase II: structure of the His-94-->Cys apoenzyme in a new crystalline form, Biochemistry 32 (1993) 1510-1518.

[64]   L.L. Kiefer, C.A. Fierke, Functional characterization of human carbonic anhydrase II variants with altered zinc binding sites, Biochemistry 33 (1994) 15233-15240.

[65]   C.A. Lesburg, C. Huang, D.W. Christianson, C.A. Fierke, Histidine --> carboxamide ligand substitutions in the zinc binding site of carbonic anhydrase II alter metal coordination geometry but retain catalytic activity, Biochemistry 36 (1997) 15780-15791.

[66]   K.A. McCall, C.A. Fierke, Probing determinants of the metal ion selectivity in carbonic anhydrase using mutagenesis, Biochemistry 43 (2004) 3979-3986.

[67]   L.L. Kiefer, S.A. Paterno, C.A. Fierke, Hydrogen bond network in the metal binding site of carbonic anhydrase enhances zinc affinity and catalytic efficiency, Journal of the American Chemical Society 117 (1995) 6831-6837.

[68]   C.C. Huang, C.A. Lesburg, L.L. Kiefer, C.A. Fierke, D.W. Christianson, Reversal of the hydrogen bond to zinc ligand histidine-119 dramatically diminishes catalysis and enhances metal equilibration kinetics in carbonic anhydrase II, Biochemistry 35 (1996) 3439-3446.

[69]   C.A. DiTusa, K.A. McCall, T. Christensen, M. Mahapatro, C.A. Fierke, E.J. Toone, Thermodynamics of metal ion binding. 2. Metal ion binding by carbonic anhydrase variants, Biochemistry 40 (2001) 5345-5351.

[70]   J.A. Hunt, C.A. Fierke, Selection of carbonic anhydrase variants displayed on phage. Aromatic residues in zinc binding site enhance metal affinity and equilibration kinetics, J Biol Chem 272 (1997) 20364-20372.

[71]   J.A. Hunt, M. Ahmed, C.A. Fierke, Metal binding specificity in carbonic anhydrase is influenced by conserved hydrophobic core residues, Biochemistry 38 (1999) 9054-9062.

[72]   J.D. Cox, J.A. Hunt, K.M. Compher, C.A. Fierke, D.W. Christianson, Structural influence of hydrophobic core residues on metal binding and specificity in carbonic anhydrase II, Biochemistry 39 (2000) 13687 - 13694.

[73]   R.W. Henkens, J.M. Sturtevant, The kinetics of the binding of Zn(II) by apocarbonic anhydrase, Journal of the American Chemical Society 90 (1968) 2669 - 2676.

[74] J.B. Hunt, M.J. Rhee, C.B. Storm, A rapid and convenient preparation of apocarbonic anhydrase, Anal Biochem 79 (1977) 614-617.

[75] Y. Pocker, C.T.O. Fong, Inactivation of bovine carbonic anhydrase by dipicolinate: Kinetic studies and mechanistic implications, Biochemistry 22 (1983) 813 - 818.

[76] C.E. Outten, T.V. O'Halloran, Femtomolar sensitivity of metalloregulatory proteins controlling zinc homeostasis, Science 292 (2001) 2488-2492.

[77] D.G. Nicholls, Mitochondria and calcium signaling, Cell Calcium 38 (2005) 311-317.

[78] J.T. Taylor, X.B. Zeng, J.E. Pottle, K. Lee, A.R. Wang, S.G. Yi, J.A.S. Scruggs, S.S. Sikka, M. Li, Calcium signaling and T-type calcium channels in cancer cell cycling, World Journal of Gastroenterology 14 (2008) 4984-4991.

[79] W. Breuer, S. Epsztejn, Z.I. Cabantchik, Iron acquired from transferrin by K562 cells is delivered into a cytoplasmic pool of chelatable iron(II), J Biol Chem 270 (1995) 24209-24215.

[80] G.J. Kress, K.E. Dineley, I.J. Reynolds, The relationship between intracellular free iron and cell injury in cultured neurons, astrocytes, and oligodendrocytes, J Neurosci 22 (2002) 5848-5855.

[81] F. Petrat, U. Rauen, H. de Groot, Determination of the chelatable iron pool of isolated rat hepatocytes by digital fluorescence microscopy using the fluorescent probe, phen green SK, Hepatology 29 (1999) 1171-1179.

[82] A.N. Woodmansee, J.A. Imlay, Quantitation of intracellular free iron by electron paramagnetic resonance spectroscopy, Methods Enzymol 349 (2002) 3-9.

[83] T.D. Rae, P.J. Schmidt, R.A. Pufahl, V.C. Culotta, T.V. O'Halloran, Undetectable intracellular free copper: the requirement of a copper chaperone for superoxide dismutase, Science 284 (1999) 805-808.

[84] S. Lindskog, P.O. Nyman, Metal-Binding Properties of Human Erythrocyte Carbonic Anhydrases, Biochim Biophys Acta 85 (1964) 462-474.

[85] K.A. McCall, C.A. Fierke, Colorimetric and fluorimetric assays to quantitate micromolar concentrations of transition metals, Anal Biochem 284 (2000) 307-315.

[86] L.A. Finney, T.V. O'Halloran, Transition metal speciation in the cell: insights from the chemistry of metal ion receptors, Science 300 (2003) 931-936.

[87] K. Hakansson, A. Wehnert, A. Liljas, X-ray analysis of metal-substituted human carbonic anhydrase II derivatives, Acta Crystallogr D Biol Crystallogr 50 (1994) 93-100.

[88] C.A. DiTusa, T. Christensen, K.A. McCall, C.A. Fierke, E.J. Toone, Thermodynamics of metal ion binding. 1. Metal ion binding by wild-type carbonic anhydrase, Biochemistry 40 (2001) 5338-5344.

[89] J.A. Hunt, C.A. Fierke, Selection of carbonic anhydrase variants displayed on phage: aromatic residues in zinc binding site enhance metal affinity and equilibration kinetics, Journal of Biological Chemistry 272 (1997) 20364-20372.

[90]   T.H. Maren, Use of inhibitors in physiological studies of carbonic anhydrase, American Journal of Physiology 232 (1977) F291-F297.

[91]   S.K. Nair, J.F. Krebs, D.W. Christianson, C.A. Fierke, Structural basis of inhibitor affinity to variants of human carbonic anhydrase II, Biochemistry 34 (1995) 3981-3989.

[92]   R.F. Chen, J.C. Kernohan, Combination of bovine carbonic anhydrase with a fluorescent sulfonamide, J Biol Chem 242 (1967) 5813-5823.

[93]   R.B. Thompson, E.R. Jones, Enzyme-based fiber optic zinc biosensor, Analytical Chemistry 65 (1993) 730-734.

[94]   R.B. Thompson, W.O. Whetsell, Jr., B.P. Maliwal, C.A. Fierke, C.J. Frederickson, Fluorescence microscopy of stimulated Zn(II) release from organotypic cultures of mammalian hippocampus using a carbonic anhydrase-based biosensor system, J Neurosci Methods 96 (2000) 35-45.

[95]   R.B. Thompson, B.P. Maliwal, C.A. Fierke, Selectivity and sensitivity of fluorescence lifetime-based metal ion biosensing using a carbonic anhydrase transducer, Anal Biochem 267 (1999) 185-195.

[96]   R.B. Thompson, B.P. Maliwal, V. Feliccia, C.A. Fierke, High sensitivity determination of Zn(II) and Cu(II) *in vitro* by fluorescence polarization, in: G.E. Cohn (Ed.), Systems and Technologies for Clinical Diagnostics and Drug Discovery, vol. 3259, SPIE, San Jose, CA, 1998, pp. 40-47.

[97]   R.B. Thompson, M.W. Patchan, Lifetime-based fluorescence energy transfer biosensing of zinc, Anal Biochem 227 (1995) 123-128.

[98]   C.J. Frederickson, L.J. Giblin, 3rd, R.V. Balaji, R. Masalha, C.J. Frederickson, Y. Zeng, E.V. Lopez, J.Y. Koh, U. Chorin, L. Besser, M. Hershfinkel, Y. Li, R.B. Thompson, A. Krezel, Synaptic release of zinc from brain slices: factors governing release, imaging, and accurate calculation of concentration, J Neurosci Methods 154 (2006) 19-29.

[99]   T. Forster, Intermolecular energy migration and fluorescence (Ger.), Annalen der Physik 2 (1948) 55 - 75.

[100]   R.B. Thompson, M.L. Cramer, R. Bozym, Excitation ratiometric fluorescent biosensor for zinc ion at picomolar levels, J Biomed Opt 7 (2002) 555-560.

[101]   J.S. Wadia, S.F. Dowdy, Transmembrane delivery of protein and peptide drugs by TAT-mediated transduction in the treatment of cancer, Adv Drug Deliv Rev 57 (2005) 579-596.

[102]   L.L. Kiefer, S.A. Paterno, C.A. Fierke, Second shell hydrogen bonds to histidine ligands enhance zinc affinity and catalytic efficiency, Journal of the American Chemical Society 117 (1995) 6831 - 6837.

[103]   C.J. Frederickson, J.-Y. Koh, A.I. Bush, The neurobiology of zinc in health and disease, Nature Reviews Neuroscience 6 (2005) 449 - 462.

[104]   Y. Li, C.J. Hough, S.W. Suh, J.M. Sarvey, C.J. Frederickson, Rapid translocation of Zn(2+) from presynaptic terminals into postsynaptic hippocampal neurons after physiological stimulation, J Neurophysiol 86 (2001) 2597-2604.

[105]   C.A. Fierke, R.B. Thompson, Fluorescence-based biosensing of zinc using carbonic anhydrase, Biometals 14 (2001) 205-222.

[106] R.B. Thompson, B.P. Maliwal, V.L. Feliccia, C.A. Fierke, K. McCall, Determination of picomolar concentrations of metal ions using fluorescence anisotropy: biosensing with a "reagentless" enzyme transducer, Anal Chem 70 (1998) 4717-4723.

[107] R.B. Thompson, B.P. Maliwal, H.H. Zeng, Zinc biosensing with multiphoton excitation using carbonic anhydrase and improved fluorophores, J Biomed Opt 5 (2000) 17-22.

[108] D. Elbaum, S.K. Nair, M.W. Patchan, R.B. Thompson, D.W. Christianson, Structure-based design of a sulfonamide probe for fluorescence anisotropy detection of zinc with a carbonic anhydrase-based biosensor, Journal of the American Chemical Society 118 (1996) 8381-8387.

[109] R. Bozym, T.K. Hurst, N. Westerberg, A. Stoddard, C.A. Fierke, C.J. Frederickson, R.B. Thompson, Determination of Zinc Using Carbonic Anhydrase-Based Fluorescence Biosensors, Fluorescence Spectroscopy 450 (2008) 287-309.

[110] W. Stumm, J.J. Morgan, Aquatic Chemistry: Chemical Equilibria and Rates in Natural Waters, Third ed., Wiley-Interscience, New York, 1996.

[111] L.E. Brand, W.G. Sunda, Reduction of marine phytoplankton reproduction rates by copper and cadmium, Journal of Experimental Marine Biological Ecology 96 (1986) 225 - 250.

[112] M. Martin, K.E. Osborn, P. Billig, N. Glickstein, Toxicities of ten metals to Crassostrea gigas and Mytilus edulis embryos and Cancer magister larvae, Marine Pollution Bulletin 12 (1981) 305 - 308.

[113] J.W. Moffett, L.E. Brand, P.L. Croot, K.A. Barbeau, Cu speciation and cyanobacterial distribution in harbors subject to anthropogenic Cu inputs, Limnology and Oceanography 42 (1997) 789 - 799.

[114] R.B. Thompson, H.H. Zeng, C.A. Fierke, G. Fones, J. Moffett, Real-time *in situ* determination of free Cu(II) at picomolar levels in sea water using a fluorescence lifetime-based fiber optic biosensor, in: G.E. Cohn (Ed.), Clinical Diagnostic Systems: Technologies and Instrumentation, vol. 4625, Society of Photooptical Instrumentation Engineers, San Jose, CA, 2002, pp. 137 - 143.

[115] R.B. Thompson, Z.F. Ge, M. Patchan, C.C. Huang, C.A. Fierke, Fiber optic biosensor for Co(II) and Cu(II) based on fluorescence energy transfer with an enzyme transducer, Biosensors & Bioelectronics 11 (1996) 557-564.

[116] R.B. Thompson, Z. Ge, M.W. Patchan, C.A. Fierke, Energy transfer-based fiber optic metal ion biosensor, in: J.R. Lakowicz (Ed.), SPIE Conference on Advances in Fluorescence Sensing Technology II, vol. 2388, SPIE, San Jose, CA, 1995, pp. 138 - 147.

[117] C. van den Berg, Determining the copper complexing capacity and conditional stability constants of complexes of copper (II) with natural organic ligands in seawater by cathodic stripping voltammetry of copper-catechol complex ions, Marine Chemistry 15 (1984) 1 - 18.

[118] S.L. Belli, A. Zirino, Behavior and calibration of the copper(II) ion-selective electrode in high chloride media and marine waters, Analytical Chemistry 65 (1993) 2583-2589.

[119] K.W. Bruland, E.L. Rue, J.R. Donat, S.A. Skrabal, J.W. Moffat, Intercomparison of voltammetric techniques to determine the chemical speciation of dissolved copper in a coastal seawater sample, Analytica Chimica Acta 405 (1999) 99 - 113.

[120] Y. Zheng, X. Cao, J. Orbulescu, V. Konka, F.M. Andreopoulos, S.M. Pham, R.M. Leblanc, Peptidyl fluorescent chemosensors for the detection of divalent copper, Anal Chem 75 (2003) 1706-1712.

[121] C. Palm, S. Netzereab, M. Hallbrink, Quantitatively determined uptake of cell-penetrating peptides in non-mammalian cells with an evaluation of degradation and antimicrobial effects, Peptides 27 (2006) 1710-1716.

[122] P.J. Dittmer, J.G. Miranda, J.A. Gorski, A.E. Palmer, Genetically encoded sensors to elucidate spatial distribution of cellular zinc, J Biol Chem 284 (2009) 16289-16297.

[123] J.L. Vinkenborg, T.J. Nicolson, E.A. Bellomo, M.S. Koay, G.A. Rutter, M. Merkx, Genetically encoded FRET sensors to monitor intracellular Zn(2+) homeostasis, Nat Methods (2009).

[124] N.C. Shaner, G.H. Patterson, M.W. Davidson, Advances in fluorescent protein technology, J Cell Sci 120 (2007) 4247-4260.

[125] B.J. Bevis, B.S. Glick, Rapidly maturing variants of the Discosoma red fluorescent protein (DsRed), Nat Biotechnol 20 (2002) 83-87.

[126] E.M. Merzlyak, J. Goedhart, D. Shcherbo, M.E. Bulina, A.S. Shcheglov, A.F. Fradkov, A. Gaintzeva, K.A. Lukyanov, S. Lukyanov, T.W. Gadella, D.M. Chudakov, Bright monomeric red fluorescent protein with an extended fluorescence lifetime, Nat Methods 4 (2007) 555-557.

[127] N.C. Shaner, R.E. Campbell, P.A. Steinbach, B.N. Giepmans, A.E. Palmer, R.Y. Tsien, Improved monomeric red, orange and yellow fluorescent proteins derived from Discosoma sp. red fluorescent protein, Nat Biotechnol 22 (2004) 1567-1572.

[128] D.J. Eide, Zinc transporters and the cellular trafficking of zinc, Biochim Biophys Acta 1763 (2006) 711-722.

[129] J.A. Tainer, E.D. Getzoff, K.M. Beem, J.S. Richardson, D.C. Richardson, Determination and analysis of the 2 A-structure of copper, zinc superoxide dismutase, J Mol Biol 160 (1982) 181-217.

[130] C.A. Fierke, R.B. Thompson, Fluorescence-based biosensing of zinc using carbonic anhydrase, Biometals 14 (2001) 205-222.

[131] L.L. Kiefer, S.A. Paterno, C.A. Fierek, Hydrogen Bond Network in the Metal Binding Site of Carbonic Anhydrase Enhances Zinc Affinity and Catalytic Efficiency, Journal of the American Chemical Society 117 (1995) 6831-6837.

[132] J.D. Cox, J.A. Hunt, K.M. Compher, C.A. Fierke, D.W. Christianson, Structural influence of hydrophobic core residues on metal binding and specificity in carbonic anhydrase II, Biochemistry 39 (2000) 13687-13694.

[133] K. Hakansson, M. Carlsson, L.A. Svensson, A. Liljas, Structure of Native and Apo Carbonic Anhydrase-Ii and Structure of Some of Its Anion Ligand Complexes, Journal of Molecular Biology 227 (1992) 1192-1204.

[134] S.K. Nair, T.L. Calderone, D.W. Christianson, C.A. Fierke, Altering the mouth of a hydrophobic pocket. Structure and kinetics of human carbonic anhydrase II mutants at residue Val-121, J Biol Chem 266 (1991) 17320-17325.

[135] M.M. Ling, B.H. Robinson, Approaches to DNA mutagenesis: an overview, Anal Biochem 254 (1997) 157-178.

[136] F. Sanger, G.M. Air, B.G. Barrell, N.L. Brown, A.R. Coulson, C.A. Fiddes, C.A. Hutchison, P.M. Slocombe, M. Smith, Nucleotide sequence of bacteriophage phi X174 DNA, Nature 265 (1977) 687-695.

[137] H. Edelhoch, Spectroscopic determination of tryptophan and tyrosine in proteins, Biochemistry 6 (1967) 1948-1954.

[138] R. Bozym, T.K. Hurst, N. Westerberg, A. Stoddard, C.A. Fierke, C.J. Frederickson, R.B. Thompson, Determination of zinc using carbonic anhydrase-based fluorescence biosensors, Methods Enzymol 450 (2008) 287-309.

[139] Y. Xue, A. Liljas, B.H. Jonsson, S. Lindskog, Structural analysis of the zinc hydroxide-Thr-199-Glu-106 hydrogen-bond network in human carbonic anhydrase II, Proteins 17 (1993) 93-106.

[140] J.F. Krebs, C.A. Fierke, Determinants of Catalytic Activity and Stability of Carbonic Anhydrase II as Revealed by Random Mutagenesis, Journal of Biological Chemistry 268 (1993) 948-954.

[141] C.A. Lesburg, M.D. Lloyd, D.E. Cane, D.W. Christianson, Crystallization and preliminary X-ray diffraction analysis of recombinant pentalenene synthase, Protein Sci 4 (1995) 2436-2438.

[142] D.J. Eide, Multiple regulatory mechanisms maintain zinc homeostasis in Saccharomyces cerevisiae, J Nutr 133 (2003) 1532S-1535S.

[143] C.J. Chang, E.M. Nolan, J. Jaworski, K. Okamoto, Y. Hayashi, M. Sheng, S.J. Lippard, ZP8, a neuronal zinc sensor with improved dynamic range; imaging zinc in hippocampal slices with two-photon microscopy, Inorg Chem 43 (2004) 6774-6779.

[144] C.J. Chang, J. Jaworski, E.M. Nolan, M. Sheng, S.J. Lippard, A tautomeric zinc sensor for ratiometric fluorescence imaging: application to nitric oxide-induced release of intracellular zinc, Proc Natl Acad Sci U S A 101 (2004) 1129-1134.

[145] N.C. Lim, H.C. Freake, C. Bruckner, Illuminating zinc in biological systems, Chemistry 11 (2004) 38-49.

[146] J.L. Vinkenborg, T.J. Nicolson, E.A. Bellomo, M.S. Koay, G.A. Rutter, M. Merkx, Genetically encoded FRET sensors to monitor intracellular Zn2+ homeostasis, Nat Methods 6 (2009) 737-740.

[147] O. Shimomura, F.H. Johnson, Y. Saiga, Extraction, purification and properties of aequorin, a bioluminescent protein from the luminous hydromedusan, Aequorea, J Cell Comp Physiol 59 (1962) 223-239.

[148] M. Ormo, A.B. Cubitt, K. Kallio, L.A. Gross, R.Y. Tsien, S.J. Remington, Crystal structure of the Aequorea victoria green fluorescent protein, Science 273 (1996) 1392-1395.

[149] R. Heim, D.C. Prasher, R.Y. Tsien, Wavelength mutations and posttranslational autoxidation of green fluorescent protein, Proc Natl Acad Sci U S A 91 (1994) 12501-12504.

[150] R. Heim, Green fluorescent protein forms for energy transfer, Methods Enzymol 302 (1999) 408-423.

[151] G.H. Patterson, J. Lippincott-Schwartz, A photoactivatable GFP for selective photolabeling of proteins and cells, Science 297 (2002) 1873-1877.

[152] X. Shu, N.C. Shaner, C.A. Yarbrough, R.Y. Tsien, S.J. Remington, Novel chromophores and buried charges control color in mFruits, Biochemistry 45 (2006) 9639-9647.

[153] S.N. Ho, H.D. Hunt, R.M. Horton, J.K. Pullen, L.R. Pease, Site-directed mutagenesis by overlap extension using the polymerase chain reaction, Gene 77 (1989) 51-59.

[154] L.L. Kiefer, C.A. Fierke, Functional-Characterization of Human Carbonic-Anhydrase-Ii Variants With Altered Zinc-Binding Sites, Biochemistry 33 (1994) 15233-15240.

[155] A.G. Aslamkhan, A. Aslamkhan, G.A. Ahearn, Preparation of metal ion buffers for biological experimentation: a methods approach with emphasis on iron and zinc, J Exp Zool 292 (2002) 507-522.

[156] Y. Yang, J. Ma, Z. Song, M. Wu, HIV-1 TAT-mediated protein transduction and subcellular localization using novel expression vectors, FEBS Lett 532 (2002) 36-44.

[157] R.A. Bozym, R.B. Thompson, A.K. Stoddard, C.A. Fierke, Measuring picomolar intracellular exchangeable zinc in PC-12 cells using a ratiometric fluorescence biosensor, ACS Chem Biol 1 (2006) 103-111.

[158] D.J. Eide, The molecular biology of metal ion transport in Saccharomyces cerevisiae, Annual Review of Nutrition 18 (1998) 441-469.

[159] A.C. Ward, Single-step purification of shuttle vectors from yeast for high frequency back-transformation into *E. coli*, Nucleic Acids Res 18 (1990) 5319.

[160] H. Zhao, D. Eide, The yeast ZRT1 gene encodes the zinc transporter protein of a high-affinity uptake system induced by zinc limitation, Proc Natl Acad Sci U S A 93 (1996) 2454-2458.

[161] A. Miyawaki, O. Griesbeck, R. Heim, R.Y. Tsien, Dynamic and quantitative Ca2+ measurements using improved cameleons, Proc Natl Acad Sci U S A 96 (1999) 2135-2140.

[162] M. Tramier, M. Zahid, J.C. Mevel, M.J. Masse, M. Coppey-Moisan, Sensitivity of CFP/YFP and GFP/mCherry pairs to donor photobleaching on FRET determination by fluorescence lifetime imaging microscopy in living cells, Microsc Res Tech 69 (2006) 933-939.

[163] L.M. DiPilato, X. Cheng, J. Zhang, Fluorescent indicators of cAMP and Epac activation reveal differential dynamics of cAMP signaling within

discrete subcellular compartments, Proc Natl Acad Sci U S A 101 (2004) 16513-16518.

[164] M. Fehr, W.B. Frommer, S. Lalonde, Visualization of maltose uptake in living yeast cells by fluorescent nanosensors, Proc Natl Acad Sci U S A 99 (2002) 9846-9851.

[165] M. Sato, N. Hida, Y. Umezawa, Imaging the nanomolar range of nitric oxide with an amplifier-coupled fluorescent indicator in living cells, Proc Natl Acad Sci U S A 102 (2005) 14515-14520.

[166] M. Fehr, S. Lalonde, I. Lager, M.W. Wolff, W.B. Frommer, *In vivo* imaging of the dynamics of glucose uptake in the cytosol of COS-7 cells by fluorescent nanosensors, J Biol Chem 278 (2003) 19127-19133.

[167] R.B. Thompson, B.P. Maliwal, H.H. Zeng, Zinc biosensing with multiphoton excitation using carbonic anhydrase and improved fluorophores, J. Biomed. Opt. 5 (2000) 17-22.

[168] G.K. Walkup, B. Imperiali, Design and evaluation of a peptidyl fluorescent chemosensor for divalent zinc, J. Am. Chem. Soc. 118 (1996) 3053-3054.

[169] E.M. Nolan, S.C. Burdette, J.H. Harvey, S.A. Hilderbrand, S.J. Lippard, Synthesis and characterization of zinc sensors based on a monosubstituted fluorescein platform, Inorg Chem 43 (2004) 2624-2635.

[170] C.C. Woodroofe, R. Masalha, K.R. Barnes, C.J. Frederickson, S.J. Lippard, Membrane-permeable and -impermeable sensors of the Zinpyr family and their application to imaging of hippocampal zinc *in vivo*, Chem Biol 11 (2004) 1659-1666.

[171] K. Komatsu, K. Kikuchi, H. Kojima, Y. Urano, T. Nagano, Selective zinc sensor molecules with various affinities for Zn2+, revealing dynamics and regional distribution of synaptically released Zn2+ in hippocampal slices, J Am Chem Soc 127 (2005) 10197-10204.

[172] H.H. Zeng, R.B. Thompson, B.P. Maliwal, G.R. Fones, J.W. Moffett, C.A. Fierke, Real-time determination of picomolar free Cu(II) in seawater using a fluorescence-based fiber optic biosensor, Anal Chem 75 (2003) 6807-6812.

[173] L. Yang, R. McRae, M.M. Henary, R. Patel, B. Lai, S. Vogt, C.J. Fahrni, Imaging of the intracellular topography of copper with a fluorescent sensor and by synchrotron x-ray fluorescence microscopy, Proc Natl Acad Sci U S A 102 (2005) 11179-11184.

[174] P. Chen, C. He, A general strategy to convert the MerR family proteins into highly sensitive and selective fluorescent biosensors for metal ions, J Am Chem Soc 126 (2004) 728-729.

[175] R.B. Thompson, D. Peterson, W. Mahoney, M. Cramer, B.P. Maliwal, S.W. Suh, C. Frederickson, C. Fierke, P. Herman, Fluorescent zinc indicators for neurobiology, J Neurosci Methods 118 (2002) 63-75.

[176] S.J. Lin, R.A. Pufahl, A. Dancis, T.V. O'Halloran, V.C. Culotta, A role for the Saccharomyces cerevisiae ATX1 gene in copper trafficking and iron transport, J Biol Chem 272 (1997) 9215-9220.

[177] D. Larin, C. Mekios, K. Das, B. Ross, A.S. Yang, T.C. Gilliam, Characterization of the interaction between the Wilson and Menkes

disease proteins and the cytoplasmic copper chaperone, HAH1p, J Biol Chem 274 (1999) 28497-28504.

[178] E.M. van Dongen, T.H. Evers, L.M. Dekkers, E.W. Meijer, L.W. Klomp, M. Merkx, Variation of linker length in ratiometric fluorescent sensor proteins allows rational tuning of Zn(II) affinity in the picomolar to femtomolar range, J Am Chem Soc 129 (2007) 3494-3495.

[179] J.L. Vinkenborg, M.S. Koay, M. Merkx, Fluorescent imaging of transition metal homeostasis using genetically encoded sensors, Curr Opin Chem Biol 14 (2010) 231-237.

[180] L. Stryer, Fluorescence energy transfer as a spectroscopic ruler, Annu Rev Biochem 47 (1978) 819-846.

[181] H.F. Jenkinson, R.A. Baker, G.W. Tannock, A binding-lipoprotein-dependent oligopeptide transport system in Streptococcus gordonii essential for uptake of hexa- and heptapeptides, J Bacteriol 178 (1996) 68-77.

[182] W. Maret, Molecular aspects of human cellular zinc homeostasis: redox control of zinc potentials and zinc signals, Biometals 22 (2009) 149-157.

[183] H.L. Alakomi, A. Paananen, M.L. Suihko, I.M. Helander, M. Saarela, Weakening effect of cell permeabilizers on gram-negative bacteria causing biodeterioration, Appl Environ Microbiol 72 (2006) 4695-4703.

[184] J.A. Hunt, C.A. Lesburg, D.W. Christianson, R.B. Thompson, C.A. Fierke, Active-site engineering of carbonic anhydrase and its application to biosensors, EXS (2000) 221-240.

[185] P. Sander, S. Grunewald, G. Maul, H. Reilander, H. Michel, Constitutive expression of the human D2S-dopamine receptor in the unicellular yeast Saccharomyces cerevisiae, Biochim Biophys Acta 1193 (1994) 255-262.

[186] N.C. Shaner, P.A. Steinbach, R.Y. Tsien, A guide to choosing fluorescent proteins, Nat Methods 2 (2005) 905-909.

[187] K.R. Brocklehurst, A.P. Morby, Metal-ion tolerance in Escherichia coli: analysis of transcriptional profiles by gene-array technology, Microbiology 146 (Pt 9) (2000) 2277-2282.